UPTEC F06 055
Examensarbete 20 p
Augusti 2006

Plasma flow along auroral arcs

Åsa Engström

UPPSALA
UNIVERSITET

Teknisk- naturvetenskaplig fakultet
UTH-enheten

Besöksadress:
Ångströmlaboratoriet
Lägerhyddsvägen 1
Hus 4, Plan 0

Postadress:
Box 536
751 21 Uppsala

Telefon:
018 – 471 30 03

Telefax:
018 – 471 30 00

Hemsida:
http://www.teknat.uu.se/student

Abstract

Plasma flow along auroral arcs

Åsa Engström

Strong E-field peaks are associated with electrons accelerated by parallel E-fields. High energetic electrons can cause discrete auroral arcs in the auroral oval as well as along the so called polar arcs occurring in the polar cap. According to Haerendel (1992) the discrete auroral arcs have an important role in transporting a surplus of energy out of the magnetosphere. Magnetic field lines, with footprints on the auroral oval, map to the plasma sheet. Therefore the plasma flow is sunward at the auroral oval.

To get an image of how the plasma flux in the ionosphere is related to discrete arcs, data from the Cluster satellites have been studied. One of the main objectives is to investigate the contribution of plasma flow caused by strong E-peaks to the plasma convection in the ionosphere.

We find that the particle flux is in many cases in anti-sunward direction and that the particle flux peaks do, in most cases, contribute very little to the netto particle flux. This indicates that maybe the discrete arcs do not have such an important role for the particle flux transport.

We also examine transpolar arcs. Resent results show that the particle flux of nightside extension of the transpolar arcs is in anti-sunward direction (Liou et al, 2005). Our results confirm that there exist transpolar arc cases where the particle flux is anti-sunward.

Handledare: Anita Kullen
Ämnesgranskare: Stephan Buchert
Examinator: Tomas Nyberg
ISSN: 1401-5757, UPTEC F06 055
Tryckt av: Ångströmlaboratoriet, Uppsala Universitet

Plasma flow along auroral arcs

Åsa Engström

Swedish Institute of Space Physics
Uppsala

August 24, 2006

Abstract

Strong E-field peaks are associated with electrons accelerated by parallel E-fields. High energetic electrons can cause discrete auroral arcs in the auroral oval as well as along the so called polar arcs occurring in the polar cap. According to Haerendel (1992) the discrete auroral arcs have an important role in transporting a surplus of energy out of the magnetosphere. Magnetic field lines, with footprints on the auroral oval, map to the plasma sheet. Therefore the plasma flow is sunward at the auroral oval.

To get an image of how the plasma flux in the ionosphere is related to discrete arcs, data from the Cluster satellites have been studied. One of the main objectives is to investigate the contribution of plasma flow caused by strong E-peaks to the plasma convection in the ionosphere.

We find that the particle flux is in many cases in anti-sunward direction and that the particle flux peaks do, in most cases, contribute very little to the netto particle flux. This indicates that maybe the discrete arcs do not have such an important role for the particle flux transport.

We also examine transpolar arcs. Resent results show that the particle flux of nightside extension of the transpolar arcs is in anti-sunward direction (Liou et al, 2005). Our results confirm that there exist transpolar arc cases where the particle flux is anti-sunward.

Contents

Chapter 1

Introduction to basic plasma physics

1.1 Plasma

A plasma is a gas of charged particles. A gas can be consist of particles carrying no electric charge, be partly ionized or fully ionized. For a gas to be called a plasma three criteria need to be fulfilled:

1. Quasineutrality ($\lambda_D << L$)
2. Collective behavior ($N_p >>> 1$)
3. ($\omega\tau > 1$)

The first criteria, quasineutrality, means that the plasma is so neutral that we can assume that $n_i \simeq n_e \simeq n$ where n_i is the ion density, n_e the electron density and n is the plasma density. At the same time electromagnetic forces control the motion of the particles so the gas is not neutral at all scale lengths. If a charged sphere is put in a plasma, charges of the opposite sign will accumulate in a cloud around the sphere. This cancels out the charged sphere and there is no electric field present outside the cloud of charged particles. This is called shielding. The width of this cloud or layer of charged particles is called the Debye length and is denoted as

$$\lambda_D = \frac{\epsilon k T_e}{n_e e^2}^{\frac{1}{2}} \tag{1.1}$$

where ϵ is the free space permittivity, k the Boltzmann constant, n_e the electron density, and T_e the electron temperature.

In a dense plasma λ_D is shorter and the shielding more effective. To be quasineutral the shielding effect is effective enough for $\lambda_D << L$ where L is the dimension of the system, i.e. the plasma behaves like a neutral gas in the presence of charge probes for distances $\geq$ L.

In a neutral gas electromagnetic forces are absent and the gravitational force is so small that it can be neglected. Therefore the motion in a neutral gas is controlled by collisions with other neutrals. In a plasma, which contains charged particles, electromagnetic forces are of significant importance. When the charged particles move, local concentrations of positive and negative charges arise. These concentrations of charges create electric fields. The motion generates currents and magnetic fields, which affects the motion of other charged particles (The Coulomb force). Collective behaviour requires not only $\lambda_D << L$ but also $N_p >>> 1$, where N_p is the number of particles in the Debye sphere. If there are not enough particles the Debye shielding does not work.

The third condition to be fulfilled concerns collisions. In a weakly ionized gas the collisions with neutrals are so common that this has a greater importance for the motion than the electromagnetic forces. For a gas to be a plasma it is required that $\omega\tau > 1$ where ω is the frequency of typical plasma oscillations and τ is the time between collisions with neutrals. (For an overview on this subject, see e.g. Chen, 1984)

1.2 The solar wind

In the universe 99% of the known matter is plasma. The Sun, as well as the space between the Earth and the Sun, consists of plasma. A plasma flow spreading out from the Sun into the surrounding space, is called the solar wind. This is the result of the high temperature in the solar corona. The thermal energy exceeds the gravity and throws the solar plasma out as the solar wind. Another way to explain it is, that the pressure in the solar corona is higher than the pressure of the space around it, causing the outflow of solar material.

The solar wind is a collisionless, fully ionized and highly conducting plasma. When the magnetic field is weak and the conductivity is high, the so-called frozen-in-principle becomes valid. It means, a certain plasma volume is tied to a certain magnetic flux tube. The kinetic pressure from the solar wind is larger than the magnetic pressure from the solar magnetic field. Thus, the particle flow controls the magnetic field. This can be described as the magnetic field lines are frozen into the solar wind. Because of this frozen-in principle, the solar wind carries the Suns magnetic field out in the space. The solar magnetic field is a part of the interplanetary magnetic field (IMF). Close to the Earth the solar magnetic field dominates the IMF. The solar wind does not flow radial outward. Due to the rotation of the Sun it resembles a water sprinkler and the magnetic field forms a spiral. It folds like shown in Figure 1.

At the Earth the IMF varies in north-south direction, depending on weather the interplanetary current sheet is below or above the x-y-plane, of the Geocentric Solar Ecliptic coordinate system (GSE). At the Earth the x- and y-components of the IMF often have similar magnitudes but are directed in opposite direction. The z-component is generally much smaller, and changes over time. When it is positive we call the IMF northward and at negative z-component southward. For a definition of coordinate systems, see chapter 1.15.

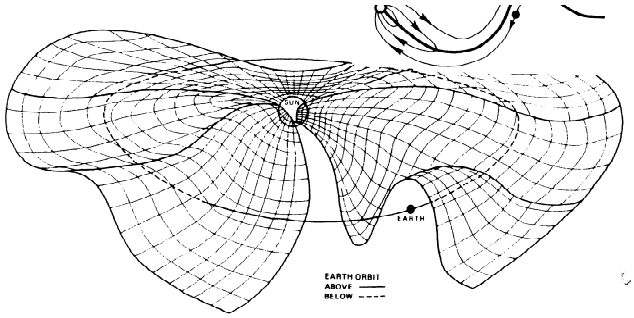

Figure 1.1: The folding of the IMF caused by the rotation of the Sun, (Kelley, 1989).

1.3 Single particle description

The single particle approach can be used in plasmas where the particle interaction can be neglected and the external fields are strong compared to the internal magnetic field created by the particle motion so that the external field will not be affected.

If we assume that we do not have an electric field present, we can derive an expression for the motion of the electrons and ions from the reduced equation of motion in which we neglect the electric field. This shows that the electrons and ions gyrate around the magnetic field lines. The center of the path is called guiding center.

The reduced equation of motion:

$$m\frac{d\vec{v}}{dt} = q(\vec{v} \times \vec{B}) \tag{1.2}$$

We get an harmonic oscillator equation with the solutions:

$$x - x_0 = r_g sin\omega_g t \tag{1.3}$$

$$y - y_0 = r_g sin\omega_g t \tag{1.4}$$

with the gyro frequency

$$\omega_g = \frac{qB}{m} \tag{1.5}$$

and the gyroradius

$$r_g = \frac{v_\perp}{\mid \omega_g \mid} \tag{1.6}$$

Equation (3) and (4) describe the motion of the particles gyrating in a circular orbit around the magnetic field line.

Normally there is also an electric field involved. When we derive the motion of the particles from the complete equation of motion, we get an extra term. Additional to the gyration around a guiding center there is a drift motion of the guiding center in the direction perpendicular to the magnetic field.

Not only the electric field but even other forces may cause drift motion of the guiding center. A general formula for the guiding center drift, valid for any force acting on on a charged particle in a magnetic field is:

$$v_F = \frac{1}{q}\frac{\vec{F} \times \vec{B}}{B^2} \tag{1.7}$$

The different drift motions are

- The electric drifts:
  - E × B-drift (electron and ions drift in the same directions)
  - Polarization drift (electron and ions drift in opposite direction)
- The magnetic drifts:
  - Gradient drift (electrons and ions drift in opposite directions)
  - Curvature drift (electron and ions drift in opposite directions)

When the drift motions of electrons and ions are in different directions, a current appear. This occurs when the drift term contains the charge sign of the particle. For example, the magnetic curvature and gradient drifts cause a current called the ring current, around the Earth. (Baumjohann and Treumann, 1996)

1.4 Magnetosphere

The Earth has a liquid core that is electrical conductive. Currents driven by thermal convection give rise to the Earth's magnetic field, which can be approximated by a dipole field. The magnetic north pole axis is tilted 11 degrees, from the geographic north pole, towards the North American continent. The angel is not constant but changes with time and research has shown that the axis flip over approximately every 100 000 year. The strength of the Earth's magnetic field, or the terrestrial field as it is also called, is at the surface, $0.6 * 10^4 T$ near the poles and $0.25 * 10^4 T$ close to the equator. The strength decreases with distance from Earth.

The solar wind flows towards the Earth with a speed of about 500 km/s. The supersonic speed relative to the Earth causes a bow shock in front of the magnetopause.

At the bow shock, most of the kinetic energy of the particles in the solar wind is converted into thermal energy. The plasma inside the bow shock is called the magnetosheath and is both hotter and denser. When the solar wind reaches the terrestrial magnetic field the IMF can not penetrate it. Since the particles are tied to the field lines, they are deflected around. The boundary between the two magnetic fields is called magnetopause. The solar magnetic field compresses the terrestrial field on the dayside through the kinetic pressure. On the night side a long tail is formed and reaches as far as $200R_E$. This tail is called magnetotail and contains two regions, the plasma sheath concentrated around the midplane and the remaining parts are the magnetotail lobes.(see e.g. Kievelson Russel, 1995)

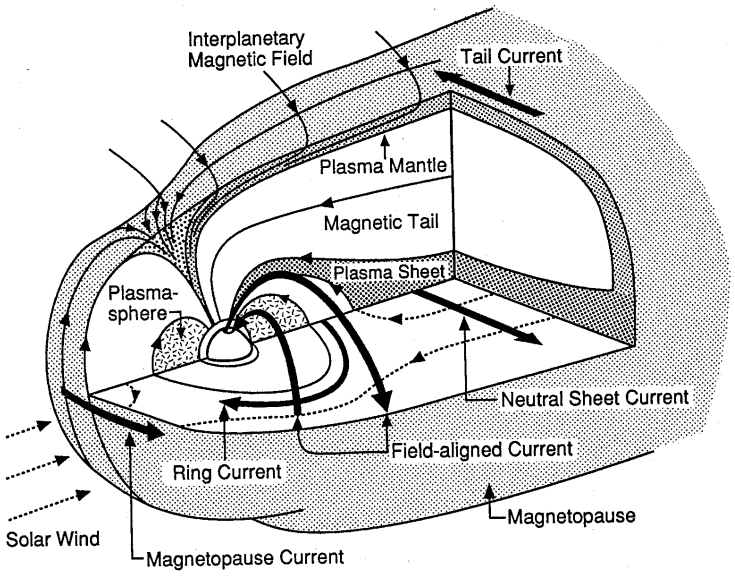

Figure 1.2: The magnetosphere (Kivelson and Russell, 1995)

1.5 Collisions and ionization

There are two types of plasmas in space. One type is collisionless plasma, where collisions are so rare that they can be neglected. The other type of plasma is collisional plasma, where the collisions are more frequent and affect or maybe even dominate the plasma behaviour. The plasma in the solar wind is collisionless while the magnetospheric and ionospheric plasmas are collisional.

Collisional plasma can also be divided into two types. Partially ionized and fully ionized. The partially ionized plasma consists of neutral atoms and molecules mixed with charged electrons and ions. The collisions between one neutral and one charged particle dominate. The heavier neutrals can be considered in rest compared to the much lighter charged particles. The collisions are direct, in other words, collisions occurs only when the neutral is in the electron's or ion's path. Fully ionized plasma contains only charged particles

and the interaction is therefore between the Coulomb fields. The result is that they are deflected at distances much longer than atomic radius. (Baumjohann Treumann, 1996)

Another type of collisions is the solar UltraViolet ionization. When the sunlight hits the atmosphere, the ultraviolet (UV) light ionizes the neutral atoms and molecules of the atmosphere. For the solar photons to be able to ionize the atoms, the energy must be higher than the ionization energy of the atoms. The only radiation with such a high energy is the UV-radiation and radiation with higher frequencies. At those frequencies the solar intensity is very weak and is for that reason not vital for the average state of the ionosphere.(see e.g. Baumjohan Treumann, 1996)

At low altitudes the atmosphere remains neutral due to recombination. At higher altitudes where the density is lower, the collisions are not frequent enough to neutralize the atmosphere through recombination. In the magnetosphere where the density is even lower, the plasma is fully ionized. The layer between the neutral atmosphere and the fully ionized magnetosphere is the ionosphere, which is partly ionized.

1.6 The ionosphere

In the ionosphere, UV light is the main source of ionization but also particle precipitation is a contribution. At the dayside the UV ionization dominates while particle precipitation is most frequent in the auroral zone.

The ionosphere can be divided into two regions. One is the low latitude ionosphere which belongs to the plasmasphere, where the plasma co-rotates with the Earth. The other area is the high-latitude ionosphere, which maps outside $4 - 6R_E$ into the magnetosphere. At high altitudes of the high-latitude ionosphere the motion of the plasma is determined by the large-scale circulation of the magnetospheric flux tubes.

1.7 Reconnection

When solar wind approaches the magnetopause, the characteristics of the plasma changes. It does not fulfill the conditions of the frozen-in principle any more. This makes it possible for the IMF field lines to connect to the terrestrial field lines at the location where the field lines are anti-parallel. Reconnection opens up the magnetopause and the particles can pass. The field lines that have one end on the Earth and the other connected to the IMF are called open field lines and the ones with both ends connected to the Earth are closed field lines. When the solar wind passes the Earth and the magnetosphere, the IMF field lines continue to be connected to terrestrial field lines. Because of the frozen-in-principle the plasma drags the open field lines in the direction of the tail. The open field lines that reach down the tail are separated by a current sheet in the equator plane. The direction of the B-field is opposite south and north of the current sheet called neutral sheet. Back in the tail are the open field lines reconnected again. (See Figure 3a). It is called tail reconnection. This results in an earthward plasma flow on the closed field lines in the plasma sheet. This earthward plasma flow is related to the sunward particle flux we find on the auroral oval. In Figure 3b, is the motion of the field lines shown. Since the plasma is connected to the field lines, due to the frozen-in principle, the plasma flows in the same direction as the field lines moves.

The direction of the IMF is of decisive importance for the efficiency and the location of the reconnection. When the IMF is southward, reconnection is very efficient. The reconnection line is on the dayside of the magnetopause. The solar wind plasma that penetrates here forms a boundary layer, the low-latitude boundary layer (LLBL) that stretches along the tail flanks far downstream from Earth.

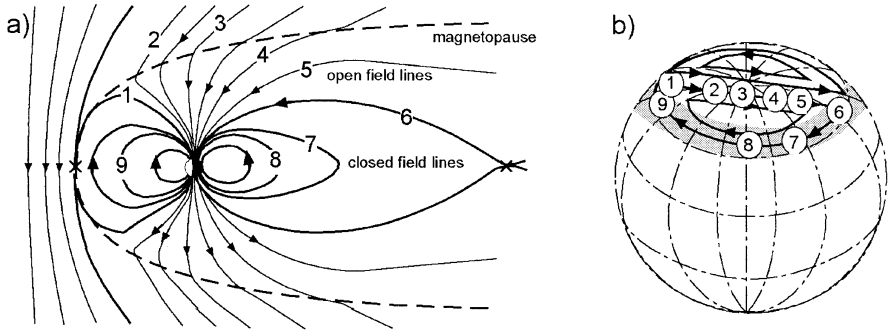

Figure 1.3: a) The reconnection between the IMF field lines and the terrestrial field lines during southward directed IMF. b) The particle flux direction during southward directed IMF. (Dungey, 1961)

When the IMF is northward, both the fields are pointing in the same z-direction, thus dayside reconnection is not possible. One suggestion is that during this time the magnetopause is closed and there is only viscous interaction at the boundaries (Axford and Hines, 1961). Viscous interaction means that momentum is transmitted through the magnetopause by waves and diffusion. This forces the plasma inside the magnetopause to move in the same direction as the plasma outside. However reconnection occurs even during northward IMF and there are a few models about reconnection during northward IMF. One of the most accepted ones is shown in Figure 4 (Lockwood, 1987). Here, the reconnection is tailward of the cusp on high latitudes. The cusp is the name of the opening where the magnetic field lines assembles and connect to the Earth. There have been a number of theories where exactly reconnection occurs. The component merging theory (Sonnerup, 1974) says that reconnection occurs where the IMF and magnetosphere first hits each other. The anti-parallel merging theory (Crooker, 1979) on the other hand says, that it occurs where the fields are completely anti-parallel to each other.

1.8 Adiabatic invariants

Adiabatic invariants are characteristic constants of the particle. They are not really constants but can be treated like that because they change slowly compared to usual periodicities of the particle motion. The magnetic moment, the longitudinal invariant and the drift invariant, are the three adiabatic invariants.
The magnetic moment μ is dependent of the mass of the particle (M), the magnetic field (B) and the speed of the particle perpendicular to the magnetic field ($V_\perp$).

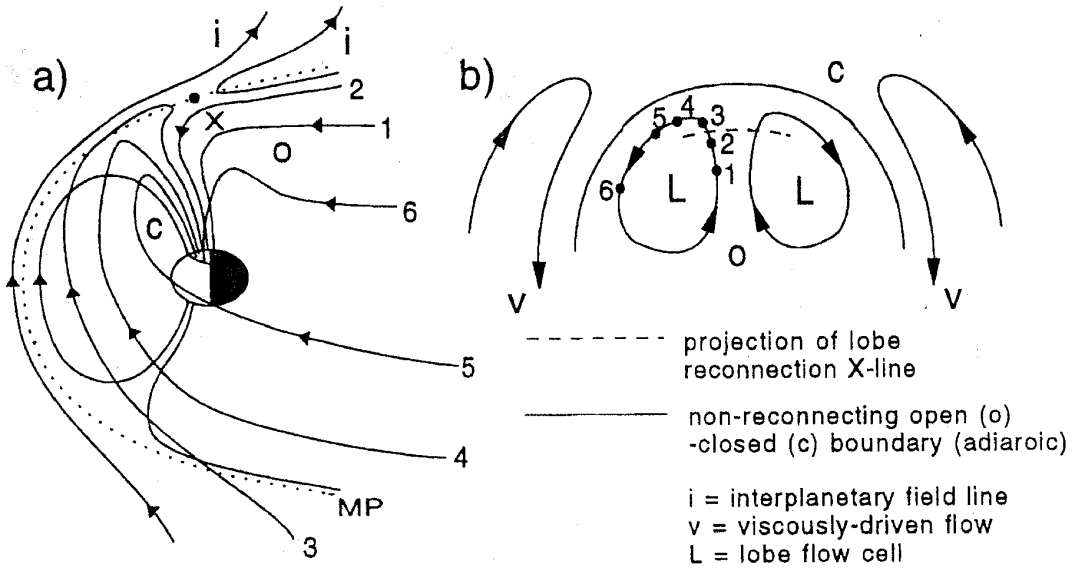

Figure 1.4: Reconnection during northward IMF. The reconnection is tailward of the cusp. (Lockwood, 1987)

$$\mu = \frac{MV_{\perp}^2}{2B} \tag{1.8}$$

When the particle moves along a magnetic field line in the Earth dipole field,the strength of the magnetic field increases but μ is conserved. The mass is constant so $V_{\perp}$ increases at the expense of $V_{\|}$. $V_{\|}$ decreases until the particle does not move at all along the field lines. Then the particle changes direction and moves back towards the other pole. The parallel speed now increases until the particle reaches the equator then it slows down again because of the magnetic field that is increasing again. The particle can continue to bounce back and forward between the poles until it is lost by collisions in the ionosphere.

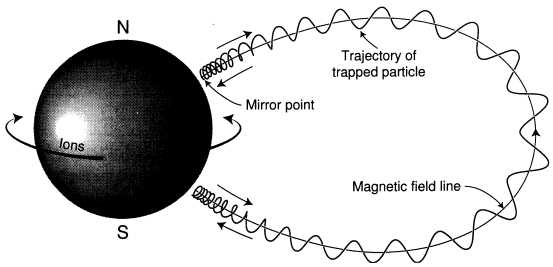

Figure 1.5: The trapped particles bounce back and forward between the northern and southern hemisphere until they are lost in the atmosphere due to collisions. (Kelley, 1989)

These particles bouncing between the poles are called trapped particles. They occur massively in a region between 2-6 R_E, the so called radiation belt, that has a very high particle density.

Chapter 2

Introduction to the auroral ionosphere

2.1 High-latitude magnetosphere

At high latitudes some of the magnetic field lines reach the magnetopause and magnetosheet. The closed field lines on high latitude reach far down the tail and into the boundary layer but are still inside the magnetopause. These field lines are connected again in the tail.

First we consider the case of southward directed IMF. IMF B_z is negative in the Geocentric Solar Magnetospheric coordinate system (GSM). It creates an electric field in the Solar wind, in the y-direction, from dawn to dusk in the reference frame of the Earth.

$$E_{SW} = -v_{SW} \cdot B_{SW} \tag{2.1}$$

The magnetic particle flux density is larger in the ionosphere than in the solar wind which makes the E-field in the ionosphere stronger. Above ionospheric height, plasma convection follows the motion of the magnetic field lines. Due to the frozen-in principle the footprints of the B-field above the ionosphere follow the motion of the solar wind. The convection pattern is different depending on the direction of IMF. As mentioned in section 1.7 about reconnection, there is a earthward plasma in the plasma sheet. The closed field lines in the plasma sheet have their footprints on the auroral oval, therefore is a sunward plasma flow always expected on the oval. For southward IMF, the convection pattern is illustrated in Figure 6. The flow is anti-sunward at high latitude over the pole and returns towards the Sun at lower latitudes.

For northward IMF the convection pattern is different. Outside the cells are two other cells presumably because of viscous interaction at the auroral zone. Observe that this is not always the case. The reality is often more complicated and the particle flux in the polar cap tend to be more chaotic. In the case of northward IMF is it common with more than two cells, the size and shape of them also varies. The B_y component of IMF influences the size and shape of the cells. Figure 7 shows the results of a statistical study of the convection pattern for different IMF orientations (Weimer, 1995)

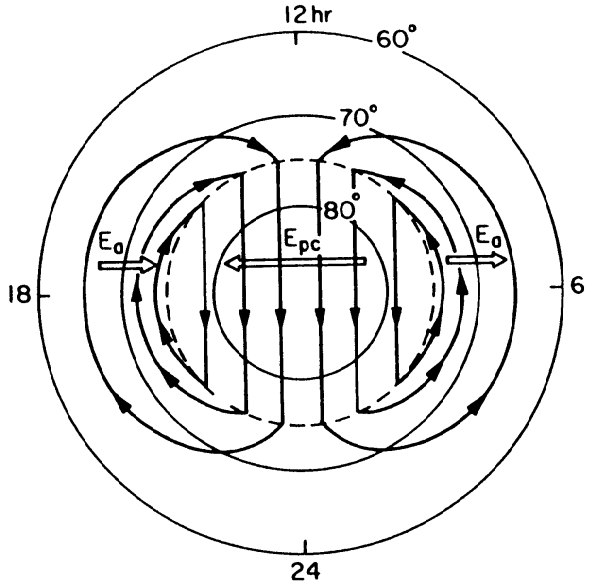

Figure 2.1: The convection pattern during southward IMF. (Kelley, 1989)

The subsonic solar wind outside the bow shock has a thermal energy of a few eV. When it slows down the kinetic energy transforms into thermal energy. The electrons in the magnetosheath have a thermal energy of 10 or 100 eV. Some of the electrons penetrate directly into the ionosphere in the connection phase or through the cusp. This shows as aurora at the dayside. Some of the remaining electrons spurt back in the reconnection phase in the tail. The electrons thermal energy in the plasma sheet is about 1keV. These electrons create diffuse aurora. The collisions between the electrons and the ionospheric atoms are an important source of ionization in the ionosphere.

2.2 The aurora

The aurora is caused by particles exciting neutral atoms and molecules in the atmosphere. When the excited atoms return to the ground energy level the energy is emitted as photons. Depending on what atom and to what energy level it is excited, the wave length is different. The aurora has colours of the wavelengths corresponding to the emitted energies. The aurora occurs at an approximate height of 100 kilometres.

The main auroral oval consists of diffuse aurora. It is quite weak in intensity and caused by particles with a energy of about 1keV. These particles have their origin in the tail plasma sheet. The auroral oval is always glowing more or less, but the size and intensity varies. The direction of IMF strongly influences both the size and luminosity of the oval. When B_z is southward the aurora is active and bright. During this time, phenomena such as substorms occur. During quiet time, (when the IMF is northward) the auroral oval is small and weak. At this time there are small-scale arcs in the polar cap almost all the time. Large-scale arcs also occur, but not that often.

Discrete auroral arcs are very bright and can be seen from the ground. These particles

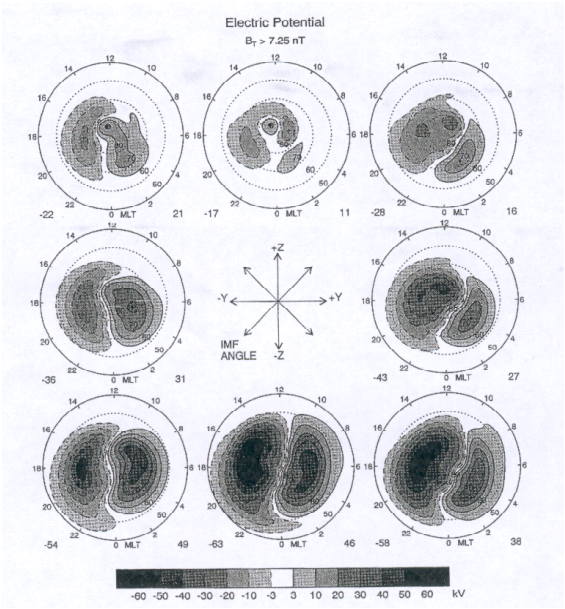

Figure 2.2: Statistical ionospheric convection patterns. From Weimer (1995)

probably have their origin in the plasma sheet boundary layer. Discrete aurora is caused by energetic electrons accelerated by parallel E-fields above the ionosphere.

Ionospheric currents are coupled to the magnetosphere through field-aligned currents. There are upward and downward field-aligned currents that create a current system.

The current is calculated from:

$$j = v_i \cdot n_i - v_e \cdot n_e \tag{2.2}$$

where v_i is the ion velocity, v_e the electron velocity, n_i the ion density and n_e the electron density. The electrons and ions can move freely along the magnetic field lines in the magnetosphere as the conductivity is extremely high. Since the B-field is stronger closer to the Earth, the particles have a turning point due to the conservation of the magnetic moment. (See chapter 1.8). In a consequence, fewer electrons reach the ionosphere. To maintain the current the velocity of the particles must increase when the density decreases. An E-field structure, shown in Figure 9, takes shape. The E-field accelerates the electrons to energies of several keV. Downward accelerated electrons cause discrete auroral arcs when they collide with the atoms in the atmosphere. Data from a spacecraft that measure the E-field at higher altitudes shows a converging E-field and a potential drop. Above the ionosphere very fast convection can exist free from frictional control. This is possible due to the parallel potential drop. The potential drop is responsible for whether the electrons are accelerated to energies high enough to cause a discrete arc. Recent results show that discrete aurora occur mainly at plasma population boundaries (Johansson et al.,2005)

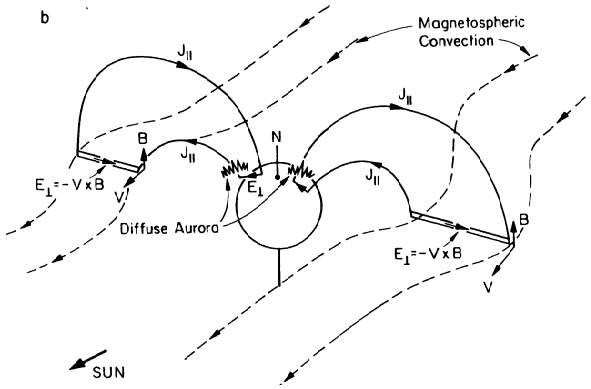

Figure 2.3: Three-dimensional view of the electric and magnetic field geometry on auroral zone flux tubes (Kelley, 1989).

2.3 Polar arcs

Arcs stretching from the auroral oval towards high latitudes are called polar arcs. They are usually sun-aligned. There are several different types of polar arcs and it is not clear if they are all the same auroral phenomenon or not. They differ in spatial extent and magnetospheric source regions. There are small-scale, sun-aligned polar arcs, stretching a few kilometres in length and large-scale polar arcs stretching from 100km to across the entire polar cap. The ones stretching from one side of the auroral oval to the other are called transpolar arcs or theta auroras. Some arcs are also moving across the polarcap. This motion is controlled by the direction of IMF.

To separate the types of arcs we use the polar arc classification by Kullen et al., (2002). See Figure 10.

1. Oval-aligned arcs - separates from the oval and stay there
2. Moving arcs - separates from the oval and starts moving across the polarcap toward the other side.
3. Bending arcs - a outgrowth, from either dusk or dawn, that bends inside the polarcap.
4. Midnight arcs - the arc arises from a thickening on the midnightside of the oval. The thickening turn into a outgrowth that stretches toward the dayside and eventually forms a transpolar arc.

Polar arcs are in many way controlled by IMF and its direction. Transpolar arcs are mainly found during quiet times, when the IMF is northward. The transpolar arcs existing during southward IMF has been explained as arc formed during northward IMF and persist after a sign change to southward directed IMF (Frank and Craven, 1988).

Transpolar arcs are believed to lie on closed field lines and the particle flux is sunward (e.g., Frank et al., 1986; Chang et al., 1998). A study with events with a transpolar arc

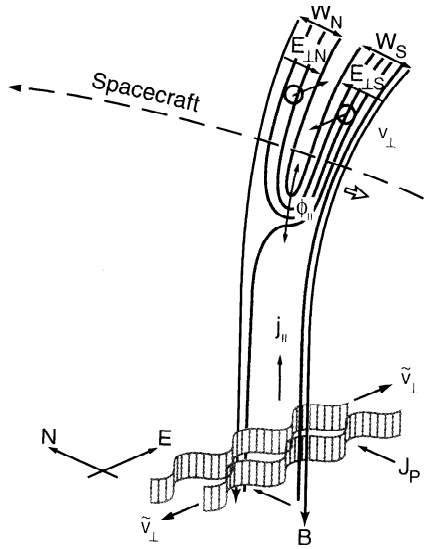

Figure 2.4: Parallel E-fields (Paschmann el al., 2003).

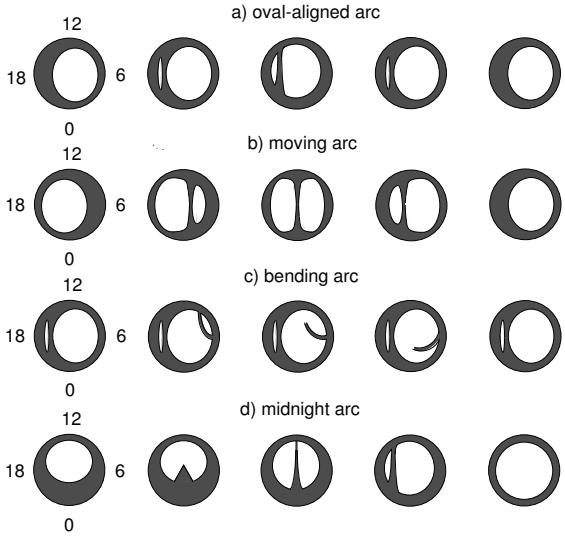

Figure 2.5: Arc types (Kullen et al., 2002).

on 8 November 2000 showed a different result. SuperDARN radar and Polar UVI image data were used. The result proved that the plasma on the nightside where drifting anti-sunward. On the dayside there was no consistent pattern of the flow. This indicate that the transpolar arcs would be on open field lines on the nightside and not on closed as according to previous theories (Liou et al., 2005).

2.4 The role of auroral arcs

All aurora is caused by particle precipitation, but all aurora is not of the same kind. As mentioned earlier in the text, the reason for the precipitation can differ as well as the source of the energy. Now concentrating on the convection related aurora and what importance it has for the magnetospheric plasma transport. The plasma in the magnetosphere is constantly in motion and is driven by the solar wind. There is an constant energy input from the solar wind plasma flowing in through the open magnetopause or by viscous interaction at the magnetopause boundaries. The convection pattern is different depending on the direction of the IMF, which can be read about in chapter 2.1. The convection is normally relative slow and controlled by the friction. The convection is associated with the flow of field-aligned currents. If the solar wind would disappear, the convection would eventually stop, except for some effects caused by the atmospheric tides. If there instead is high momentum and high energy input from the solar wind, we would see a significant increase of the currents. In the formation of elongated, narrow and structured auroral arcs are field-aligned currents an important condition. When the energy input is high, and the field-aligned currents greatly enhanced, rich auroral displays can be observed. The auroral arcs are therefore traces of enhanced energy release from the magnetosphere. This role of the arcs as a efficient way to fast transport the energy out of the magnetosphere, Haerendel (1992) cast the name 'auroral pressure valve'.

In most cases the discrete arcs are to be found on the boundary region of the auroral oval. We make the assumption that the E-field peak is bipolar and there is a density distribution with higher density on one side of the arc. We start from the statement that the discrete arcs play an important role in effective releasing energy from the magnetosphere (Haerendel, 1992). For this to be possible it requires a netto particle flux, i.e. the particle flux has to be stronger on one side of the discrete arc so that the particle fluxes do not cancel out each other. The particle flux is dependent of both the E-field and the density. Since we assumed that the E-field peaks were bipolar, the density has a great importance. The Flux is the velocity multiplied with number of particles. If the density is higher on one side of the arc this means that, presupposed that the strength of the E-field is equal, we get a higher particle flux on this side of the arc.

Chapter 3

Coordinate systems

3.1 Geocentric Solar Ecliptic (GSE)

The x-axis points from the Earth towards the Sun. The y-axis points towards dusk in the ecliptic plane and the z-axis is parallel to the ecliptic pole.

3.2 Geocentric Solar Magnetospheric coordinates (GSM)

The x-axis points from the Earth towards the Sun. The y-axis is perpendicular to the x-axis and the magnetic dipole axis and the z-axis perpendicular to x and y and is chosen to have it's positive direction in the same sense as the northern magnetic pole. The only difference between the GSM and the GSE coordinate system is a rotation about the x-axis. This coordinate-system reduces the three dimensional motion of the Earth's dipole, to motion in only one plane. The system is for example useful for large-scale magnetosphere studies.

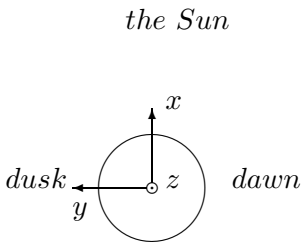

Figure 3.1: The GSM coordinate system

3.3 Geomagnetic (GM or MAG)

The z-axis is parallel to the magnetic dipole axis and points towards north. The y-axis is orthogonal to the line through the geographic poles and the x-axis completes the right handed orthogonal set. It is often expressed in longitudes and latitudes.

3.4 The Solar magnetic coordinate system (SM)

The y-axis is perpendicular to the line from the Earth to the Sun. The z-axis is parallel to the magnetic north pole. The x-axis completes the set. Observe, that the x-axis does not point directly towards the Sun. Sometimes the solar magnetic coordinate system is expressed in geomagnetic latitude (lat) and magnetic local time (MLT). The magnetic local time is used instead of longitude. 12.00 MLT is the point closest to the Sun. 18.00 refer to dusk and 06.00 refer to dawn. 00.00 MLT is located furthest away from the Sun and referred to as midnight. Sometimes the satellite location is expressed in corrected magnetic latitude (CGLat) and MLT. Corrected magnetic latitude is the latitude we get when following the magnetic field lines down instead of drawing a straight line towards the Earth.

3.5 Magnetic field, East, Equator system (MEE)

A coordinate system developed at KTH. The z-axis is directed in the direction of the magnetic field, so on the northern hemisphere it is directed towards the Earth and on the southern hemisphere away from the Earth. The y-axis is always directed towards the equator and the x-axis points eastward. Since this coordinate system is fixed on the rotating Earth, it is useful for high-latitude ionospheric measurement.

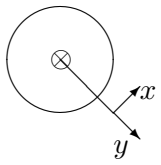

Figure 3.2: The MEE coordinate system. The northern hemisphere seen from above.

Chapter 4

Instruments

4.1 Cluster (ESA/NASA)

The first launch of Cluster was in 1996 with one of the Ariane-5 rockets. Unfortunately it exploded shortly after the start. The now present Cluster satellites were launched from Baikonur Cosmodrome in Kazakhstan the 16th July 2000, with two Russian Soyuz launchers, each with a Fregat upper stage.

Cluster consists of four spacecrafts orbiting around the Earth in polar orbits with high eccentric coefficient. The minimum distance from the Earth is $4R_E$ and the largest distance is $18{,}7R_E$. The Cluster satellites fly in a tetrahedron formation and the distance between them varies between a few kilometres up to 20 000 km. The Cluster spacecrafts examine how the solar wind affects the Earth and it's space environment. Because there are four spacecrafts, it is possible to do measurements in three dimensions. When they are close to each other we can look at small scale physics like reconnection processes and when they are wide apart we can study temporal variations of physical quantities. The spacecrafts are all identical and are each formed like a disk with a diameter of 2.9 meters and a height of 1.3 meters.

The Electric field measurements are made by an instrument called EFW (Electric field and wave experiment). The instrument includes sensors attached to 50 meter long booms. Totally there are four booms. The potential between the booms are measured and then a three-dimensional E-field is calculated. When the sun shines on the spacecraft it emits electrons. A situation similar to plasma shielding come up and that is why the long booms are necessary.

PEACE (Plasma Electron And Current Experiment) detects particles with low and medium energies. There are two parts, one that handle the fast particles and another part for the slower ones. The sensors count them and measure the direction and value of the velocity as well.

CIS (Cluster Ion Spectrometry experiment) is also an instrument that handles particle data. It consists of an advanced instrument control and data processing system that can perform detailed data processing on-board. It consist of two instruments a HIA (Hot Ion Analyzer) and a time-of-flight ion Composition and Distribution Function analyzer, CODIF. CIS analyzes the ions of the magnetosphere and the solar wind every four seconds. It measures the mass, composition and distribution functions of the ions.

Figure 4.1: The cluster satellite (ESA homepage)

4.2 Image (NASA)

IMAGE is a satellite launched with the purpose to capture a global picture of the magnetosphere of the Earth and the plasma affected by the geomagnetic field. IMAGE was launched with the Boeing Delta II 7326-9.5 launch vehicle, at 25th of mars 2000. It was released and put in a polar ecliptic orbit with apogee altitude of 6,7R_E and a perigee of 1000 km. The apogee latitude changes during the mission, but started at 40 degrees north latitude and change towards 90 degrees to be back at 40 again two years after the launch. The data from the IMAGE project can easily be accessed on the internet, because of the open data policy of the mission.

The images used in this study are from WIC. WIC is a Wideband Imaging Camera with a field view of 17×17 degrees. The camera is operating in the wave length interval between 140 and 160 nm (Ultraviolet light). The spatial resolution is less than 0.1 degrees and a temporal resolution is 120 s. The final sensitivity of the image is expected to be around 100 R. The camera is constructed to photograph the Earth and the auroral oval and by taking photos from a distance greater than 4 R_E, it produces global images.

4.3 Polar UV Imager (NASA)

The UV Imager is a camera and one of eleven instruments on the Polar spacecraft. The Polar spacecraft was launched at February 23, 1996, from Vanderberg Air Force Base, California, on a Delta II rocket. From the beginning the Polar spacecraft had an orbit with apogee over the northern polar region, but the orbit changes and the apogee moves 16 % every year. Now the inclination is at 86 degrees, the apoogee is at 9 and the perigee at 1.8 Earth radii. The orbit period is 18 hours.

The UV Imager is a highly sensitive camera that produces images of the auroral regions. It's a 2-dimensional spatial imager detecting light in the UV-wave lenght between 130-190nm. It is very sensible and can detect objects over 100 times fainter than the objects that you can detect with the eye. It corresponds to a sensibility of 10 Rayleighs. The UV Imager is apart from the camera an electronic stack. The electronic stack is a support package that functions as the electrical interface with the spacecraft, controls the mechanical components

and monitors the status of the camera.

Chapter 5

Purpose of the work

The aim of this work is to find out how much the plasma flow along auroral arcs contributes to the entire plasma convection to the auroral oval. After downloading data from the Cluster satellites, times-series plots are created. The plots contain E-field, B-field, density, field-aligned currents and plasma transport. Concerning the direction of the particle flux the focus is on a few questions in the analysis. In what direction is the background particle flux on the oval? How much do the E-field peaks contribute to the background particle flux? In which direction is the particle flux contribution from the E-peaks? We also want to examine how great importance the density profile has on the particle flux peaks. The few transpolar arc cases will be treated separately. Many aspects of transpolar arcs are not very well understood. How is the particle flux directed on transpolar arcs? At the end of the study, all results will be compared to previous findings.

Chapter 6

Method

6.1 The work plan

The project started by searching for transpolar arcs from overview pictures from WIC on the Image satellite. Material from January 2000 until May 2005 was reviewed. The location for the transpolar arcs was compared with the position of Cluster at the same time, to obtain possible conjunctions. The Cluster position was chosen to be within a distance from 4-7 R_E from the Earth. This was very time demanding and did not give the expected results. Only a few conjunctions where found. The next method tried, was to look at list of strong E-field peaks. E-field peaks are often connected to discrete arcs and therefore also transpolar arcs. A list of registered strong e-field peak from Johansson, KTH, was used. The strength of the E-field peaks was 500-1000 mV/m. This method showed to be a lot more profitable and faster. After this the total number of transpolar arcs where 3. The decision was taken to increase the subject to discrete arcs in the auroral oval. Possible discrete arcs were easily found on the lists of strong E-field peaks. Not all of them were actually arcs since the direction of the current and the size of the potential drop are decisive. For some of the events found on the list there were images from either Polar or Image, but most of them had images of very low quality or no images at all. Of the 32 events included in this work have 10 of them a image from either IMAGE or POLAR. The images are attached in appendix B.

After sorting out a number of approximately 25-30 events, probable conjunction interval were chosen from PEACE data plots. The events or the part of the orbits of the events where PEACE data was missing or indistinct in any way, was sorted out. Data from Cluster 1,3 and 4 was used. Cluster 2 was skipped because there was no CIS density data available for this satellite. The CIS data is needed to calculate the particle flux from the density. The time interval was chosen to be about one to two hours to cover the entire TPA region or as large part of the oval as possible. The next step was to download high-resolution E-field data, B-field data and spacecraft potential from EFW. Particle data was downloaded from CIS. The positions of the satellites were also downloaded. It was necessary to download B-field for a longer interval to be able to subtract the background field to get the B-field variations without the background dipole field. This is needed to calculate the field-aligned currents. Even more events where discarded at this stage because of missing CIS or E-field data.

To create time-series plots several programs developed by T.Johansson and S.Figueiredo

were used. First the program despins the E- and B-fields data and changes the coordinate system from GSE to MEE. The potential along the satellites orbit is calculated by integrating the E-field. Then the program uses the B-field data of a 3 hours time interval, approximates it with a suitable polynomial and then subtracting the background field. Plots were produced containing PEACE data, spacecraft potential, potential, E-field, B-field, particle data, particle flux and field-aligned currents. A new program calculated the integrated particle flux, by adding all the previous points in the plot to see if there was more negative or positive particle flux all together. At last additional events from Kullen were included in the work to get a more extensive material to analyze. These events were taken both from the strong E-field list and another list from Johansson with weaker E-field peaks. The analysis consists of two parts. First analyze the plot with attention to some questions. Is the particle flux direction sunward or anti-sunward and have the location on the oval any significance? In what extent is the density important for the particle flux peaks? How much contribute the particle flux from a strong e-field peak to the total particle flux and do the arcs contribute to sunward or anti-sunward particle flux? The second part of the analysis was to compare the results with the theories.

6.2 Plot descriptions

We have produced five different plots that have been used in the analysis. All of them start with PEACE data on the top. The PEACE data shows the electron energy and it is easy to localize the position of the satellite with respect to large-scale plasma boundaries. The areas with many particles, the green areas on the plot, correspond to the auroral oval and the empty areas the polar cap or just outside the oval.

Figure 14, shows the downloaded spacecraft potential from which we calculated the density, the plasma potential(V), and the E-field and B-field in x- and y-direction. The plasma potential(V) is calculated from the E -field:

$$V = -\int E dx \tag{6.1}$$

We define $dx = vdt$ where v is the velocity of the spacecraft. The E-field and B-field data are shown and on the same plot there is also a blue line showing the B-field after the background B-field is subtracted. The data is presented in the MEE-coordinate system where the z-axis is directed in the same direction as the magnetic field, the y-axis towards the equator and the x-axis points eastward.

Figure 15 shows the ion density and the particle flux. The density is both taken from CIS data and calculated from the measured spacecraft potential. At the first density plot is the red line O^+, the black line H^+ and the green line density from the spacecraft potential. On the second plot is the redline corresponding to He^2, the black to He^1. The blue line shows all previous particle types added together which correspond to the total amount of particles. The green line is as in the previous plot the density calculated from the spacecraft potential. The particle flux is calculated from:

$$particleflux = n \cdot v = n \cdot \frac{E \times B}{B^2} \tag{6.2}$$

The blue line is the particle flux, using CIS data for the density and the green line shows the particle flux calculated with the density from spacecraft potential.

In Figure 16 once again the potential and the electric field are shown. The electric field is now shown in a different coordinate system since a minimum variance analysis is made. An MVA analysis gives the direction of the strongest E-field gradient. The new direction is proportional and tangential to the sheet orthogonal to the strongest E-field gradient calculated in the minimum variance steepest gradient. E-normal shows the E-field proportional to this sheet and E-tangential, the E-field in the same plane as the sheet. The last plot shows how much the sheet is rotated from the MEE-coordinate system.

Figure 17 shows, apart from the PEACE data, the potential, E-normal, B-normal, and density, also field-aligned currents and the particle flux in tangential direction. The field-aligned currents are calculated from the magnetic field without background field. It is coloured in blue for positive values and red for the negative values of the current. The blue curve means that we have upward streaming ions and downward streaming electrons. Upward mean away from the Earth and downward towards the Earth. The blue current is called primary current, it consists of accelerated electrons that cause the aurora. Further on we will refer to the upward current as primary current. The red curve describes upward streaming electrons and downward streaming ions. This current is called return current. The particle flux-tangential is calculated in the same way as the particle flux on previous plots but the in the new coordinate system after the MVA analysis.

Figure 18 contains partly the same particle flux as on Figure 15 but this time coloured to get a overview if there is more positive or negative particle flux. For the most of the events, we have chosen to plot the particle flux calculated from the spacecraft potential density. CIS only detects particles above a certain energy and therefore is the density calculated from spacecraft potential believed to be more correct. The problem is that during some periods is the instrument that measure spacecraft potential used for something else. A current is put on to get an artificial scp. During these periods the density from scp cannot be used to calculate the density and for these periods CIS more reliable. The last two plots here show the integration of the particle flux. We always start from the low density region outside the oval, which is almost always the polar cap, and then add every point to the total. This makes it easier to see how large the contribution is from the particle flux peaks caused by the strong E-field peaks. The integrated particle flux is calculated according to the formula:

$$particleflux = \int v \cdot ndx \tag{6.3}$$

Figure 19 is a overview plot created to show all parameters important for our analysis on one plot. It does not contain anything new in addition to the other plots. It displays the PEACE data, and the sheet orientation. The E-field in x- and y-direction is showed on the same plot. On the third plot, the particle flux curve is coloured in red for positive values and blue for negative ones. There are also the curves with integrated particle flux as in

Figure 18. The last plot shows the density. The black line is the density calculated from CIS data and the green line show the density calculated from the spacecraft potential. The dotted black line shows only proton density.

6.3 Analysis method

If we look at the electric field on Figure 14. We can both find bipolar and monopolar peaks. Bipolar peaks consist of one negative peak and one positive peak, one of them following the other. Monopolar peaks are either a single positive or negative peak. At a bipolar E-field peak, is a sign change of direction of the electric field. In the point where the fields converge we get a primary current, (blue on the field-aligned current (FAC) plot). As a discrete arc is caused by precipitating electrons, where there is a primary current, we might also find a discrete arc. A additional condition for a discrete arc is that the potential drop is large enough, at least 1kV. This is required for the electrons to be accelerated to high energies enough to cause aurora. The discrete arc is located in the boundary between the converging fields. The opposite case, when the electric fields diverge, we get a return current and no aurora.

Sometimes we have an even distribution of the particle flux and the positive and negative particle flux peak have equal size. In some cases is either the negative or the positive peak larger. We want to examine whether the asymmetric particle flux distribution, leading to a net particle flux, depends on the E-field or density structure. When using the words symmetric and asymmetric related to peaks, symmetric means a bipolar particle flux peak where the positive and negative has an almost equal amplitude. Asymmetric means that one of the peaks has larger amplitude or in the extreme case one of the peaks is so small that it can be considered as a monopeak.

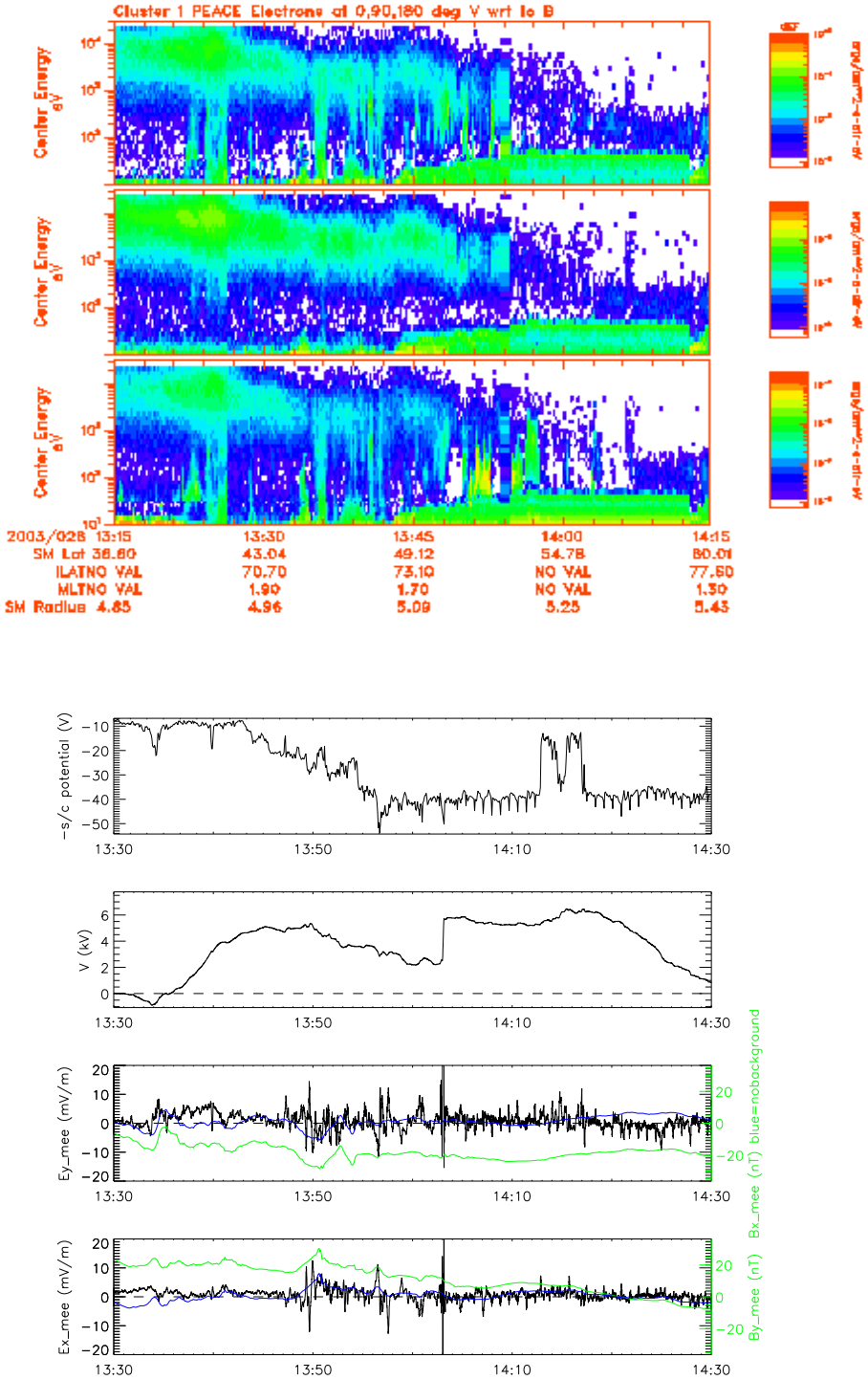

Figure 6.1: *plot_eb*

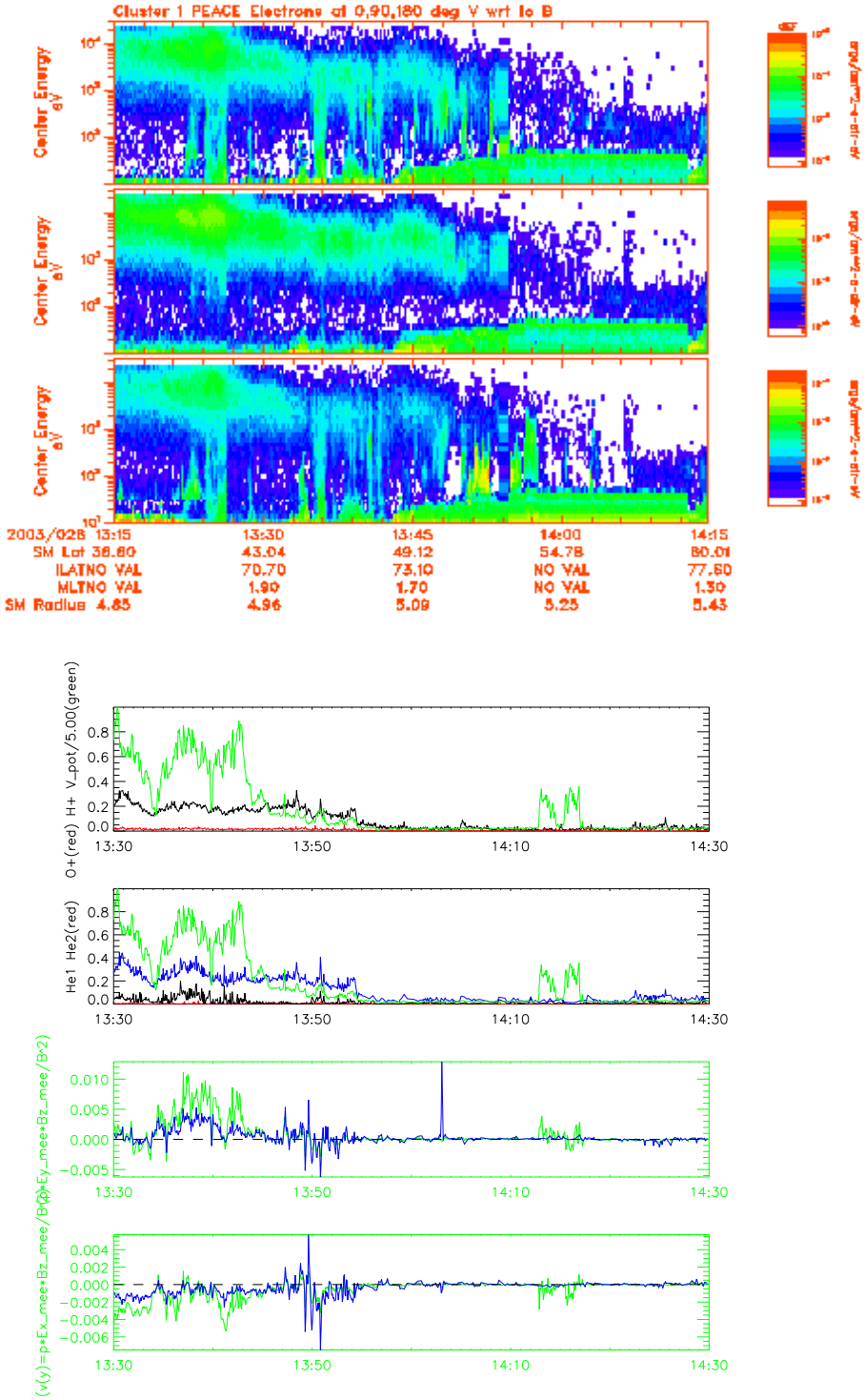

Figure 6.2: *plot_flux*

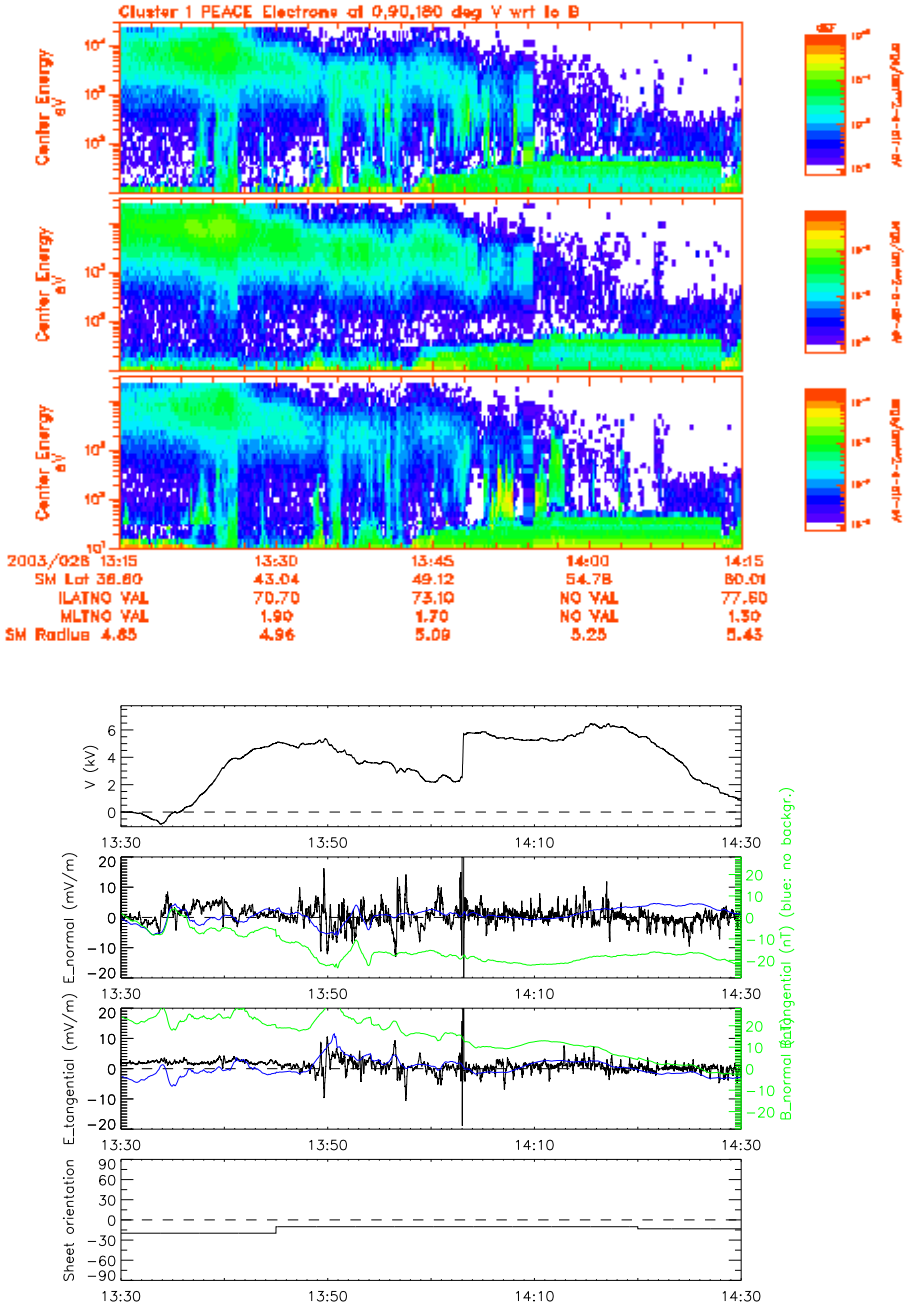

Figure 6.3: *plot_eb_mva*

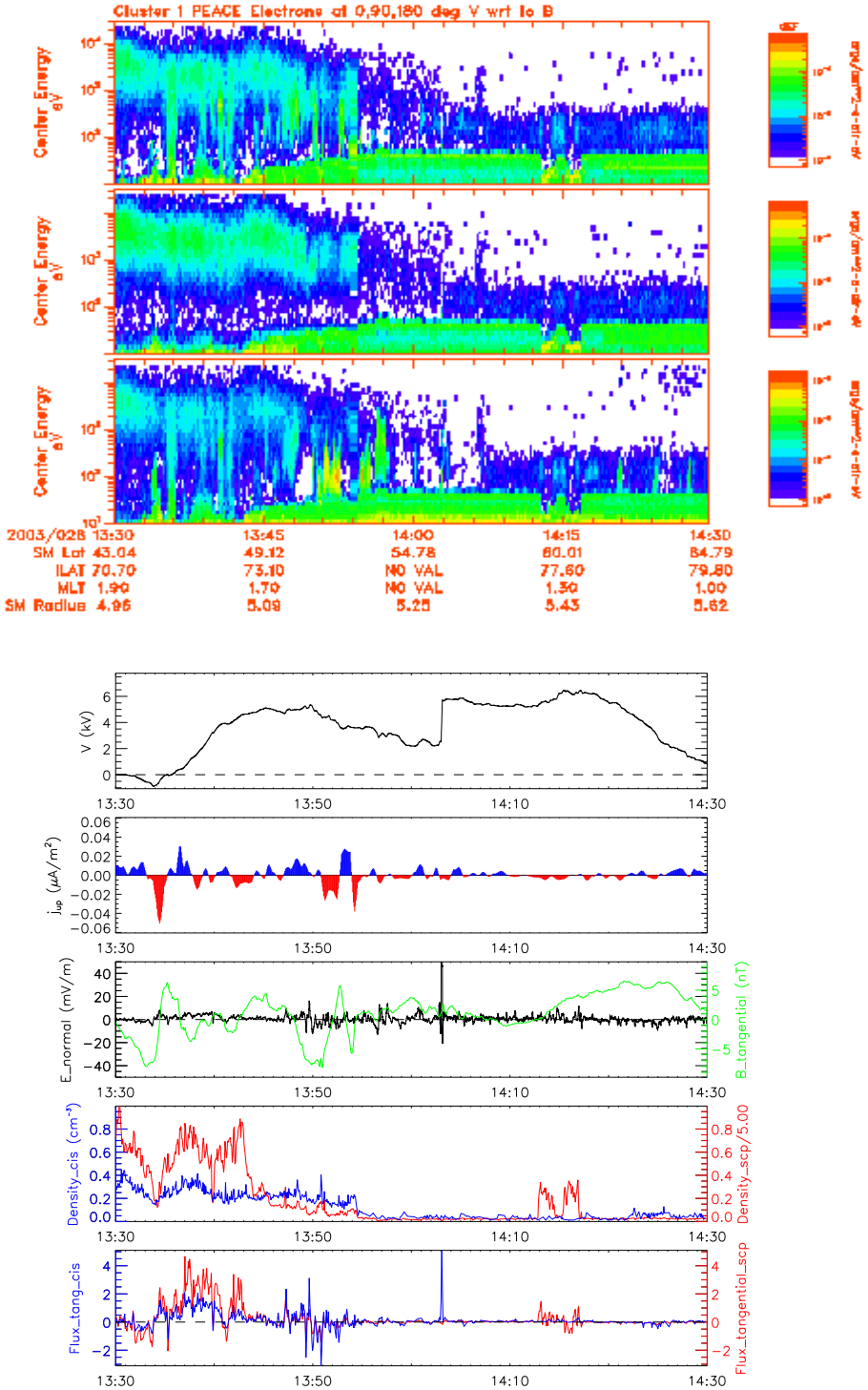

Figure 6.4: *plot_j_mva*

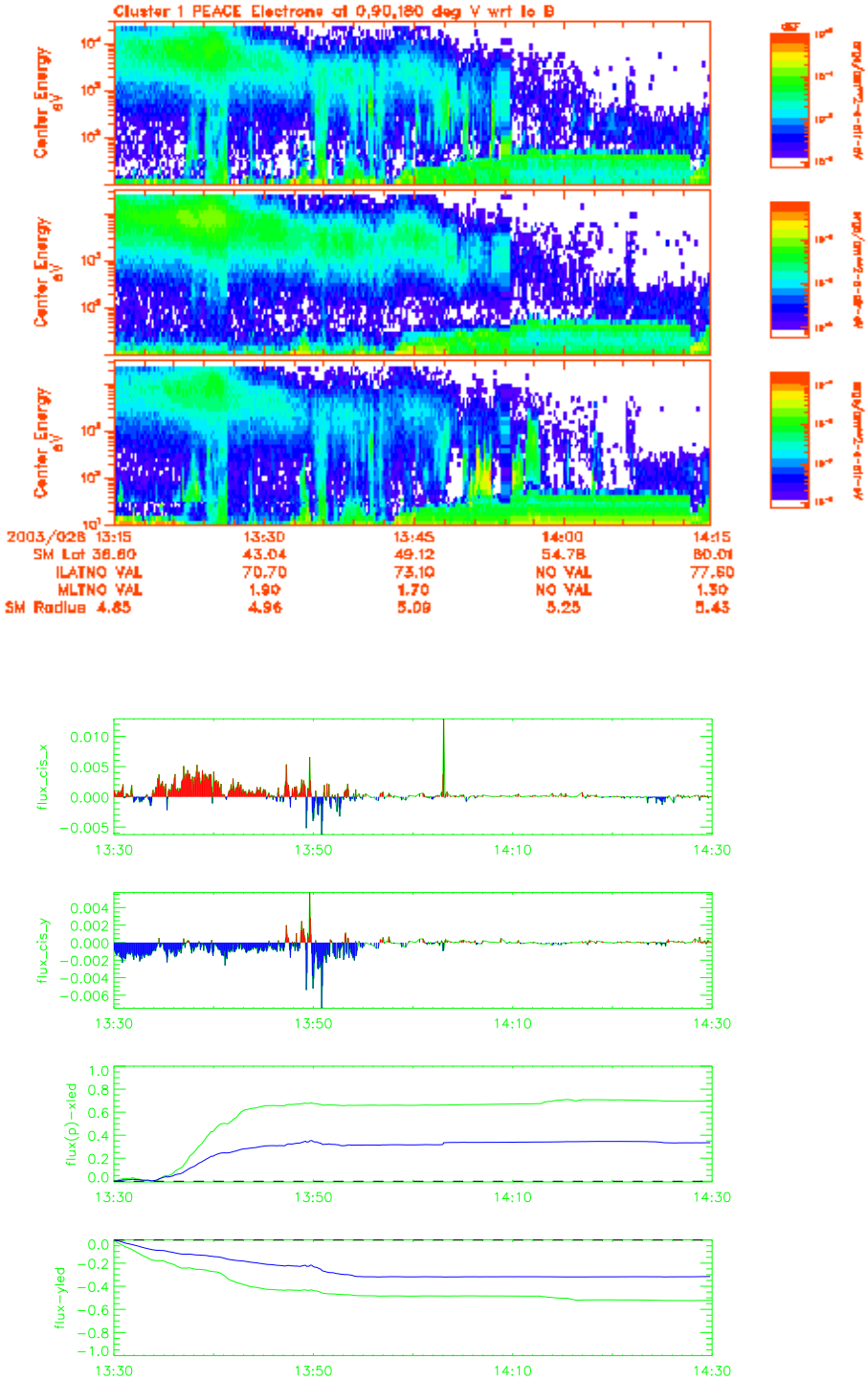

Figure 6.5: *plot_flux2*

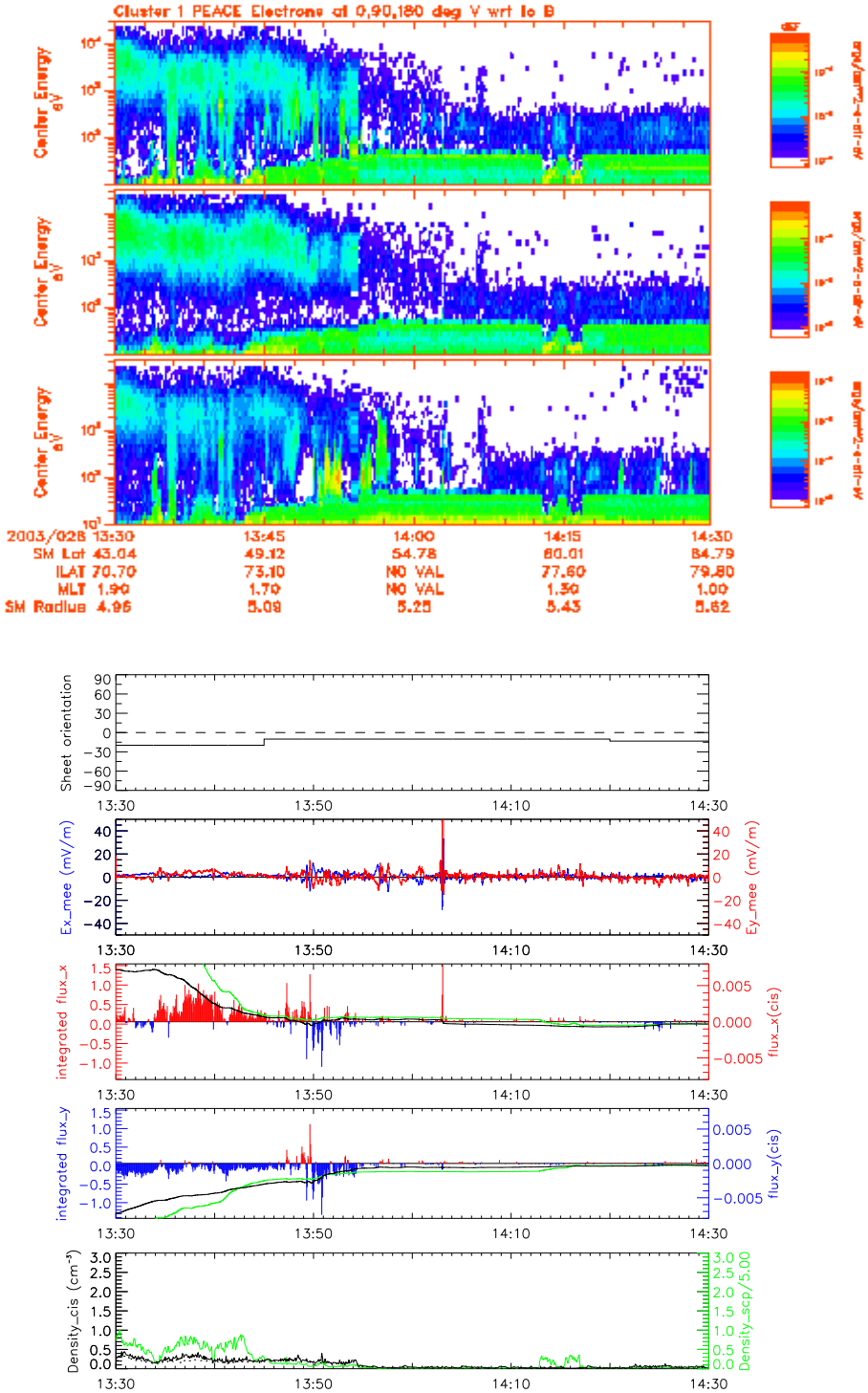

Figure 6.6: *plot_overview*

Chapter 7

Results

In this study 33 events, containing large E-field peaks, are examined in detail. Three of them are transpolar arcs. The other 30 are located on the auroral oval. 18 on the dusk side, 9 on the dawn side and 3 are located in the midnight sector (see Figure 20). The midnight sector is here defined as the region between 23.00 and 01.00 MLT. (Images of the auroral zone are often displayed with the coordinates corrected geomagnetic latitude (CGlat) and magnetic local time (MLT)).

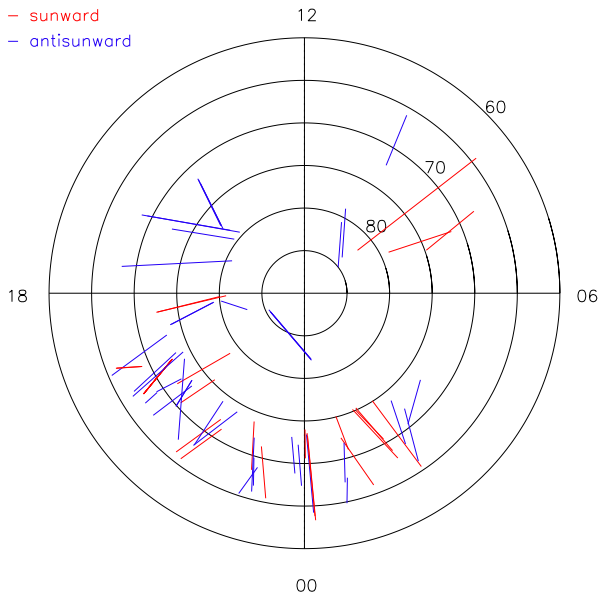

Figure 7.1: The satellite paths, from all events, traced along the B-field lines down to the Earth. Red line mean that a sunward netto particle flux is measured by the satellite, blue means that a anti-sunward particle flux is measured.

7.1 Sunward and anti-sunward particle flux

On Figure 18 and 19 it is possible to see the direction of the total particle flux, shown on the overview plots (see Appendix C). The total particle flux is displayed on the plot were the integrated particle flux curve is shown. We have looked at the entire interval displayed at the plots, not only at the region of the strong E-field peak. As shown in Table 1, we find that of the 33 events, 14 have sunward particle flux and 11 an anti-sunward particle flux. At the dawnside, 6 of 9 are sunward and 2 are anti-sunward. At the duskside, only 7 of totally 18 events have anti-sunward particle flux. The number of events with sunward particle flux is on the dusk side 6. Besides is the number of events with sunward and anti-sunward particle flux is quite even distributed on the dusk and dawnside. We also have 3 events in the midnight sector. The remaining cases are unclear. For these events it is difficult to decide what particle flux direction would be expected from theory. The reason for this is that this region is located near the boundary between the dusk and dawn convection cells, thus it looks different from time to time. A location can at one moment be on the dusk cell and another moment be on the dawn cell, of the large-scale two cell convection pattern in Figure 7, shows a statistical study of the ionospheric convection pattern for different direction of the IMF. For a few events the particle flux direction changes between the different satellites due to large time lag between them i.e., the magnetosphere has slightly changed convection pattern. If density measurements by CIS and the density calculated from the spacecraft potential of one satellite differ, one of them measures something wrong. CIS only detects particles above a certain energy so usually is the spacecraft potential more correct. During some periods a current is put on to get an artificial scp. Then the density from scp cannot be used and CIS is more reliable. If different satellites show different results, this means the structures have changed in time between the passings of the satellites. These events are very interesting since we can follow the time evaluation of the E-field structures but they are also more difficult to analyze.

	Oval		TPA		
	Duskside	Dawnside	Dayside	Nightside	
sunward	7	6	0	1	14
anti-sunward	7	2	0	2	11
unclear cases	4	1	0	0	5

Table 7.1: The total particle flux

7.2 Connection between particle flux direction and IMF direction

We compare the particle flux direction with the IMF during and up to two hours before the satellite and arc conjunction. Excluding the transpolar arcs, there are 13 events with sunward particle flux. Of them, all except one appear during southward IMF or shortly after a turn to northward IMF. The same comparison for the events with anti-sunward particle flux give more complicated results. Of 9 events 5 occur during northward IMF, or

shortly after a turn. 3 occur after or during a period of weakly southward IMF and one after southward IMF that turned toward northward IMF.

7.3 The E-field peak's influence on the background particle flux

To see how much influence the E-peaks have on the background particle flux, the curve showing the integrated particle flux is studied. The peaks contribute in most cases very little to the total plasma flow. The most common (31 of the peaks) is that just a little jump is seen on the curve. Of the remaining, 6 peaks do no contribute at all, 7 contribute a little more, but not so much that a single peak has a major importance for in what direction the background particle flux will be. Only 6 of the 50 peaks are of significant importance for the total particle flux. These peaks do not cause a larger particle flux than the peaks of the other events, but the background particle flux is so low, that the peak contribution matters. Example of events where the peak contribution is important, are May 1 (Cluster 1), 2003 and May 3 (Cluster 1), 2003, and April 15, 2002 (Cluster 3 och 4). See Appendix C.

7.4 The direction of the particle flux peak

We have looked closer at the relation between the direction of the particle flux peaks and background particle flux and if the particle flux peaks contribute to sunward or anti-sunward particle flux. We exclude the transpolar arcs and the three events in the midnight sector. We also have some unclear cases that are excluded. All bipolar peaks obviously have one peak in the same direction and one in the opposite direction from the direction of the background particle flux. Sometimes the particle flux in the bipolar peak cancel each other and the netto particle flux is zero. If one of the peaks in the bipolar peak is larger then the other we get a netto particle flux from the peak that contribute to particle flux in one direction. Altogether 25 peaks are analyzed and the result is presented in Table 2 and Table 3. The particle flux direction is equal to the background particle flux for 15 of the peaks. The remaining have particle flux in the opposite direction to the background particle flux. At the duskside, almost as many peaks contribute to particle flux in the opposite direction as in the same direction as the background particle flux. At the dawnside there are more peaks with particle flux in the same direction than peaks with particle flux in the opposite direction as the background particle flux. If only looking at if the peak contributes to sunward or anti-sunward particle flux, 14 contribute to sunward and 11 to anti-sunward particle flux. At the dawnside more peaks contribute to sunward particle flux.

	Duskside	Dawnside	Total
Sunward	6	8	14
Anti-sunward	9	2	11

Table 7.2: Flux contribution from the peaks.

	Duskside	Dawnside	Total
Same direction as background particle flux	8	7	15
Opposite direction compared to background particle flux	7	3	10

Table 7.3: Flux contribution from the peaks.

7.5 The density's influence on the particle flux

Here we analyze the influence of density on the particle flux peaks. For our events we can discern four different cases shown in Figure 21. The first is that we have a particle flux peak, symmetric or asymmetric that follows the E-field, while the density is equal on both sides of the boundary.

In the second situation we have a monopolar E-field peak and the density gradient causes an even stronger monopeak. In the third case we have an asymmetric peak but the density weakens this asymmetry. The last case is a symmetric bipolar peak, but because of higher density on one side the particle flux peak becomes larger (in some cases even a mono peak).

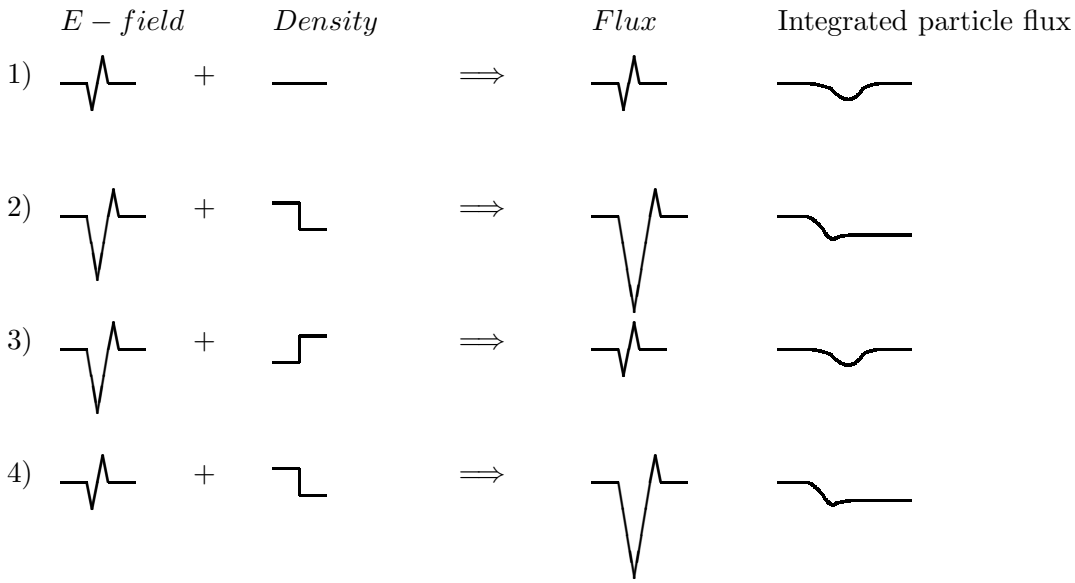

Figure 7.2: The four cases in which the densities influence on the particle flux is divided.

The first row on the table distinguishes the arcs on the oval from the transpolar arcs. The second row tells where the event is located. Duskside, dawnside or in the midnight area for the arcs on the oval and day or nightside for the transpolar arc. Observe that despite using the word arc, not all E-field peaks from our events cause arcs. If the E-field diverges there is a return current instead and no auroral arc, and often the potential drop is too small to lead to an electron acceleration high enough to cause aurora, even if the E-field is converging.

In some cases an event has more than one E-field peak. so there can be more than one peak from each event in the study. Only data from one satellite on each event is taken to avoid to counting the same peak twice. The data is not as structured as assumed in theory. It is sometimes nearly chaotic. This makes it difficult to analyze. Totally 50 peaks

have been examined. More than half of them can be categorized as case 1 in Figure 21. For these there are no density changes and the particle flux varies as the E-field. For the remaining a more even distribution is seen. There exist both monopolar and bipolar peaks. 22 of the peaks are from events on the duskside. On the dawnside are 11 peaks and 11 in the midnight sector. As many as 16 of the peaks categorized as alternative 1 are located on the duskside.

	Oval			TPA		
	Duskside	Dawnside	Midnight	Nightside	Dayside	
1)	16	5	5	3	0	29
2)	2	1	3	1	0	7
3)	2	2	2	2	0	8
4)	2	3	1	0	0	6

Table 7.4: The density's influence on the particle flux peaks

7.6 The transpolar arcs

Only three transpolar arcs are examined in the study. All of them are located at the duskside and at the nightside. According to Kullen et al.'s (2002) classification of polar arcs, the arc appearing at May 19, 2002 is an oval-aligned arc. It is formed at the dusk side and stays there until it disappears. For the December 19, 2002 arc event, no global auroral images are available. From the PEACE data it is possible to see that the arc is located at high latitude on the dusk side, not too close to the oval boundaries. The arc on July 26, 2003 is a moving arc moving from dusk to the center of polar cap before it fades out on the polar images.

At the plots, the E-field is weak across the entire transpolar arc. We can only detect one or a few strong E-field peaks. The transpolar arcs seem to consist of mainly diffuse aurora with a few discrete arcs.

At the conjunction between the Cluster satellites and the arc the particle flux is directed in anti-sunward direction for two events and in sunward direction for one of the events.

7.7 The size of the potential drop and direction of the field-aligned current

The E-field peaks are connected to auroral arcs if the electrons are accelerated downwards (primary current) and the potential drop is at least 1kV. Table 5 shows how many of the E-field peaks cause primary currents, and for how many the potential drop is high enough. Of the 50 examined E-field peaks, 21 are causing discrete auroral arcs. Most of the peaks have a high enough potential drop but approximately half of the currents are return currents that do not cause auroral arcs. Unclear direction of current means that the peak is exactly where there is sign change of the current and it is difficult to decide the direction of the current.

	Return current	Primary current	Unclear direction of current
Potential drop $<$ 1kV	7	3	0
Potential drop $\geq$ 1kV	16	21	3

Table 7.5: Number of E-field peaks causing auroral arcs.

Chapter 8

Discussion

According to previous studies of the ionospheric convection pattern, the particle flux is sunward along the auroral oval. The flow in the plasma sheet is sunward since the closed magnetic flux tubes move sunward in the tail. (see Figure 3). As the closed magnetic field lines maps to the oval, the particle flux on the oval is sunward. Our results show sunward particle flux for 14 of the 30 events on the auroral oval and anti-sunward particle flux for 11 events. This is not expected. The comparison with the IMF direction shows that during southward IMF 11 of 15 events have sunward particle flux and agree with the theory of sunward flow at the auroral oval. For northward IMF the results are more complicated to explain. Of 6 events with northward IMF 5 have anti-sunward particle flux. There may be several explanations for the anti-sunward particle flux: Since the arcs are in most cases located in the boundary region between polar cap and the auroral oval, the field lines may map to the plasma sheet boundary layer (PSBL) instead of mapping to the plasma sheet. On one side of this boundary is the plasma sheet with sunward particle flux. On the other side of the boundary are open field lines on anti-sunward particle flux. The boundary may be disordered and if the arcs end up on the side with open field lines we get an anti-sunward particle flux. Another possible reason can be that the field lines maps to the low-latitude boundary layer (LLBL) where the particle flux is always anti-sunward. In that case the LLBL should extend to unusually high latitudes.

Concerning the E-field peak influence on the total particle flux of the examined data period, we find that they have in most cases a negligible influence. Only when the background particle flux has very low values the particle flux connected to the strong E-field peaks can be decisive for the direction and strength of the netto particle flux. The important contribution is in other words not caused by a extra strong peak but a very weak background particle flux.

In a theory by Haerendel (1992), it is proposed that discrete auroral arcs serve as 'pressure valves' in the magnetospheric energy cycle. This would mean that the particle flux contribution from the discrete arcs are large and in sunward direction. Since our results show that in most cases the particle flux contribution from discrete arcs is small, this disagrees with the theory. Most of all the many detected anti-sunward events are in contradiction to Haerendel's theory. We expect the peaks to contribute to a sunward particle flux, but this is not seen in the data. Only 14 of 25 peaks contribute to sunward particle flux. Instead of increasing the sunward convection, these E-field peaks diminish the number of particles that move sunward.

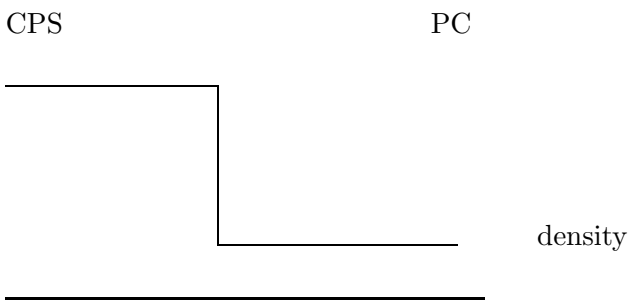

Figure 8.1: The central plasma sheet and polar cap with a steep density gradient between.

According to the idea about the density influence on the particle flux we have started from two assumptions. The first is that the peaks at the plasma boundaries would be bipolar. The second assumption is that the arc is located at a steep density gradient. This gradient is expected to be found at the boundary between the low density polar cap and the auroral oval with high density. (See Figure 22).

Many of our peaks in our study deviate from this picture, especially concerning the density change. Since there is no change of the density in most of the cases, the particle flux is mainly controlled by the E-field. This theory requires the E-field peaks to be located at the boundaries between the oval and the polar cap where we expect to find such a density gradient. These results indicate that density gradients play only a minor role for the particle flux strength and direction near E-field peaks. Also, in most cases the E-field peaks at density gradients in the PSBL are already monopolar (Johansson et al., 2005)

Why are the assumed conditions not present? Are the peaks located too far from the boundaries? From the density plots it is easy to establish that there is no sharp boundary between the oval and polar cap. The density is high at the oval and very low in polar cap. What we did not expect was that between these regions there is a transition region where the density varies very quickly, up and down. (See Figure 23). Thus, the condition for the density change is hard to fulfil. There are a few cases, for example April 15, 2002, where we have the perfect conditions. At 21:54 UT there is a strong bipolar peak. A density maximum appears when the density has a strong westward component. This leads to a net plasma transport. Here the theory about the density's influence on the particle flux is confirmed. The problem in this case is that the net particle flux is anti-sunward, and according to Haerendel's theory, in the wrong direction. The conclusion is that despite that there are cases where the assumptions are confirmed, it does not seem like discrete arcs have an important function in transporting plasma from the magnetosphere tail to the dayside.

A similar finding about strong anti-sunward particle flux is found for the nightside part of transpolar arcs. A recent study shows that the nightside extension of the transpolar arcs contains anti-sunward particle flux, which is very surprising. Liou et al.,(2005), proposed that the nightside part is mainly on field lines mapping to the low latitude boundary layer

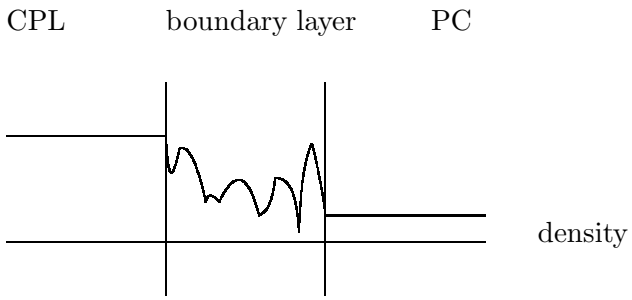

Figure 8.2: The central plasma sheet (CPS) and polar cap (PC), with a boundary layer with varying density, between.

where anti-sunward particle flux prevails. In our study we have similar results for 2 of 3 arcs. All three transpolar arcs are located on the nightside and on the duskside. Two of them confirm the observations by Liou et al., (2005), since the particle flux is anti-sunward. However one of the transpolar arcs has sunward particle flux. We can not make any conclusions of the issue since we have too few cases to analyze.

Almost half of the E-field peaks in this study cause auroral arcs. In most cases the electrons are accelerated to energies exceeding 1keV. We have as many cases where the E-field peak lies in the return current region as in the primary current region and that is the reason why only half of the E-field peaks cause arcs.

Chapter 9

Summary

Strong E-fields peaks indicate the presence of B-field parallel E-fields. The parallel E-field accelerate electrons. The high energetic electrons cause discrete auroral arcs in the ionosphere if the potential drop is large enough. We have studied data from the Cluster satellites to get an image of how the plasma flux above the ionosphere is related to discrete arcs. In this study, 33 events with strong E-field peaks 4-7 R_E above the high-latitude ionosphere have been analyzed. Plots have been produced of the E-field, B-field, density, particle flux and field-aligned currents.

- 30 of the events are located at the auroral oval and 3 are transpolar arcs.
- The events on the dawnside have more often sunward particle flux. On the duskside there are almost as many anti-sunward particle flux cases as sunward particle flux cases.
- The particle flux direction is compared to the direction of IMF. Of the events with sunward particle flux, all except one appear during southward directed IMF or shortly after a turn from southward directed IMF to northward IMF. The events with anti-sunward direction occur both during southward and northward directed IMF.
- In most cases, the particle flux peaks do, contribute very little to the netto particle flux. In the few cases where the particle flux peaks are of significant importance, the background particle flux is very weak.
- The particle flux peaks contribute to anti-sunward particle flux just as often as they contribute to sunward particle flux. Neither do we see any tendency for the particle flux peak to be more often directed in the same or opposite direction compared to the direction of the surrounding particle flux. This results cannot confirm the theory that convection related auroral arcs play an important role for the sunward convection along the auroral oval (Haerendel, 1992).
- For more than half of the examined E-field peaks there is no density change and the particle flux varies as the E-field.
- The E-field peaks appear typically in the boundary region between central plasma sheet and polar cap, not at the polar cap boundary.

- A relative new result show that the nightside extension of the transpolar arcs is on open field lines as the particle flux is anti-sunward (Liou et al, 2005). In our study we have similar results for 2 of 3 transpolar arcs which strengthens the observations by Liou et al.,(2005).
- About half of the E-field peaks in this study are connected to downward accelerated electrons and have a potential drop high enough to cause auroral arcs.

Many of the results are difficult to interpret and there are still many question marks concerning auroral arcs. It is possible to find events that confirm Haerendel's idea about discrete auroral arcs serving as magnetospheric pressure valves. However, our results indicate that this is not typically the case. In most cases the plasma flux along arcs in the return region is too weak to contribute significantly to the plasma convection and/or it is often directed in anti-sunward direction. Further examination of the subject is necessary and interesting.

Acknowledgements

First and foremost, thanks to Anita Kullen, who has been a splendid supervisor. She has devoted several hours to explain the physics and helping me with trouble shooting. She has given me useful advices and guidance during the whole project, but still always made me feel free to take the final decisions. Also thanks to her little son, who has been very patient when I was "stealing" his mum away from him to talk about "boring science". I would like to express my gratitude to Stephan Buchert, for sharing his ideas on which this project is based on. I also would like to thank my office mate Andreas Ljungberg, for the good company, for helping me with LaTeX, for giving me tricky rebuses and for sharing my frustration behind the computers. Thanks to all the nice staff at IRF-U for making me enjoy my time here. Especially thanks to Bertil and Yuri for helping me out with the "computer stuff" and all fellow diploma workers for the nice lunches and coffee breaks. Last but not least, thanks to my mother for all advices and encouragement during the report writing and to Ida for doing the dishes with a smile on her face.

Bibliography

Axford, W.I., and C. O. Hines, A unifying theory of high-latitude geophysical phenomena and geomagneic storms, *Can. J. Phys.*, *39*, 1433, 1961.

Baumjohann, W., and R. A. Treumann, *Basic space plasma physics*, Imperial College Press, 1996.

Chang, S. -W. et al., A comparison of a model for the theta aurora with observations from Polar, Wind and SuperDARN, *J. Geophys. Res.*, *103*, 17:367, 1998.

Chen, F. F., *Plasma physics and controlled fusion, volume 1: Plasma physics*, 2nd edition, Plenum Press, 1984.

Crooker, N. U., Dayside merging and cusp geometry, *J. Geophys. Res.*, *84*, 951, 1979.

Dungey, J. W., Interplanetary magnetic field and the auroral zones, *Phys. Rev. Lett., 6*, 47, 1961.

Frank, L. A., and J. D. Craven, Imaging results from Dynamics Explorer 1, *Rev. Geophys.*, *26*, 249, 1988.

Frank, L. A., et al., The theta aurora, *J. Geophys. Res. 91*, 3177, 1986.

Haerendel, G., 'Disruption, ballooning or auroral avalanche - on the cause of substorms', in: *Proceedings of the First International Conference on Substorms, Kiruna, Sweden, 23-27 March*, 1992

Johansson, T, G. Marklund, T. Karlsson, S. Liléo, P.-A. Lindqvist, A.Fazakerley, and A. Marchaudon, On the profile of the high-altitude auroral electric field and its relation to plasma boundaries, JGR, in press, 2005.
Kelley, M. C., and R. A. Heelis, *Auroral plasma physics*, Academic Press Limited, 1989.

Kivelson, M. G., and C. T. Russel, *Introduction to Space Physics*, Cambridge University Press, 1995.

Kullen, A., M. Brittnacher, J. A. Cumnock, and L. G. Blomberg, Solar wind dependence of the occurence and motion of polar auroral arcs: A statistical study, *J.*

Geophys. Res., *107*, 1362, 2002.

Kullen, A., *Polar Auroral Arcs*, PhD thesis, Alfven laboratory, Division of plasma physics, Royal institute of technology, Stockholm.

Liou, K., J. M. Ruohoniemi, P. T. Newell, R. Greenwald, C.-I. Meng, and M. R. Hairston, Observations of ionospheric plasma flows within theta auroras, *J. Geophys. Res.*, *110*, A03303, 2005.

Lockwood, M., Solar wind magnetosphere coupling, *Technical report 97/53*, EISCAT Scientific Association, 1997.

Paschmann, G.,S. Haaland, and R. Treumann (Eds.), *Auroral plasma physics*, Kluwer Academic Publishers, 2003.

Sonnerup, D. P., Magnetopause reconnection rate, *J. Geophys. Res.*, *79*, 1546, 1974.

Weimer, D, Models of high-latitude electric potentials derived with a least error fit of spherical harmonic coefficients, *J. Geophys. Res.*, *100*, 19595, 1995.

Webbsites:

Polar UV imager home page: http://uvi.nsstc.nasa.gov/, 2006-06-12

Image homepage: http://pluto.space.swri.edu/IMAGE/, 2006-06-12

Cluster homepage: http://sci.esa.int/science-e/www/object/index.cfm?fobjectid=1984, 2006-06-12

Geophysical coordinate transformations,
http://www-ssc.igpp.ucla.edu/personnel/russell/papers/gct1.html/

Appendix A

Tables

All events

Date	Time interval C1	Time interval C3	Time interval C4
20020223	15:20-16:20	15:20-16:20	15:20-16:20
20020415	-	21:45-22:15	21:45-22:15
20020420	-	19:00-19:30	18:30-19:00
20020427	-	19:30-20:00	19:30-20:00
20020502	-	16:50-17:20	16:50-17:20
20020512	-	05:00-05:30	05:00-05:30
20020519	-	05:20-05:50	05:20-05:50
20020519	-	08:20-09:05	08:20-09:10
20021001	-	-	23:50-00:20
20021028	-	-	01:00-02:30
20021106	-	-	16:15-16:45
20021125	-	-	13:30-14:30
20021219	-	-	14:30-15:30
20030126	13:30-14:30	14:20-15:20	13:40-14:30
20030131	06:45-08:15	-	-
20030202	13:10-14:40	-	-
20030207	11:15-12:15	11:15-12:15	11:00-12:00
20030221	15:25-15:55	-	15:40-16:10
20030228	18:00-18:30	19:15-19:45	18:55-19:25
20030307	-	22:15-22:45	-
20030315	00:10-01:10	01:00-02:00	00:50-01:50
20030320	00:15-01:15	-	00:15-01:15
20030329	07:10-08:10	-	-
20030417	-	09:15-10:15	08:45-09:45
20030424	-	12:30-13:30	11:45-12:45
20030501	14:55-15:40	16:00-16:30	15:35-16:20
20030503	23:45-01:10	-	-
20030511	02:15-03:15	02:45-04:15	-
20030515	20:30-22:00	-	-
20030611	-	02:15-03:25	-
20030627	17:20-18:50	17:20-18:50	17:20-18:50
20030726	13:10-14:30	13:10-14:30	13:10-14:30
20030731	02:15-03:15	02:15-03:15	02:15-03:15

At some time intervals, the Cluster satellites turn on Aspoc. This generates an artificial spacecraft potential. During this time the measured spacecraft potential cannot be used for calculation of the plasma density. Instead the density measurements from CIS data are more reliable. The events where Aspoc is switched on are listed in the table below:

Date	Satellite	Comments
20020420	c3	
20020427	c3	after 19.42
20020519	c3, c4	
20030126	c3,c4	
20030202	c3, c4	
20030221	c4	
20030228	c3	
20030307	c3	
20030315	c3	
20030417	c3	
20030511	c3	
20030611	c3	after 02.38
20030627	c3	
20030726	c3, c4	

Appendix B

Images

For some of our events global auroral images exist, taken by the Wideband Imaging Camera (WIC) on the IMAGE satellite or by the UV Imager camera on the Polar satellite.

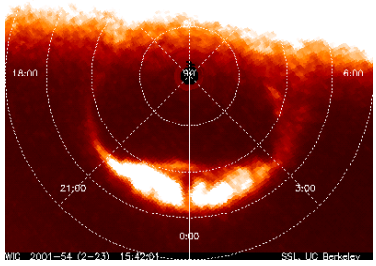

Figure B.1: 2001-02-23

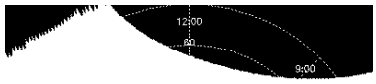

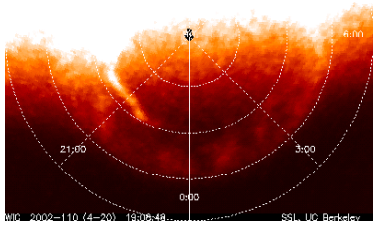

Figure B.2: 2002-04-20

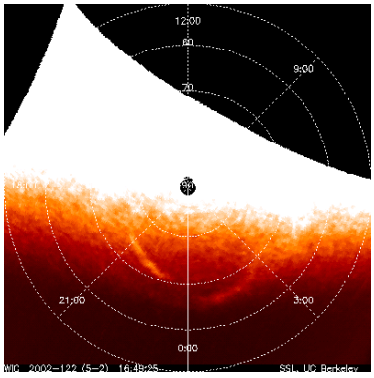

Figure B.3: 2002-05-02

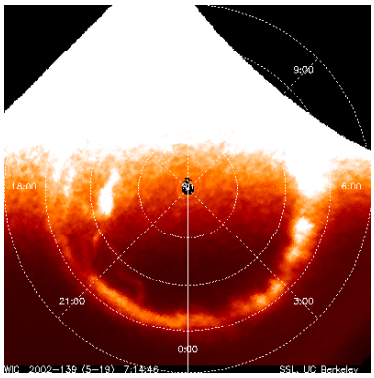

Figure B.4: 2002-05-19

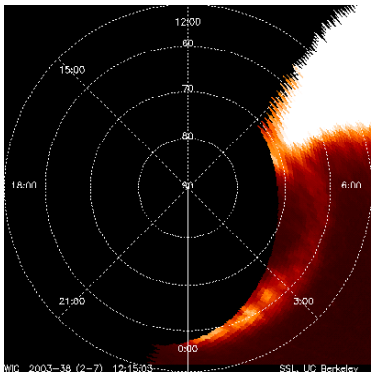

Figure B.5: 2003-02-07

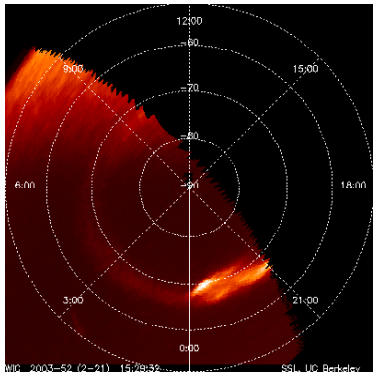

Figure B.6: 2003-02-21

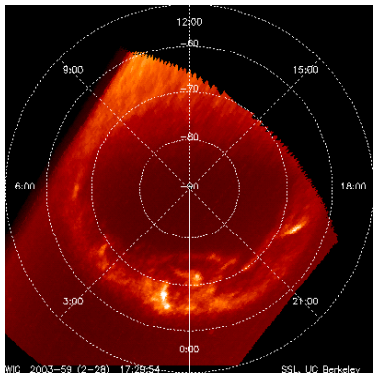

Figure B.7: 2003-02-28

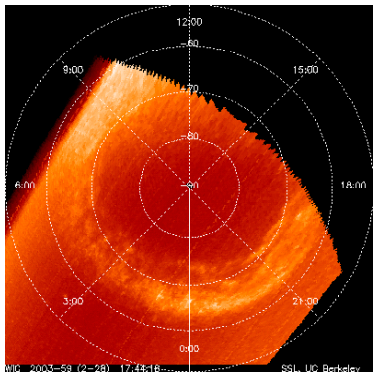

Figure B.8: 2003-02-28

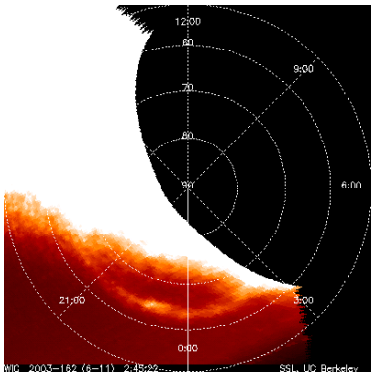

Figure B.9: 2003-06-11

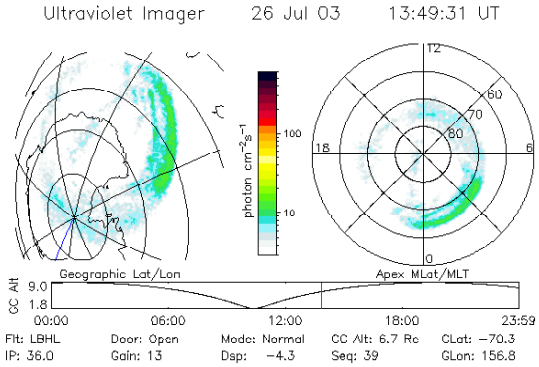

Figure B.10: 2003-07-26

Appendix C

Overview plots

Overview plots from all events used. Data from one satellite is presented irrespective of how many of the satellites that are used in the study. Plot from Cluster 1 2003-02-28 is missing because of wrong density data.

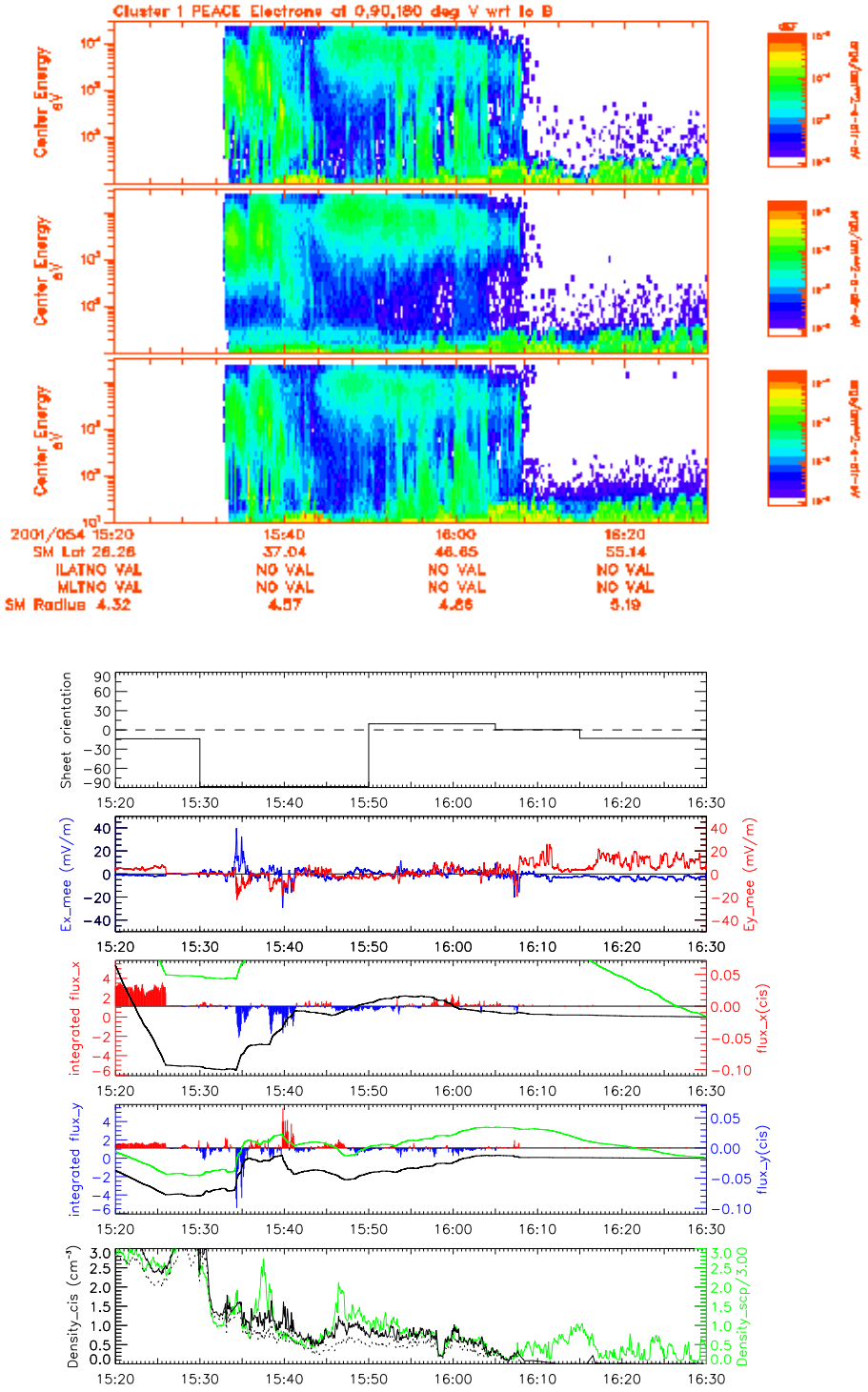

Figure C.1: 2001-02-23 Cluster 1

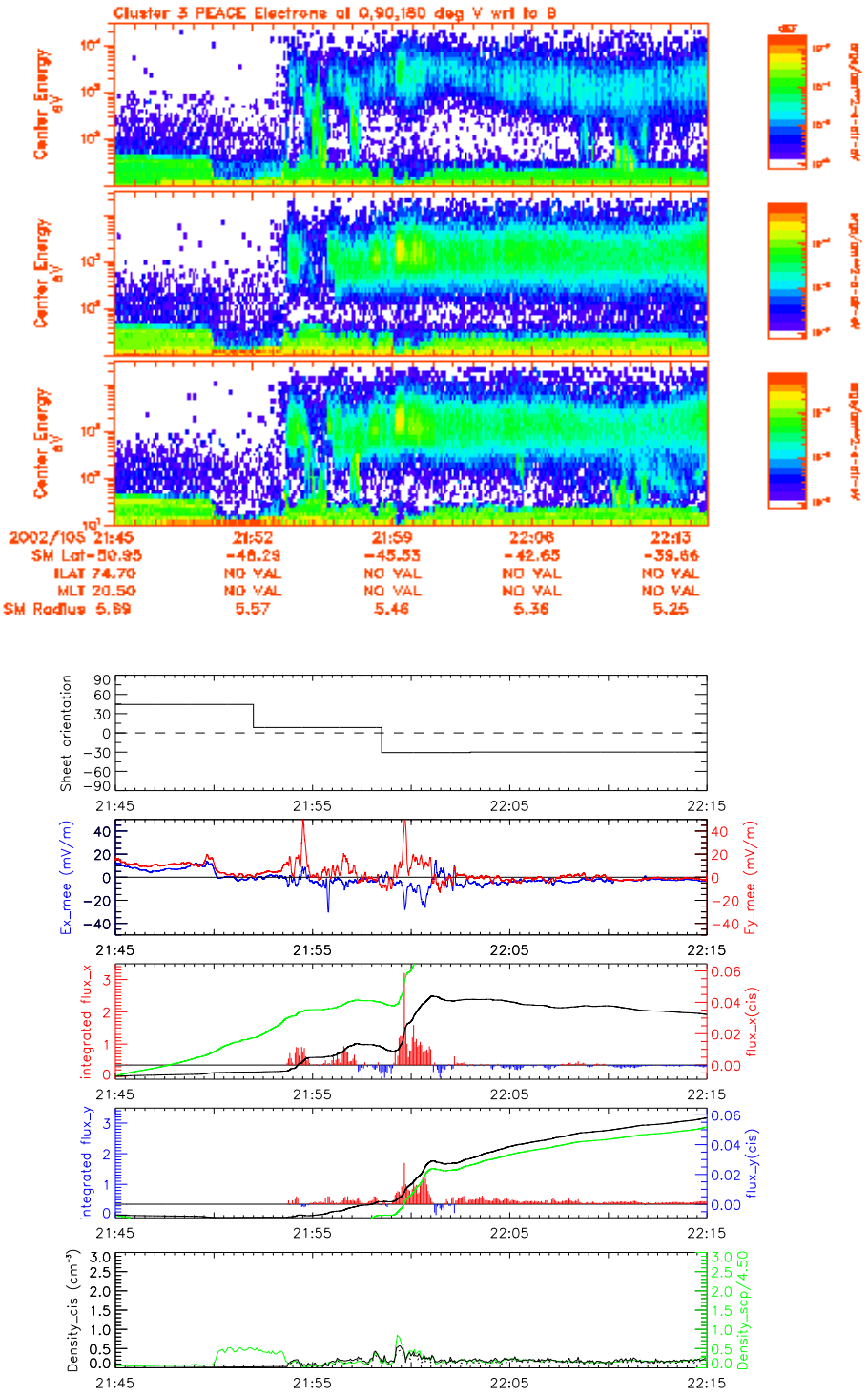

Figure C.2: 2002-04-15 Cluster 3

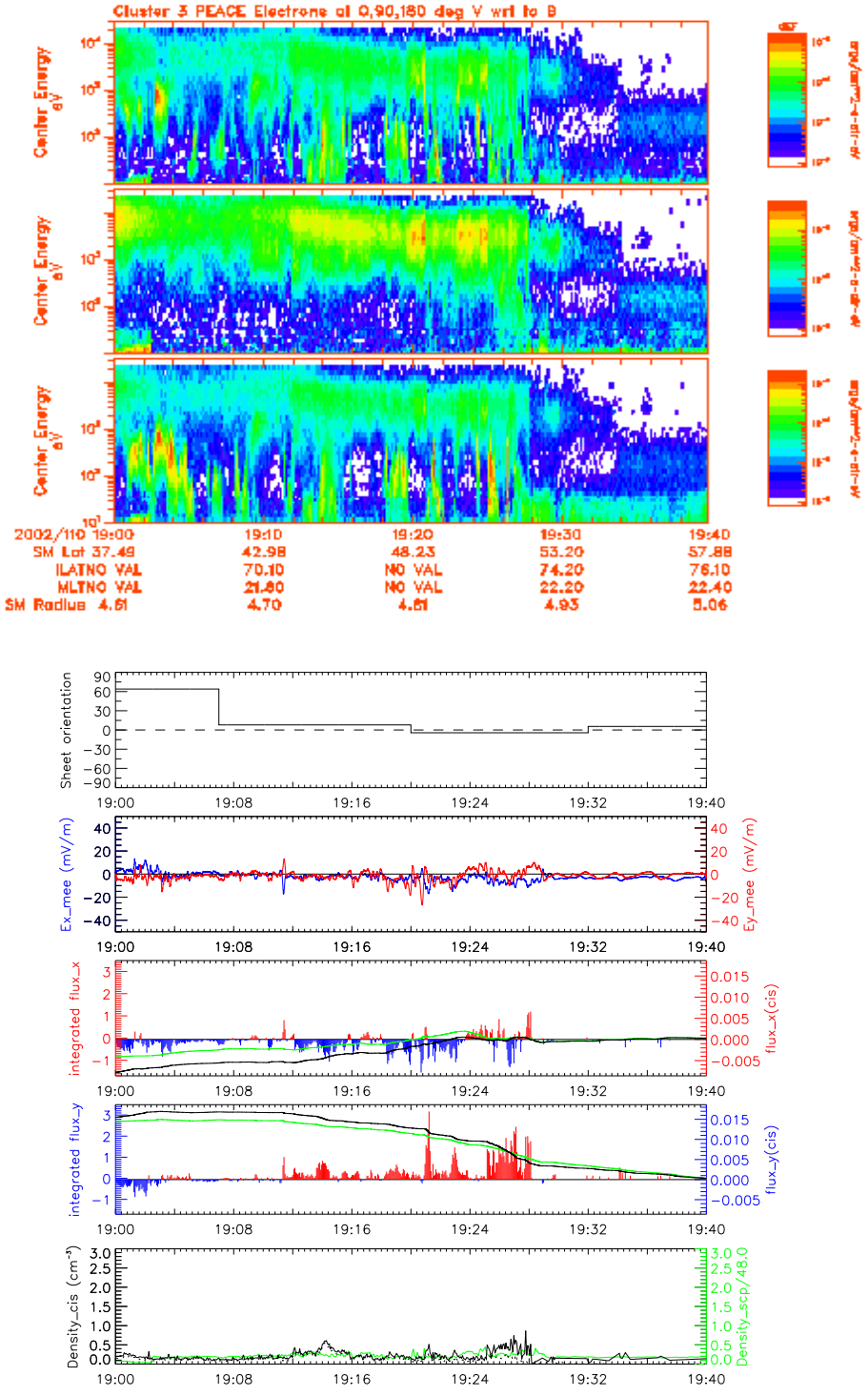

Figure C.3: 2002-04-20 Cluster 3

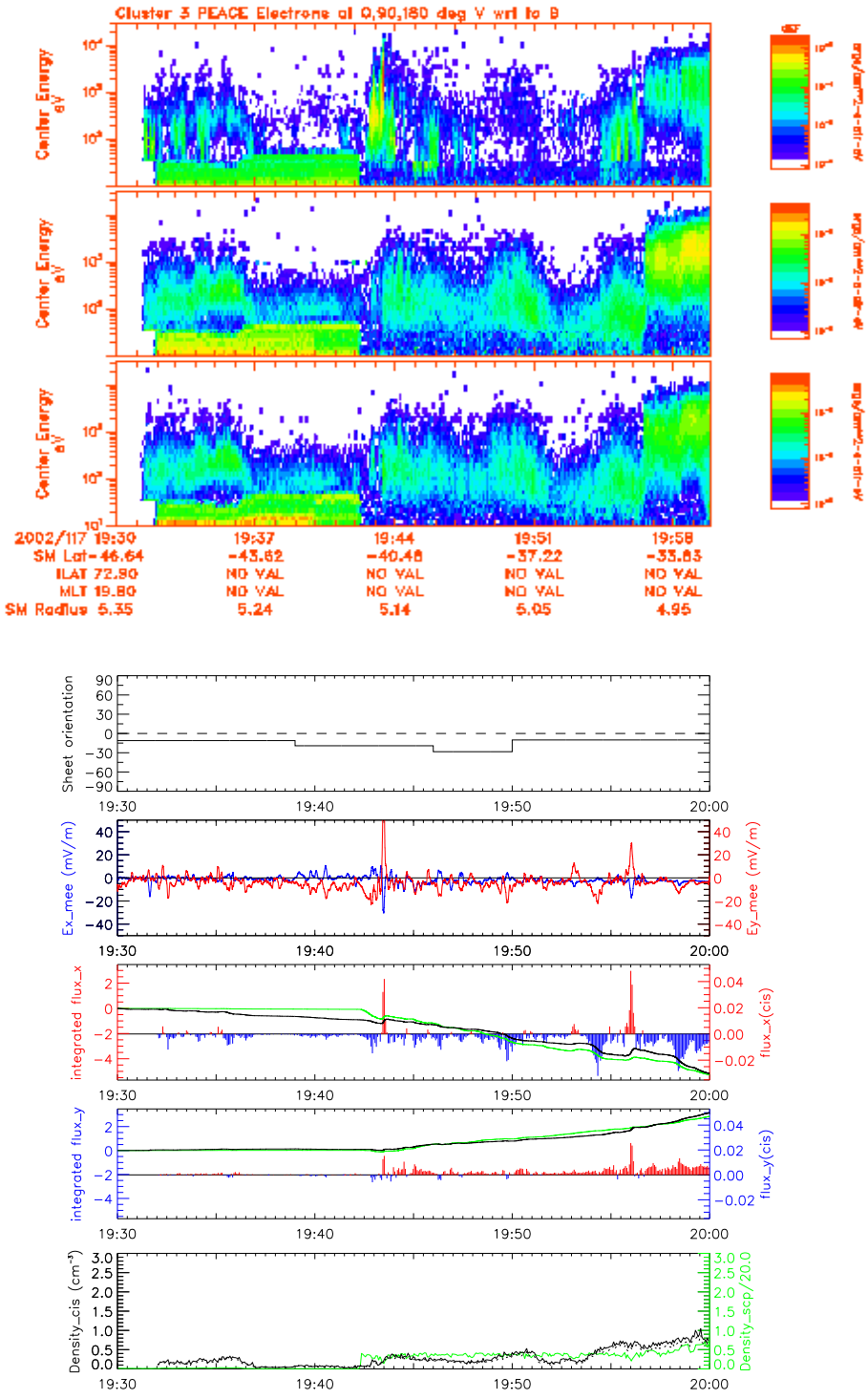

Figure C.4: 2002-04-27 Cluster 3

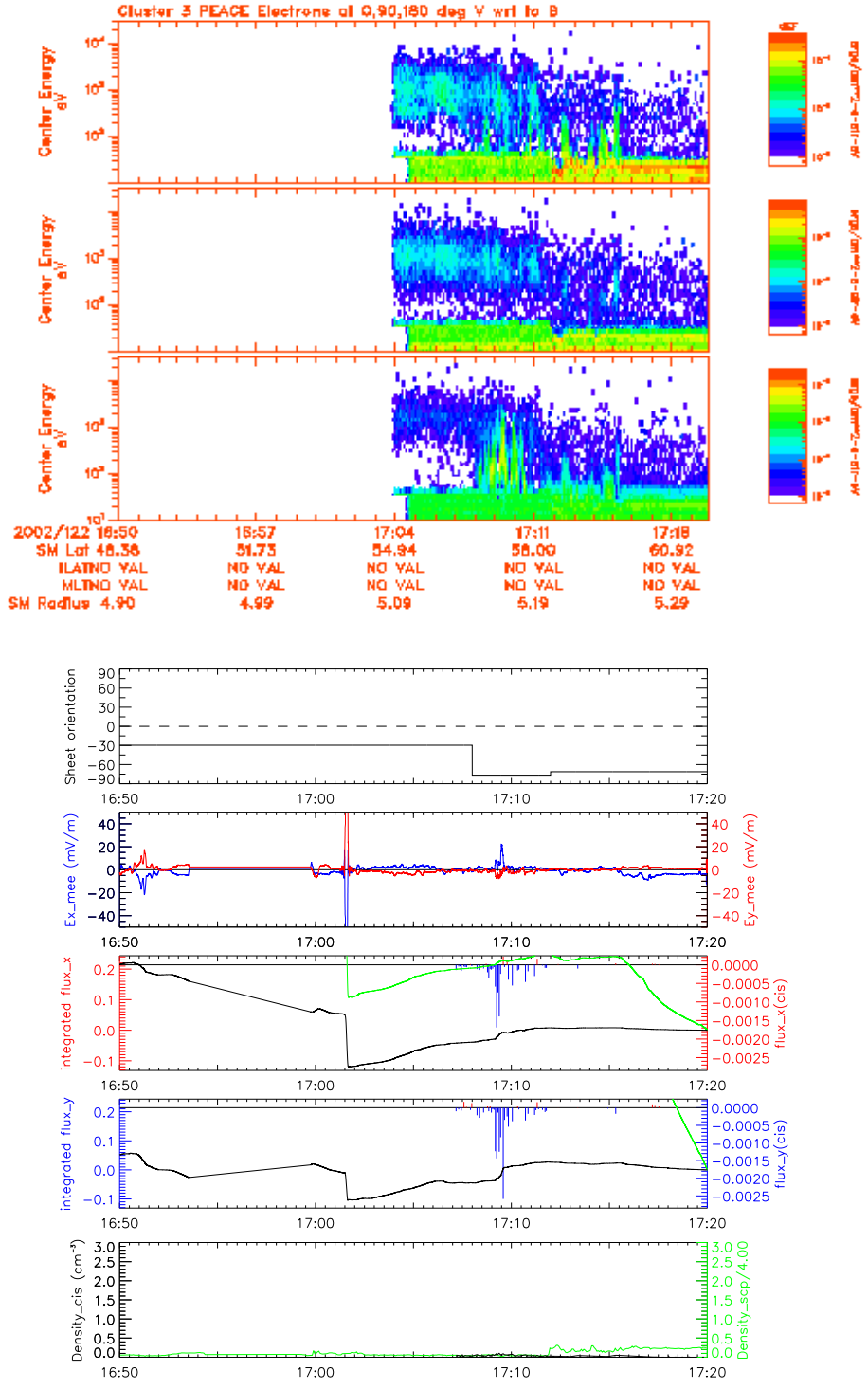

Figure C.5: 2002-05-02 Cluster 3

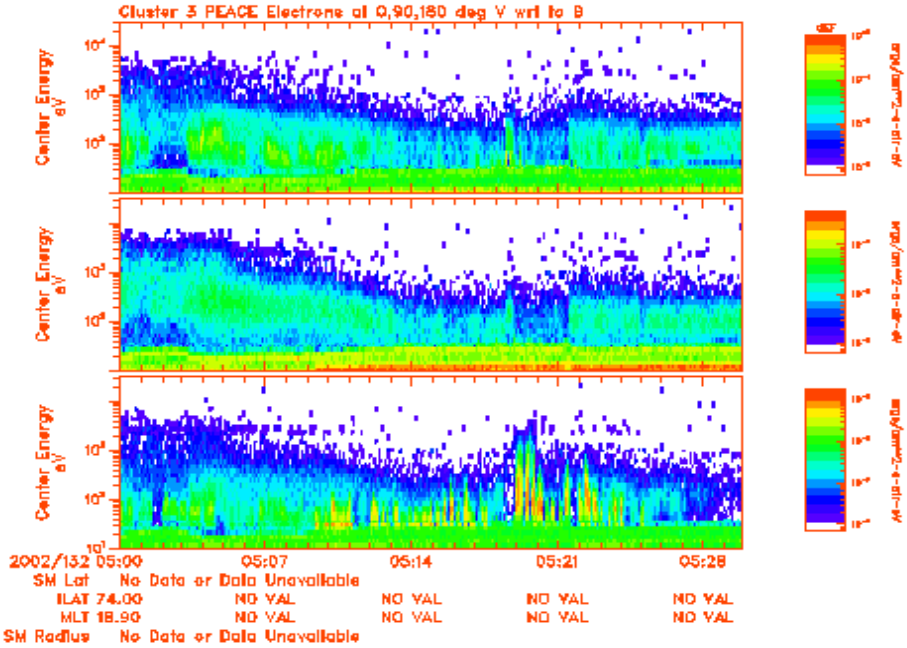

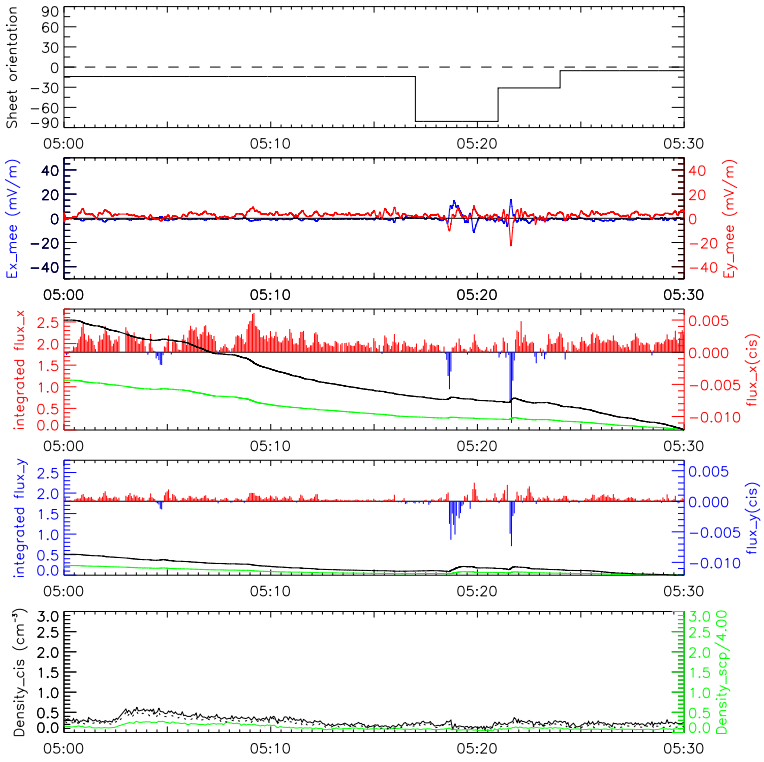

Figure C.6: 2002-05-12 Cluster 3

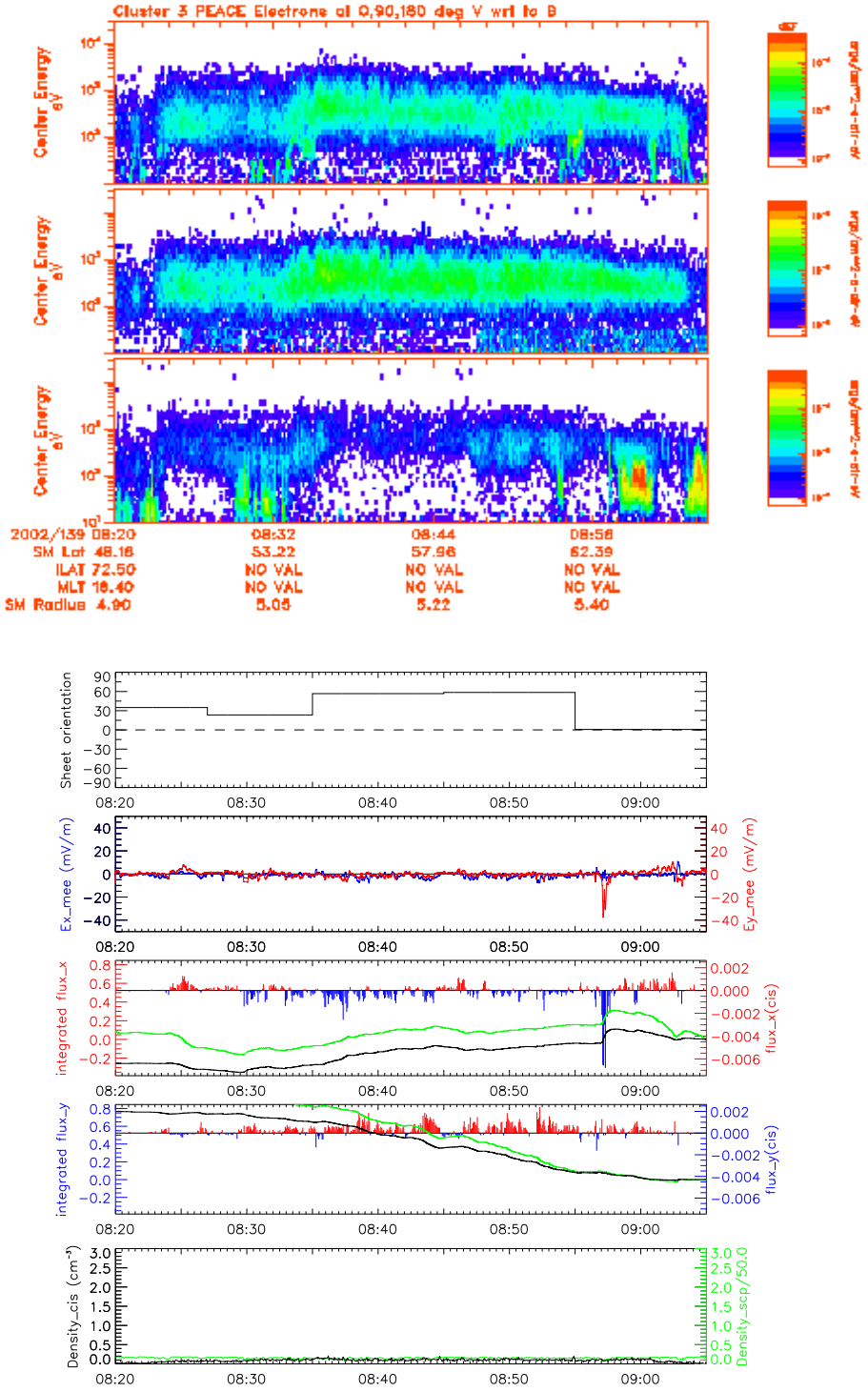

Figure C.7: 2002-05-19 Cluster 3

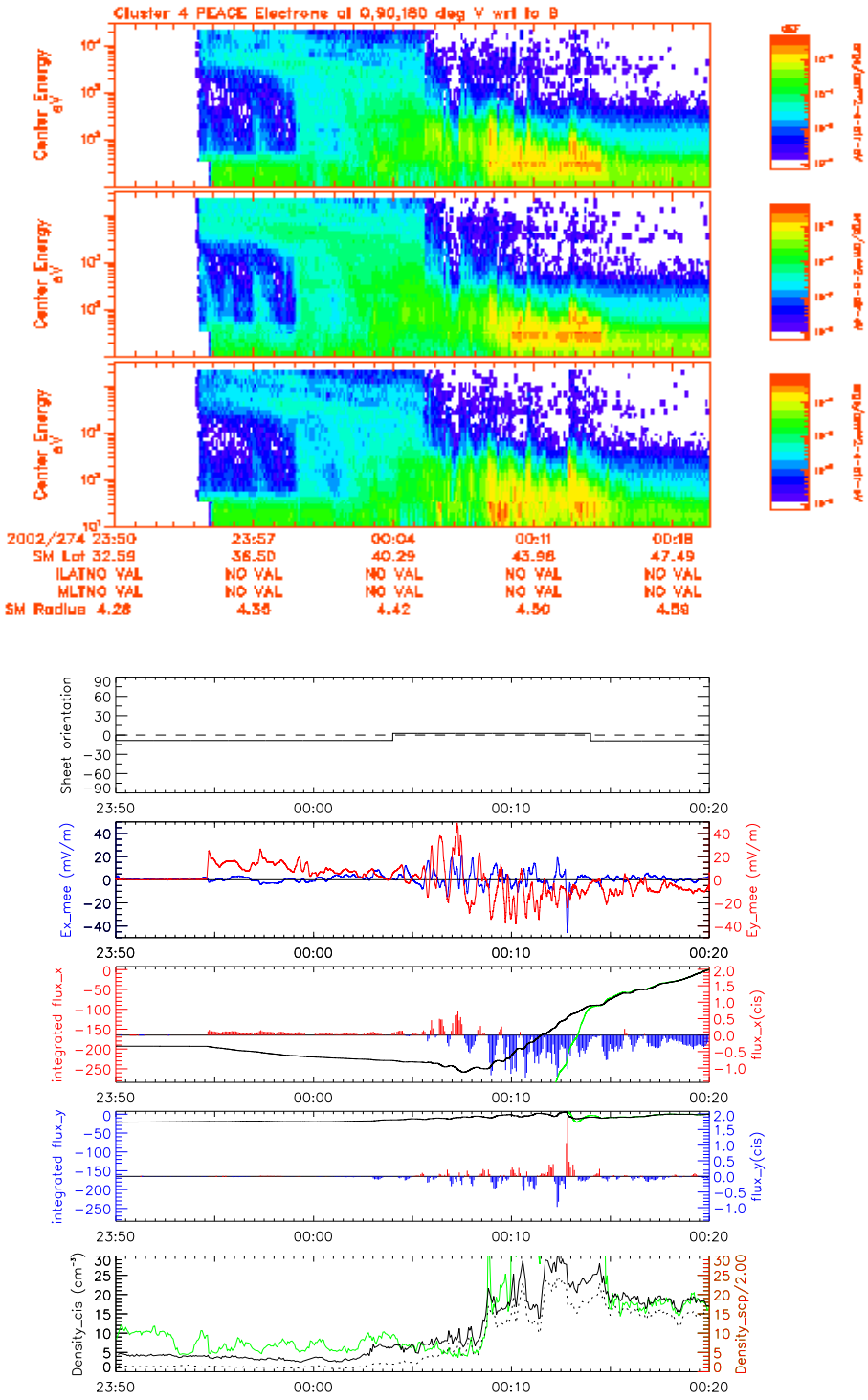

Figure C.8: 2002-10-01 Cluster 4

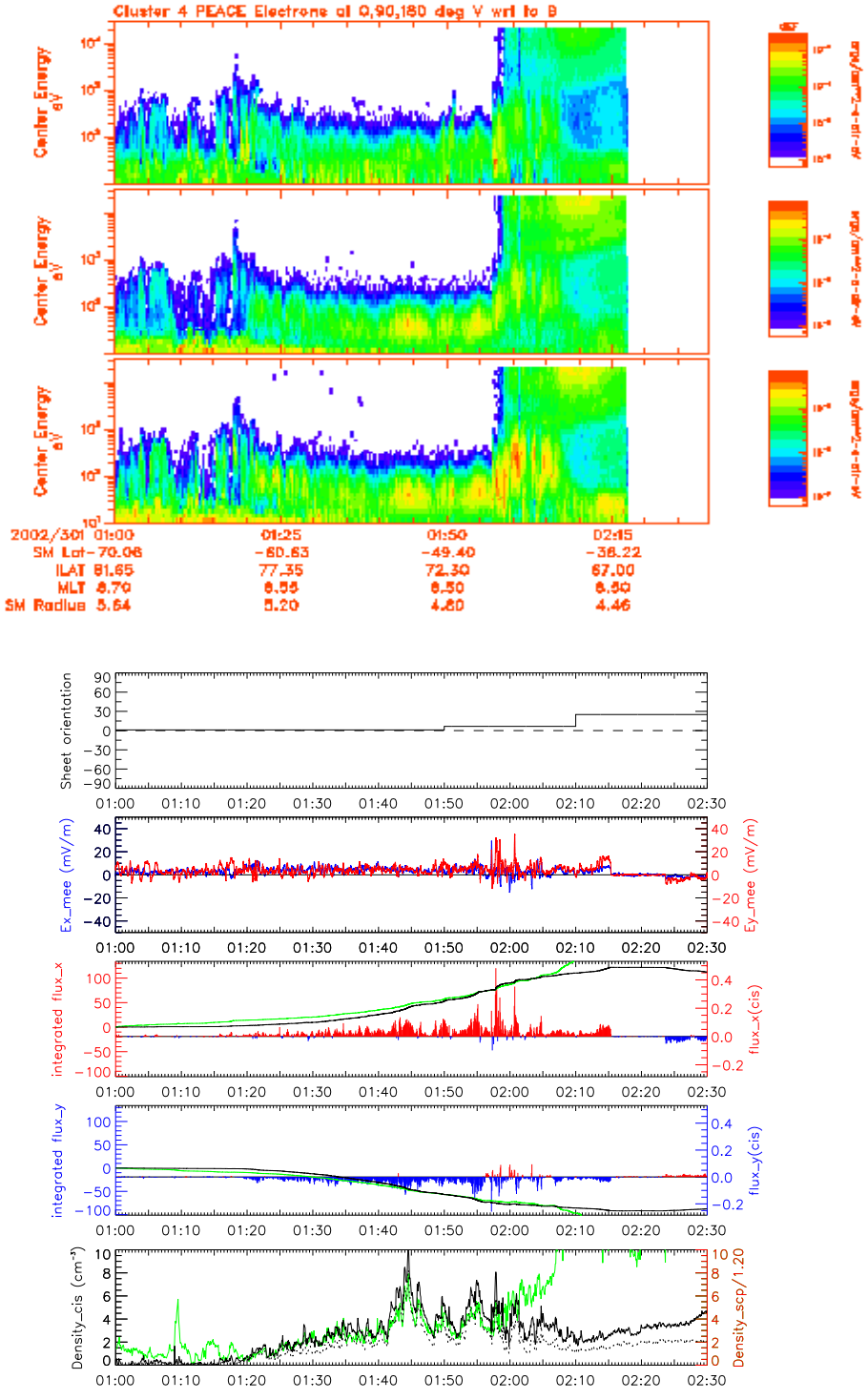

Figure C.9: 2002-10-28 Cluster 4

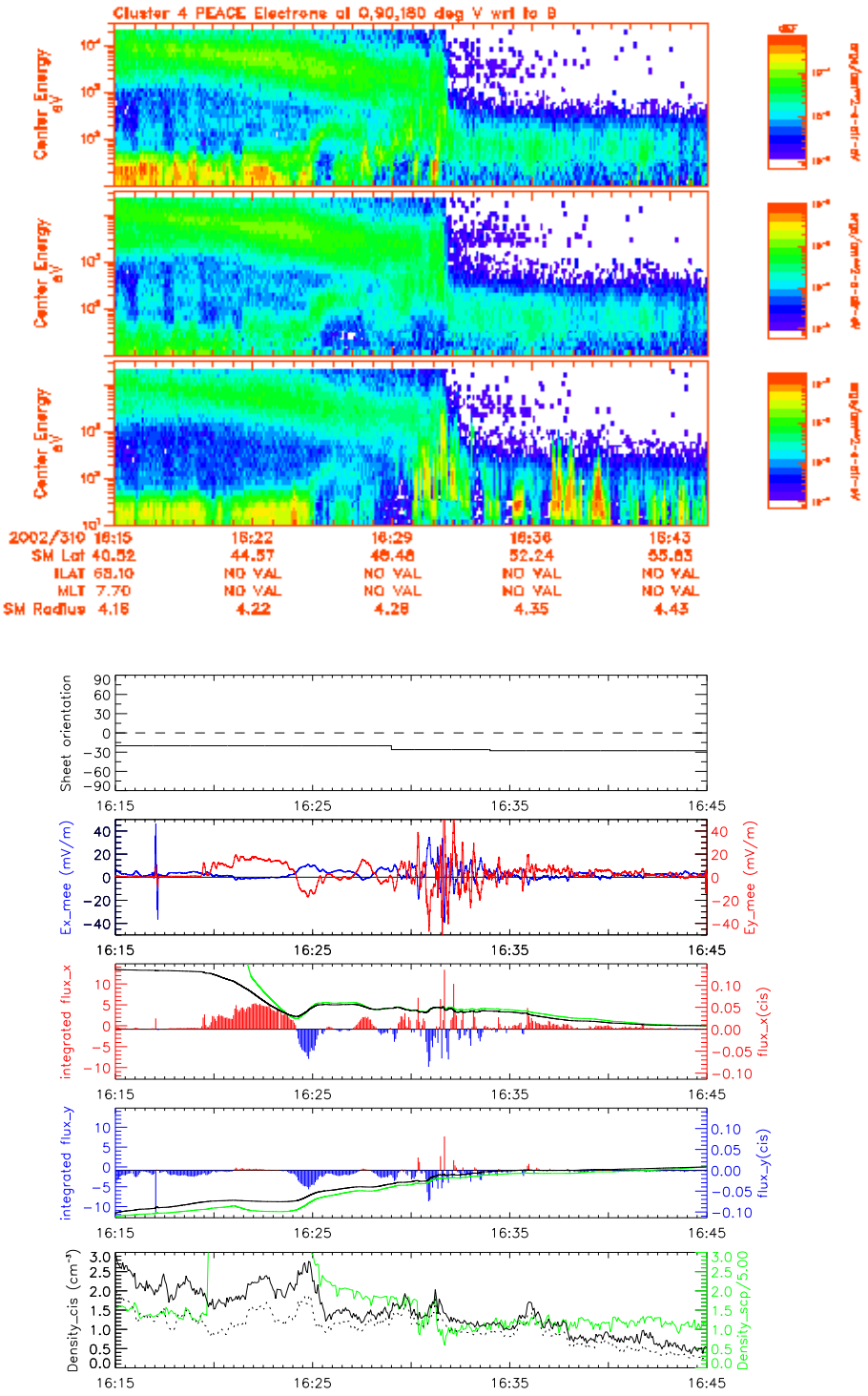

Figure C.10: 2002-11-06 Cluster 4

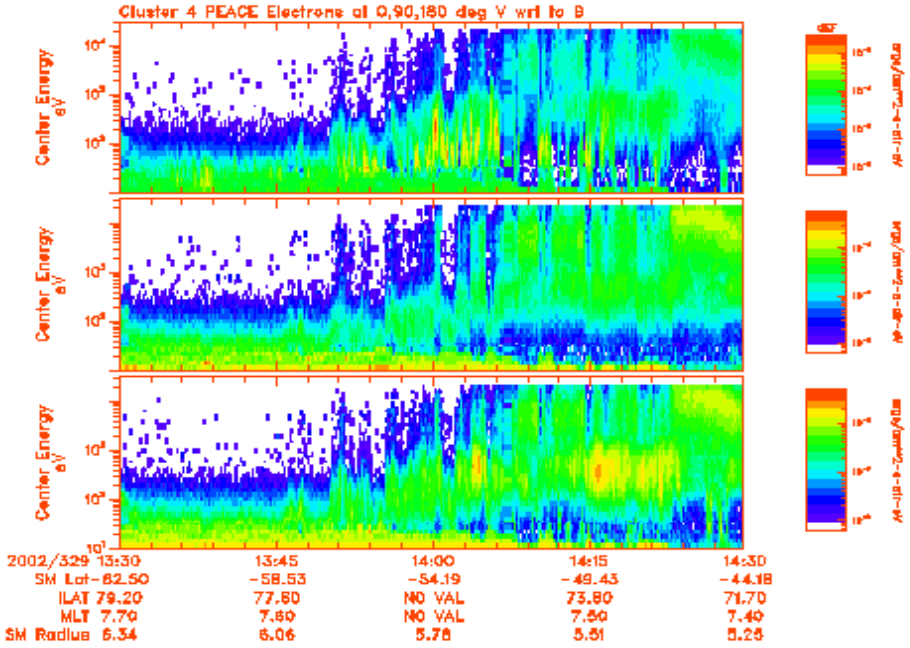

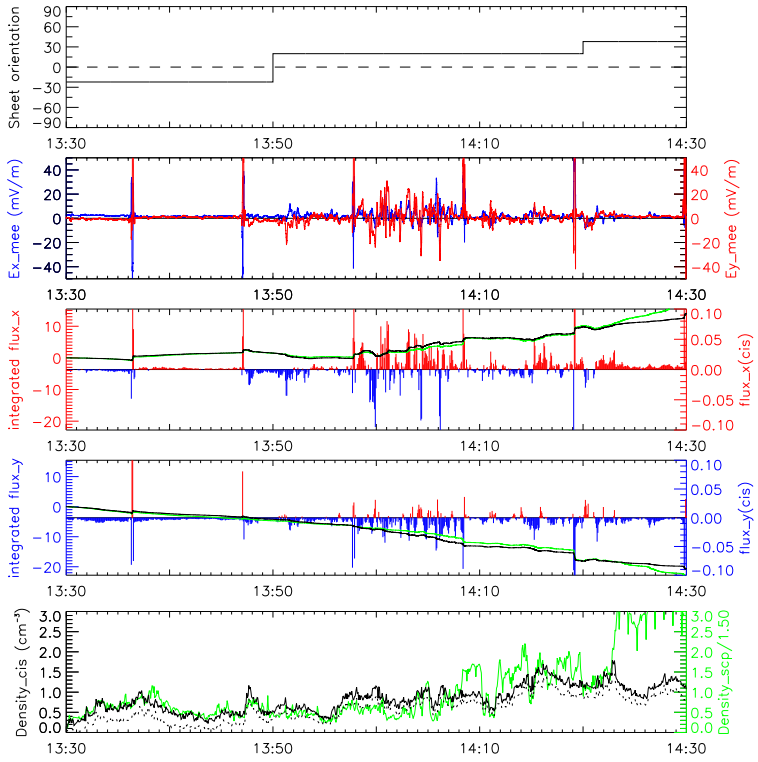

Figure C.11: 2002-11-25 Cluster 4

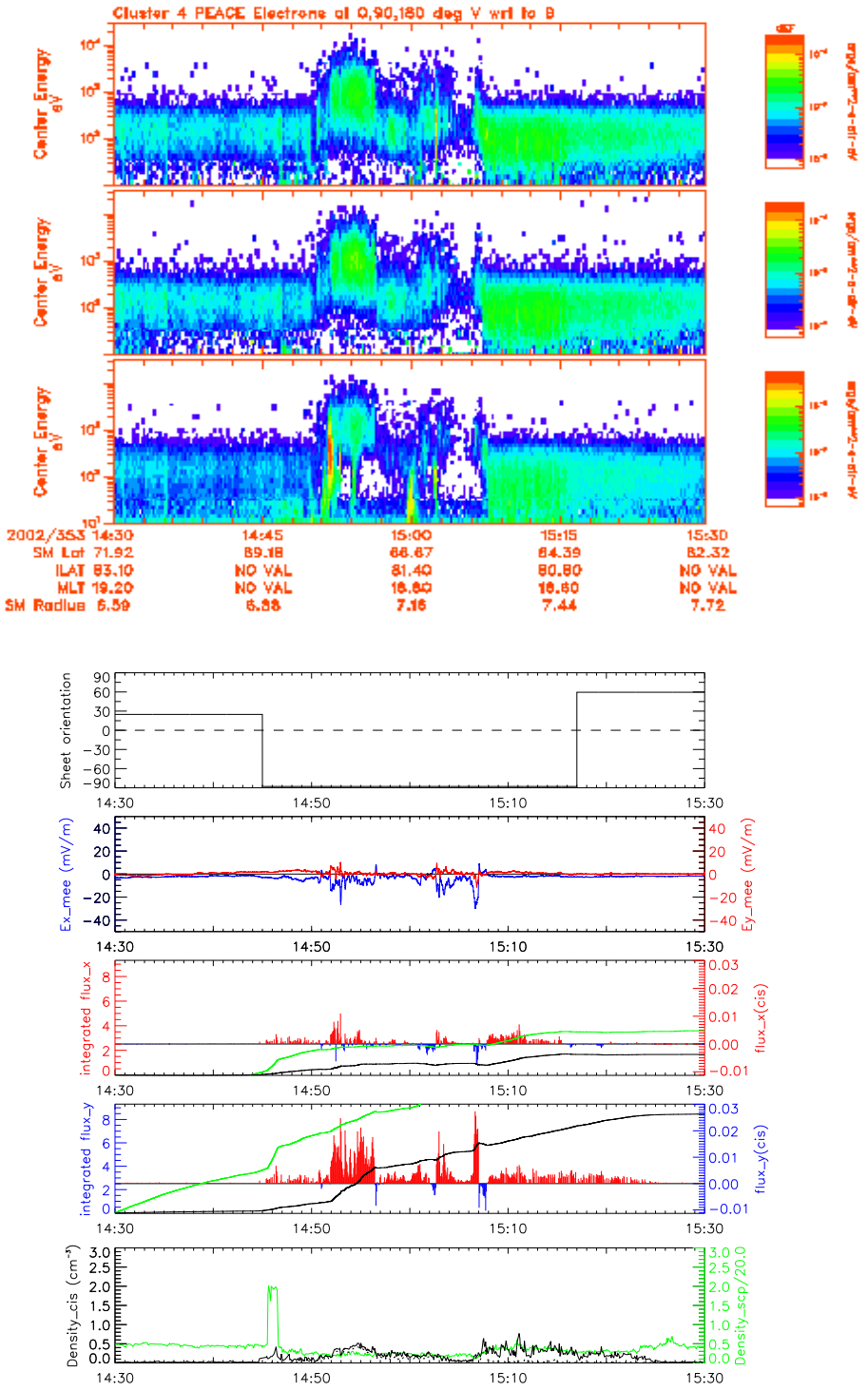

Figure C.12: 2002-12-19 Cluster 4

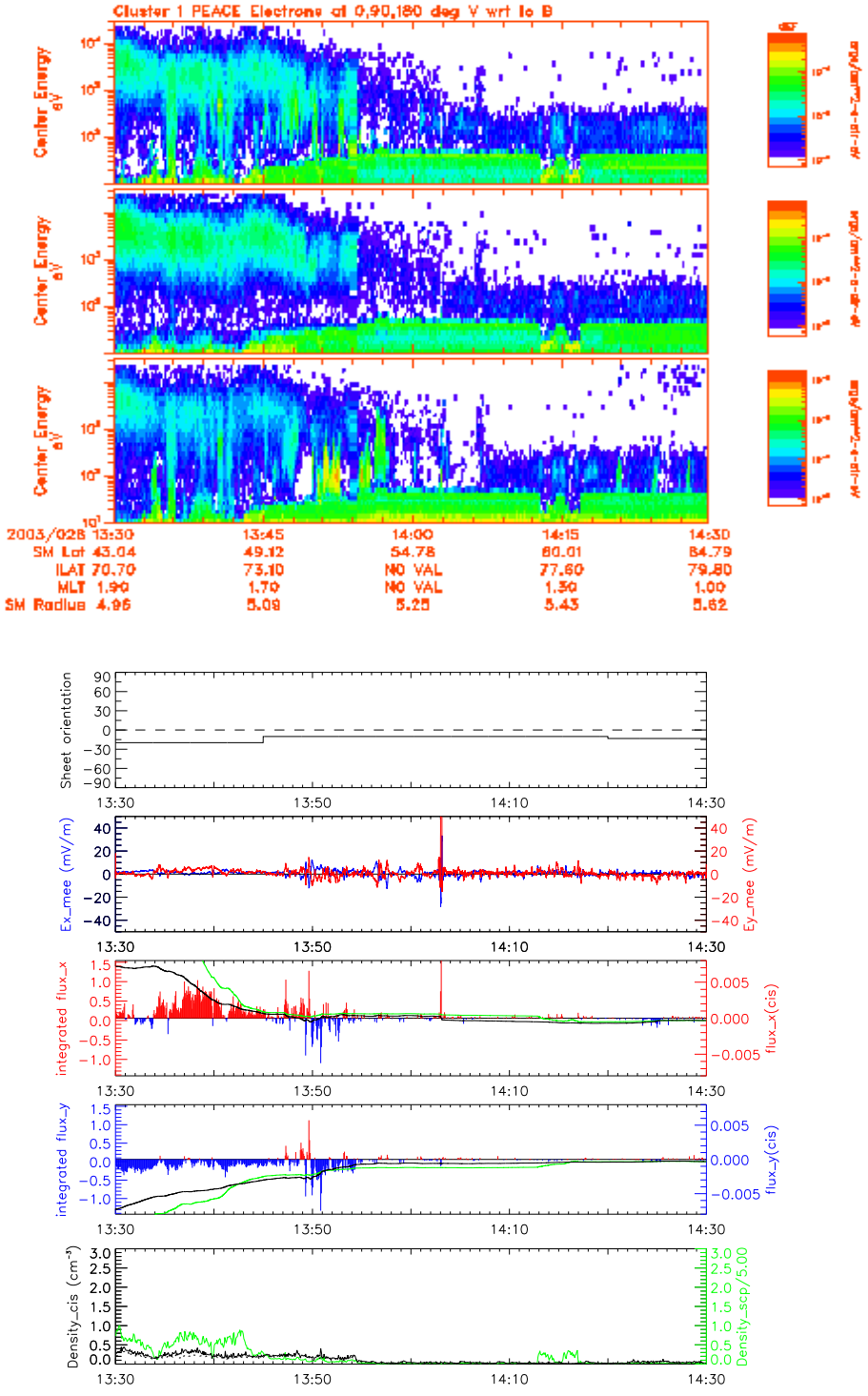

Figure C.13: 2003-01-26 Cluster 1

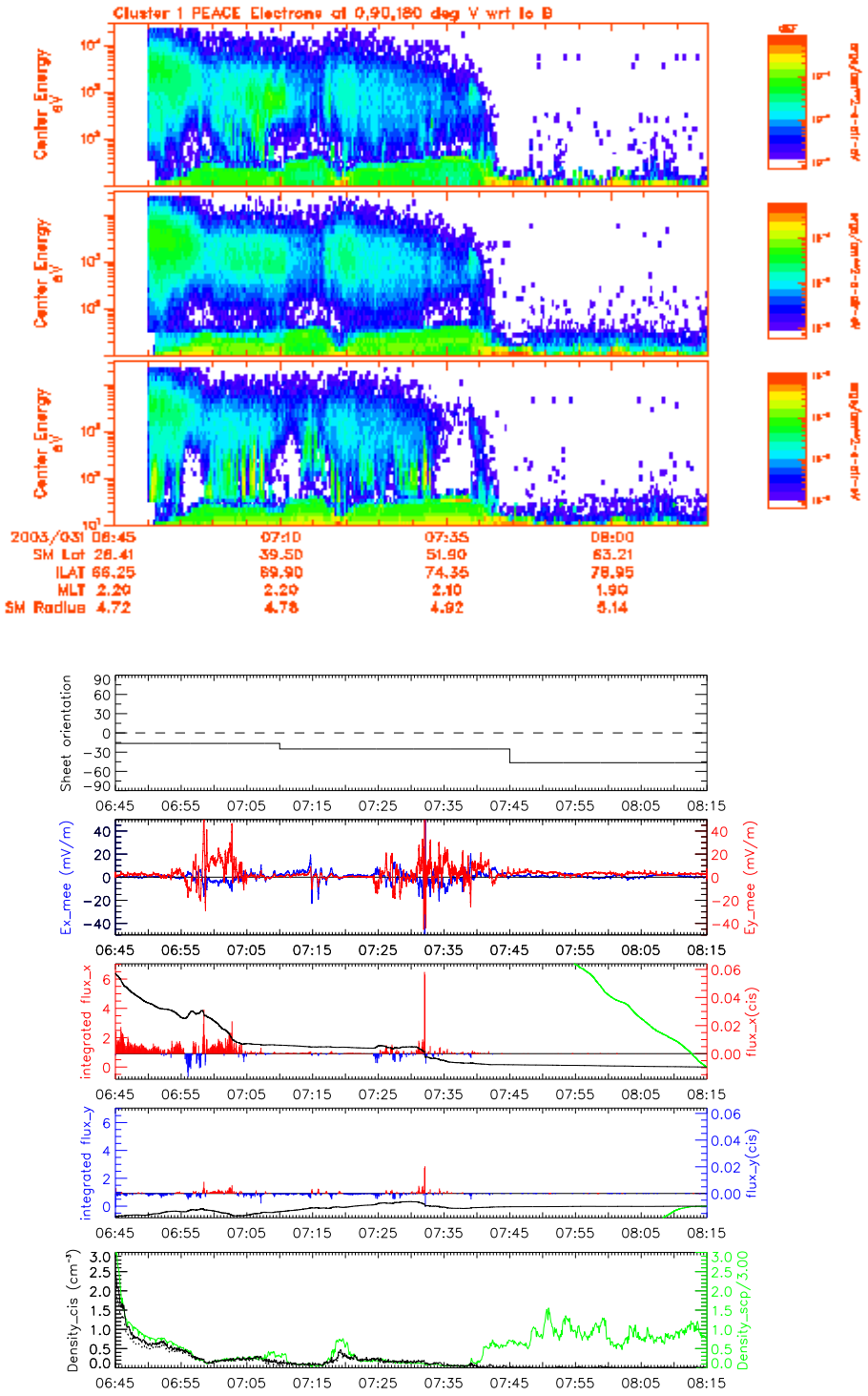

Figure C.14: 2003-01-31 Cluster 1

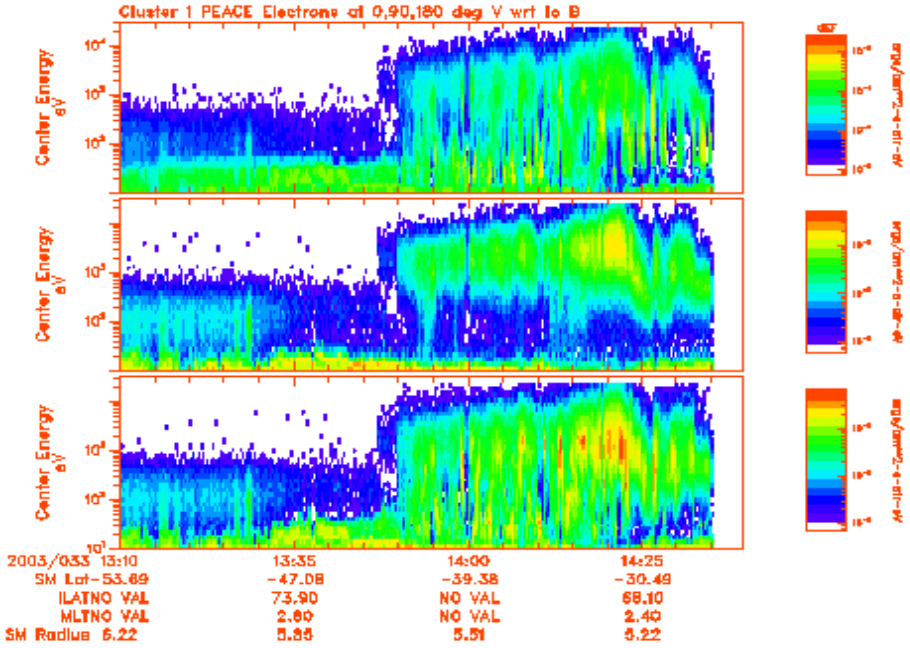

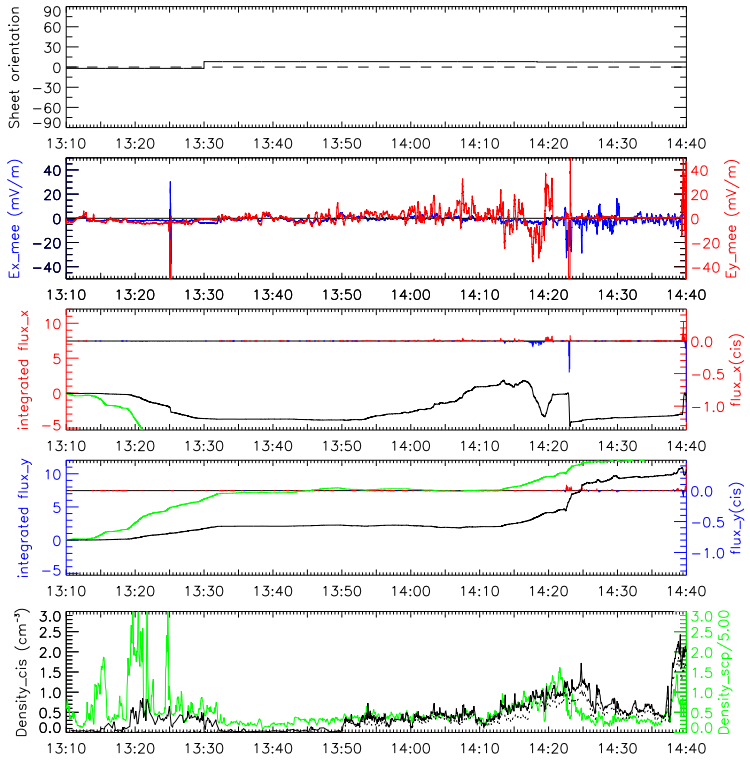

Figure C.15: 2003-02-02 Cluster 1

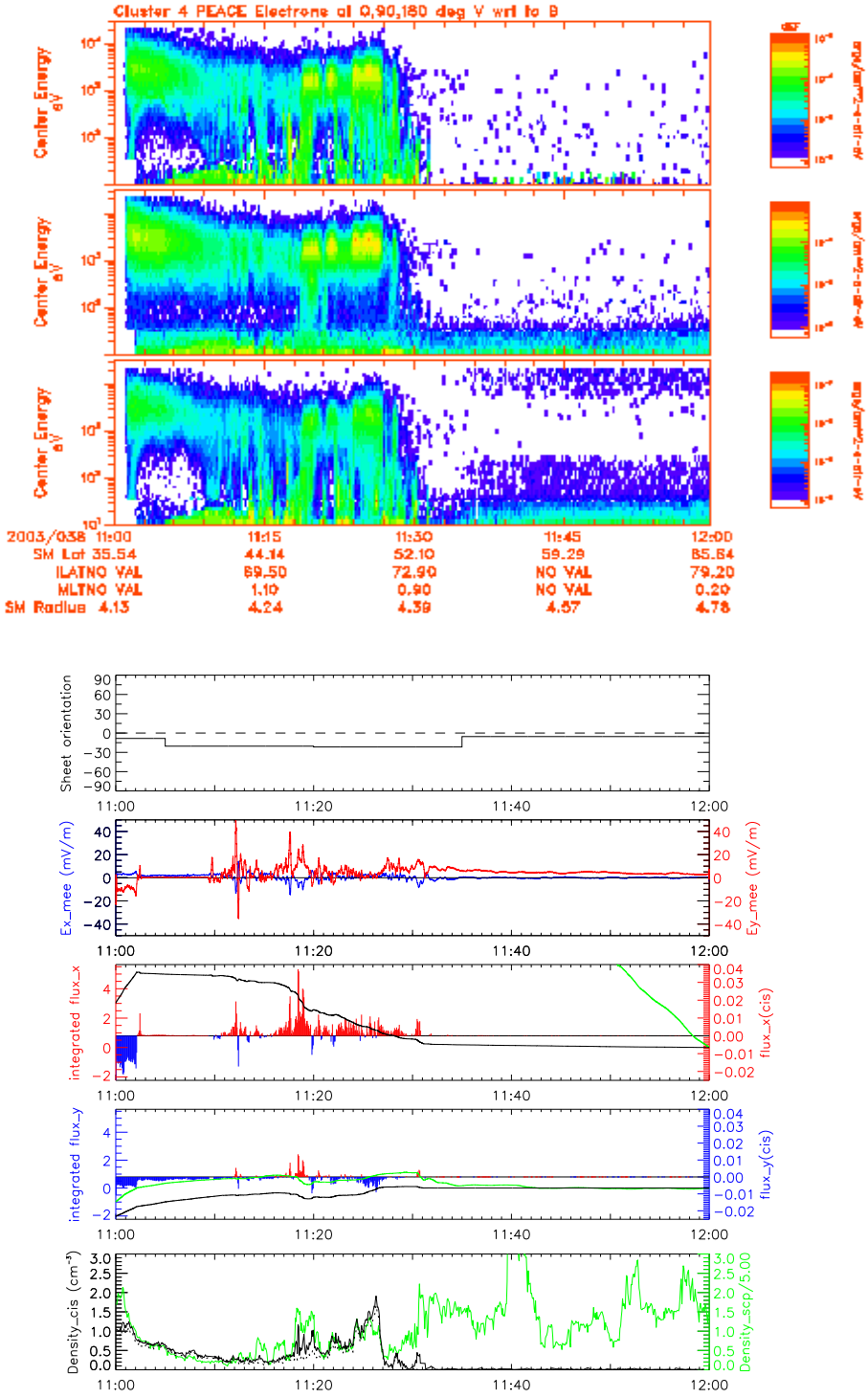

Figure C.16: 2003-02-07 Cluster 4

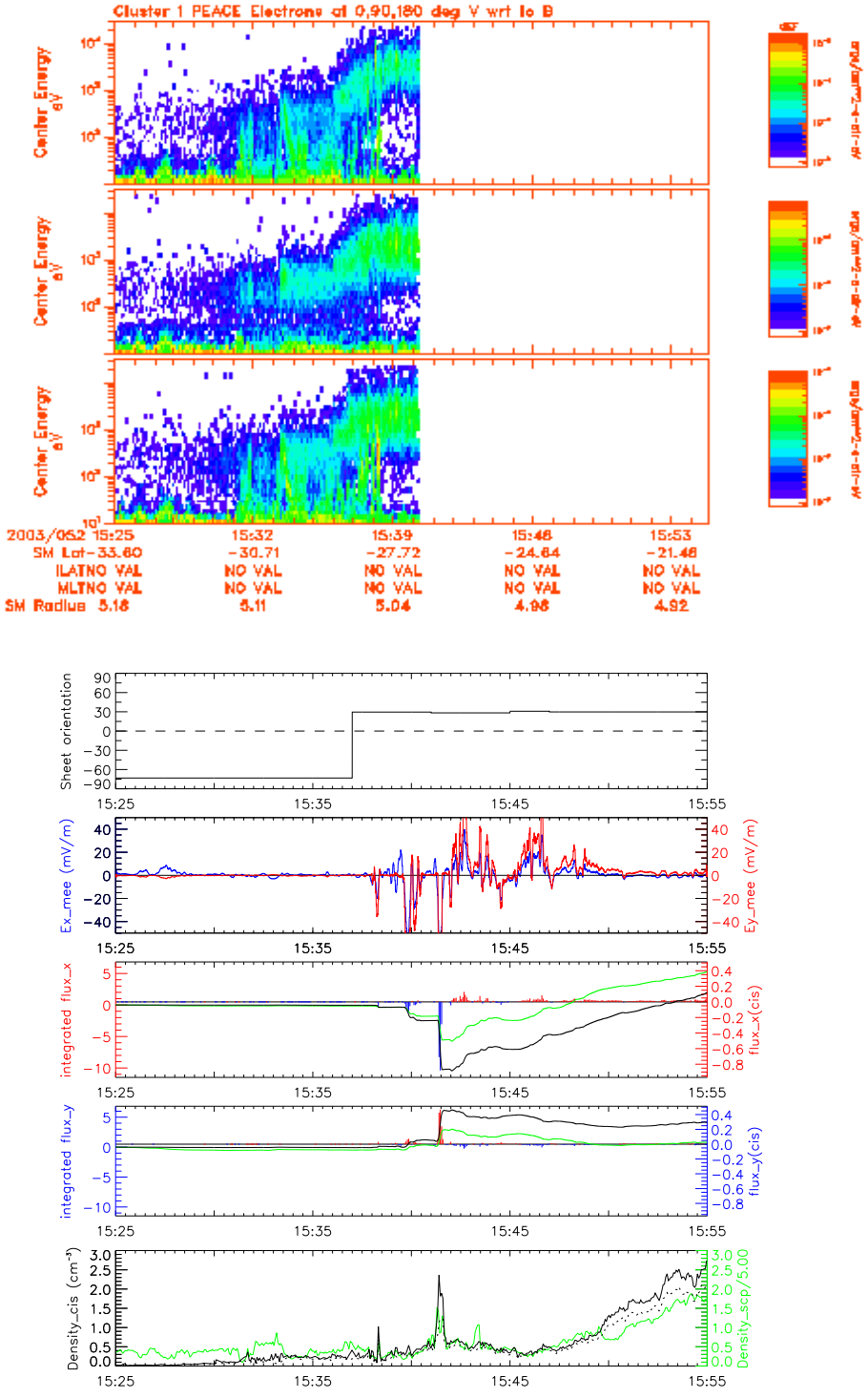

Figure C.17: 2003-02-21 Cluster 1

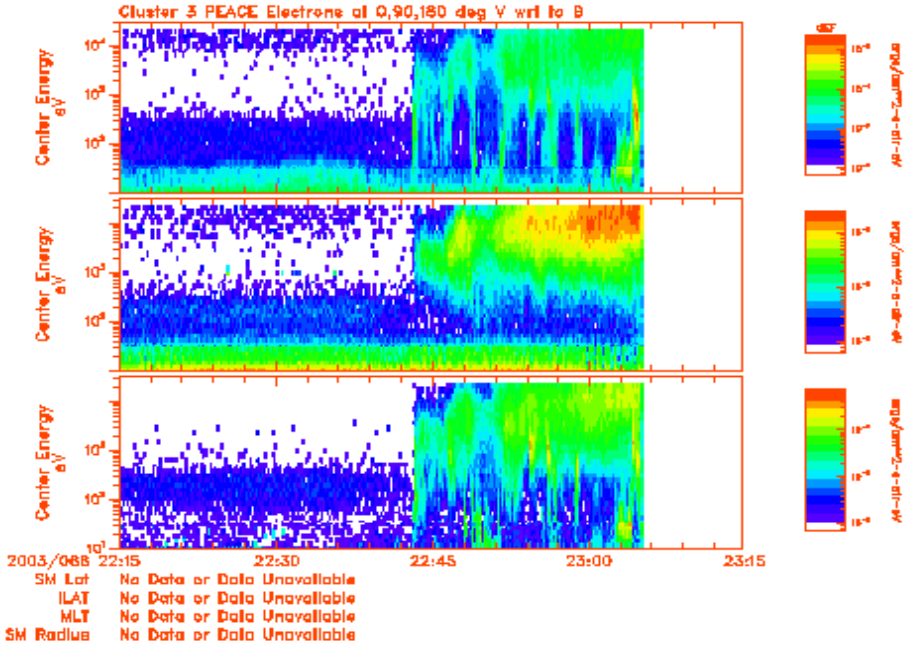

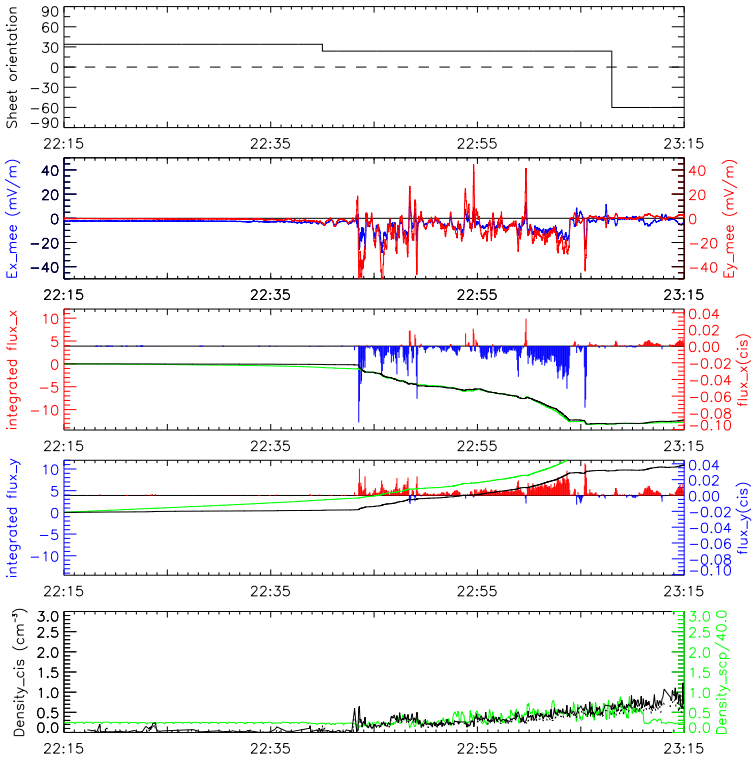

Figure C.18: 2003-03-07 Cluster 3

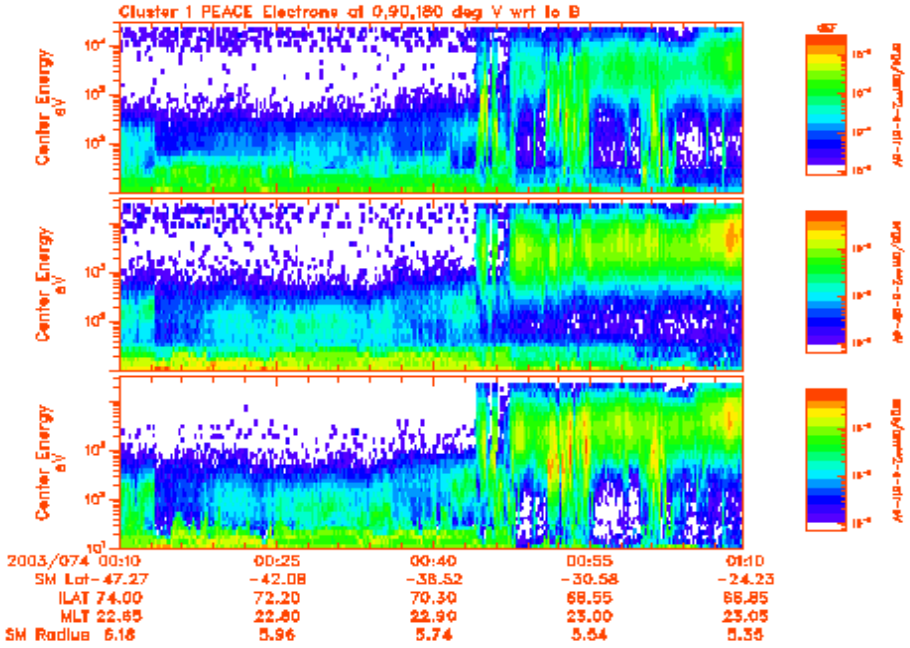

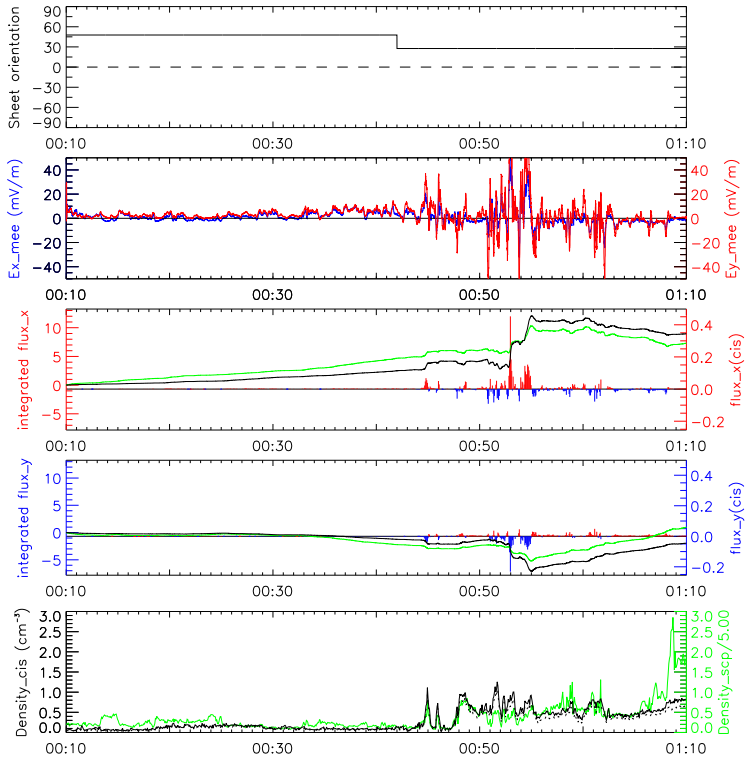

Figure C.19: 2003-03-15 Cluster 1

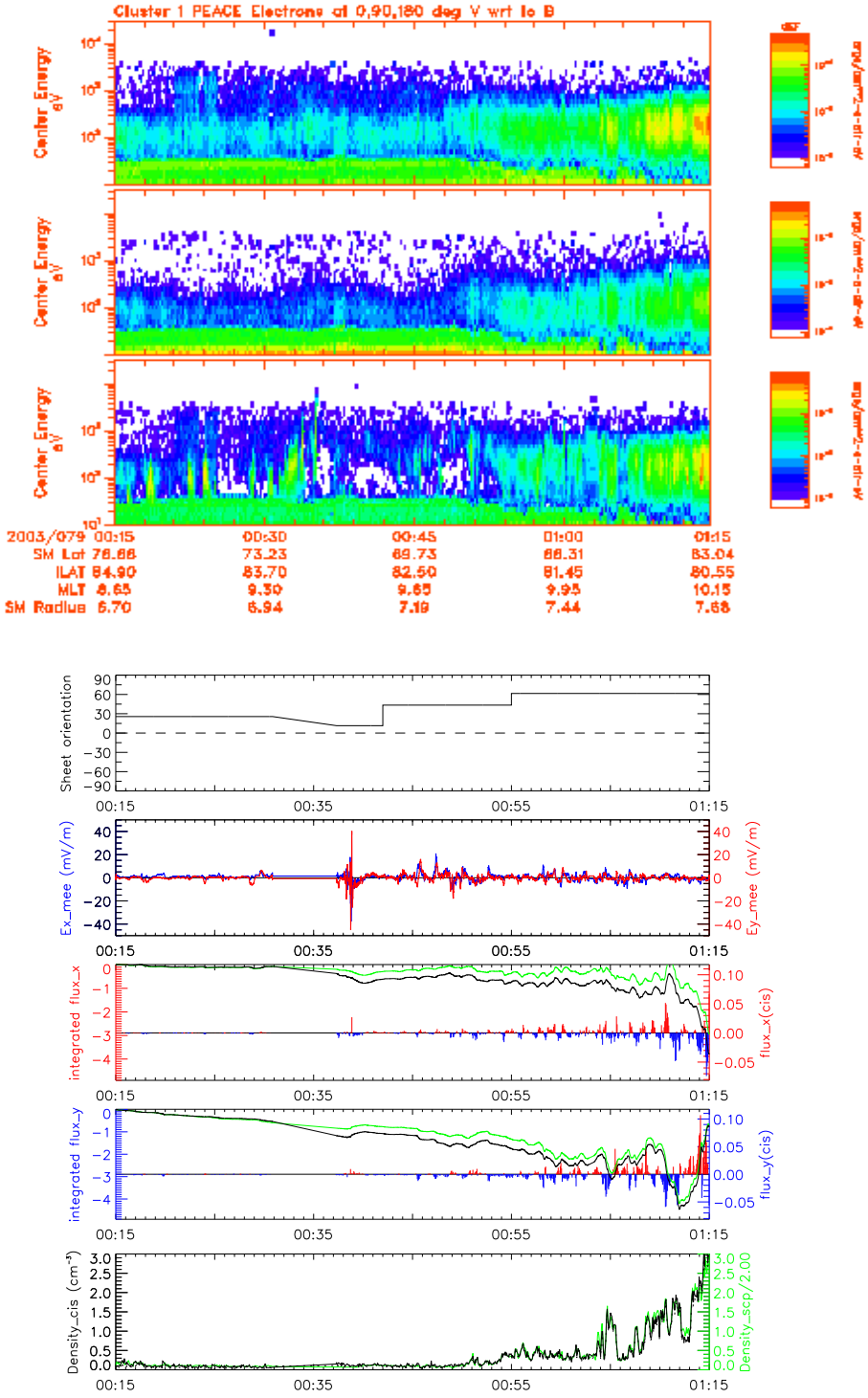

Figure C.20: 2003-03-20 Cluster 1

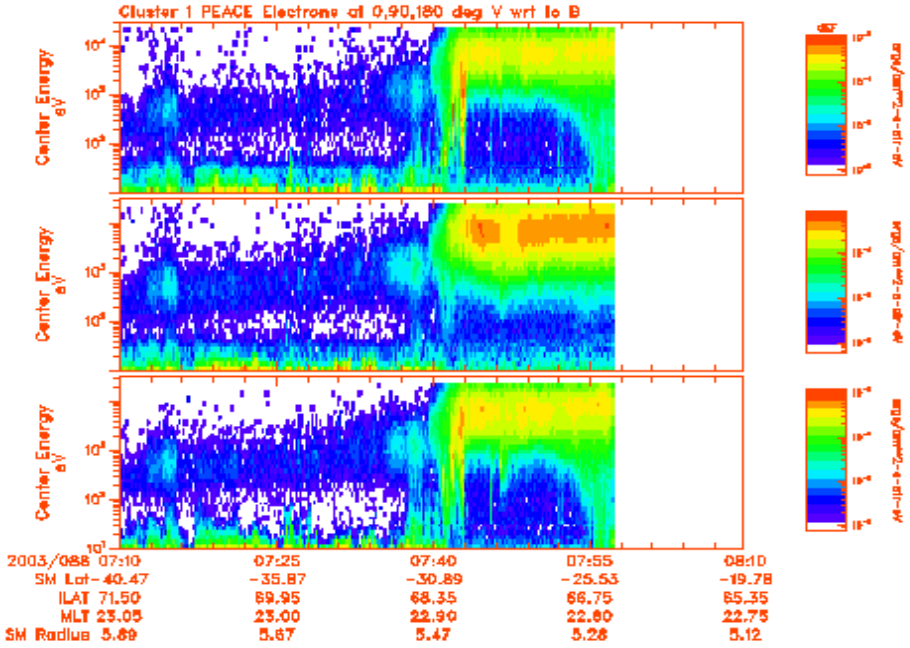

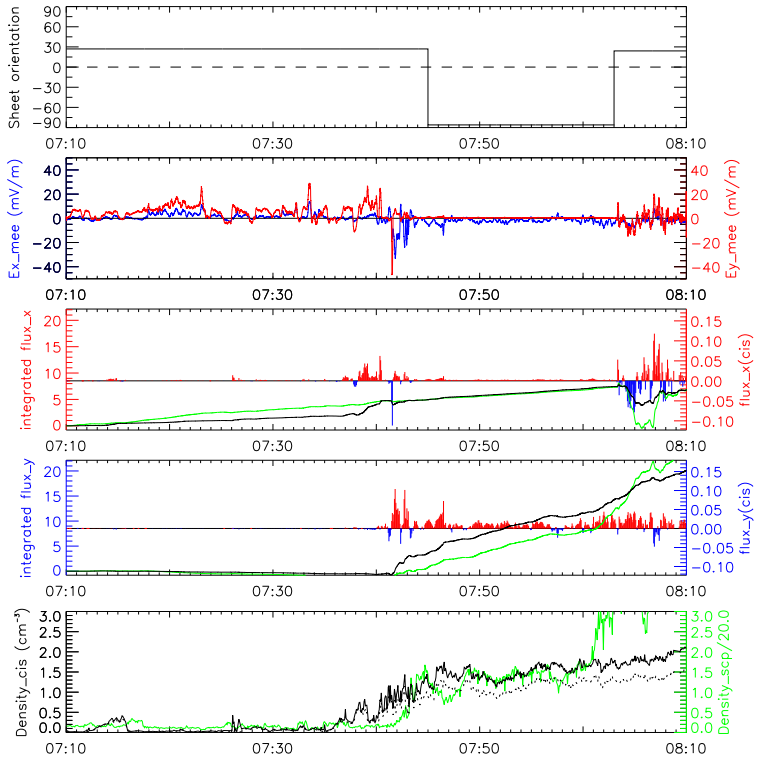

Figure C.21: 2003-03-29 Cluster 1

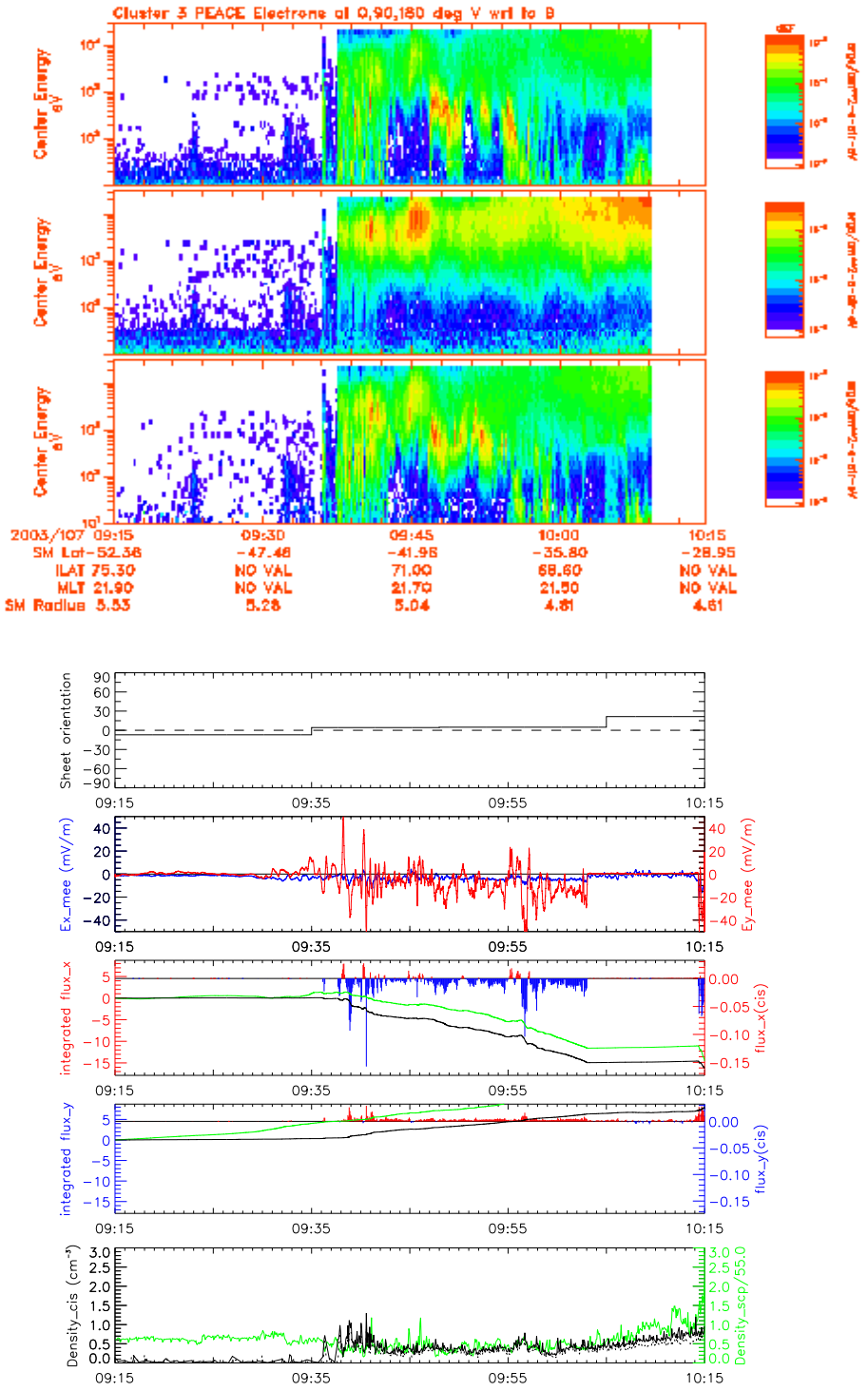

Figure C.22: 2003-04-17 Cluster 3

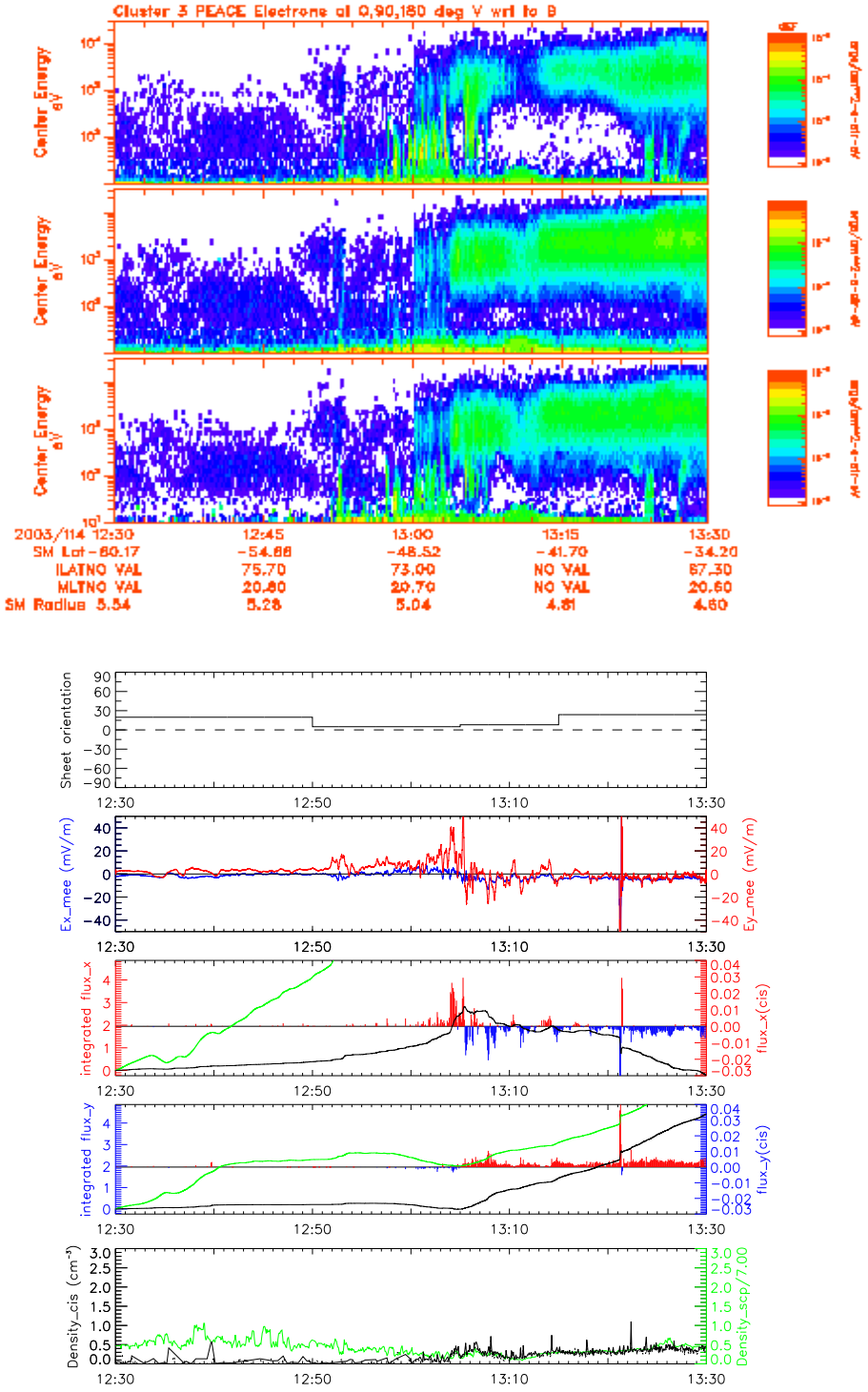

Figure C.23: 2003-04-24 Cluster 3

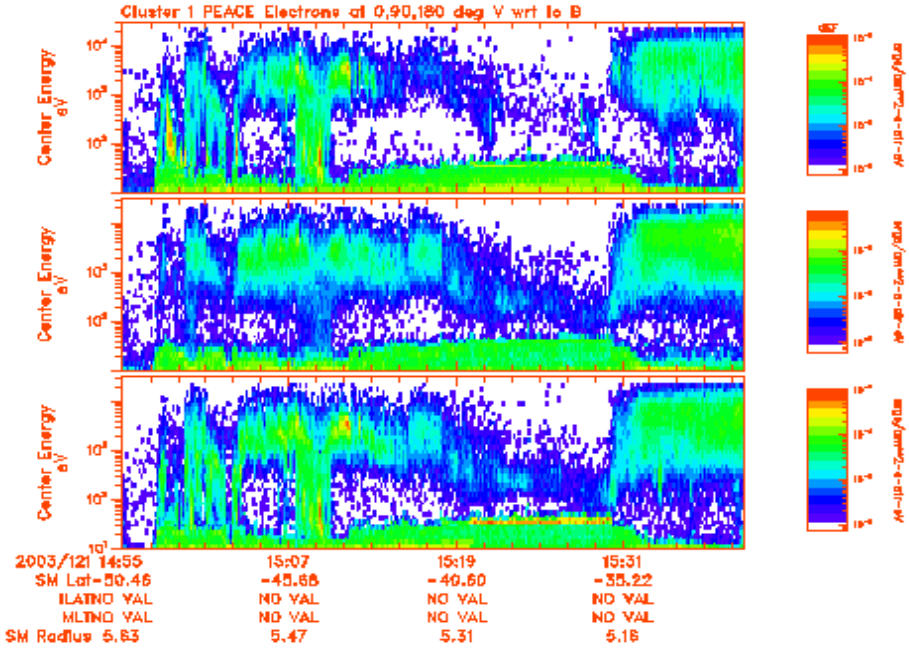

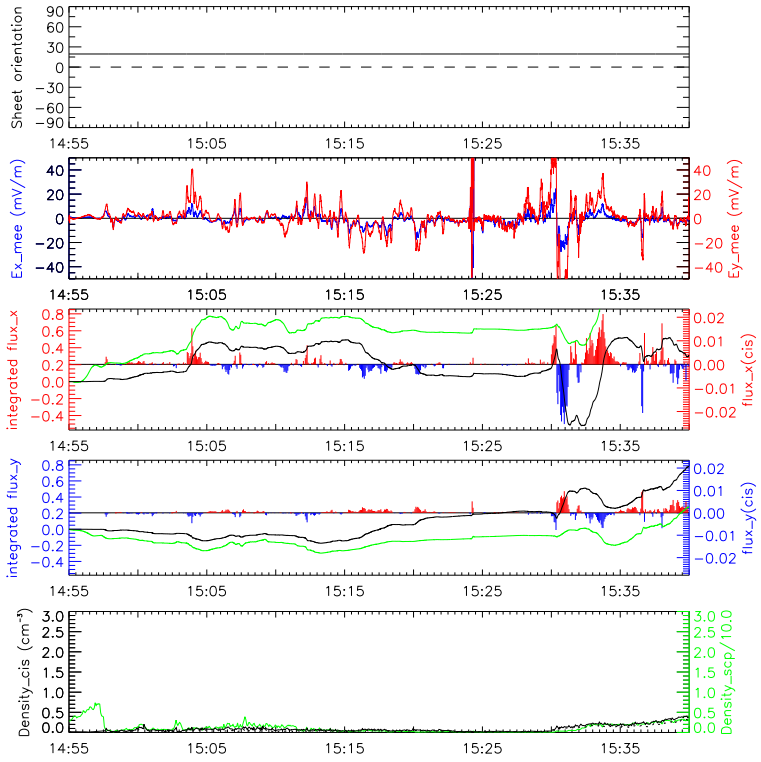

Figure C.24: 2003-05-01 Cluster 1

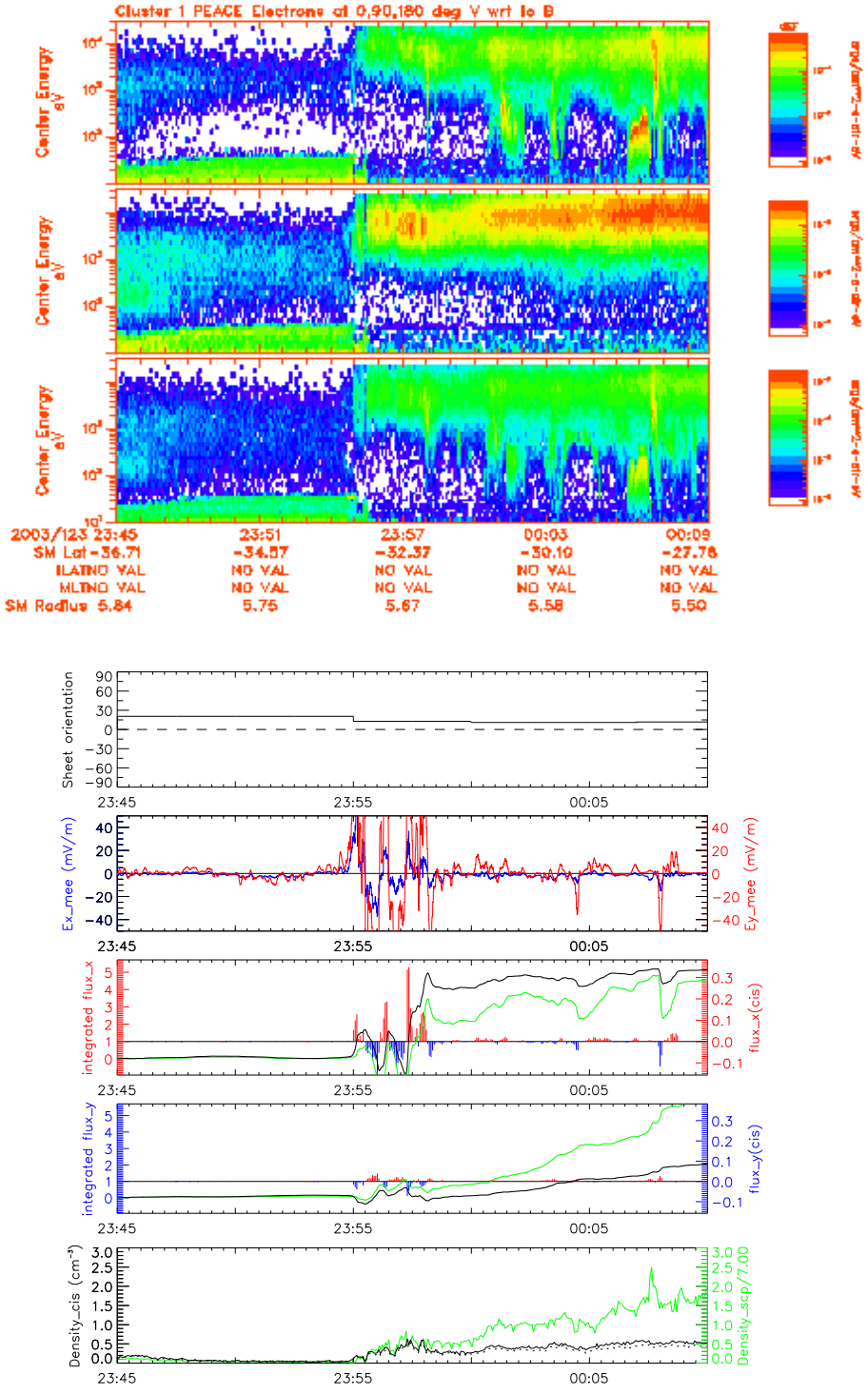

Figure C.25: 2003-05-03 Cluster 1

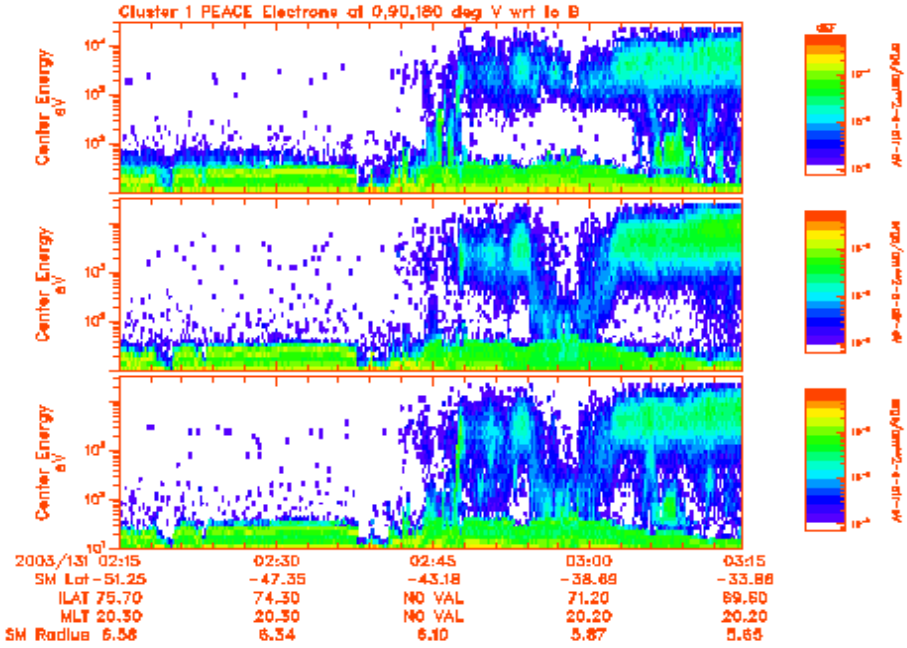

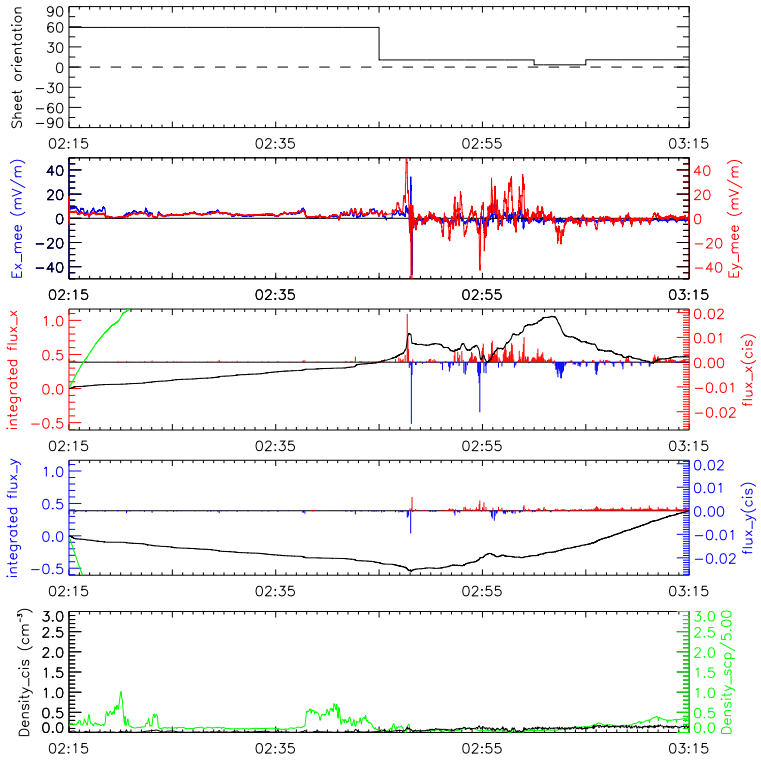

Figure C.26: 2003-05-11 Cluster 1

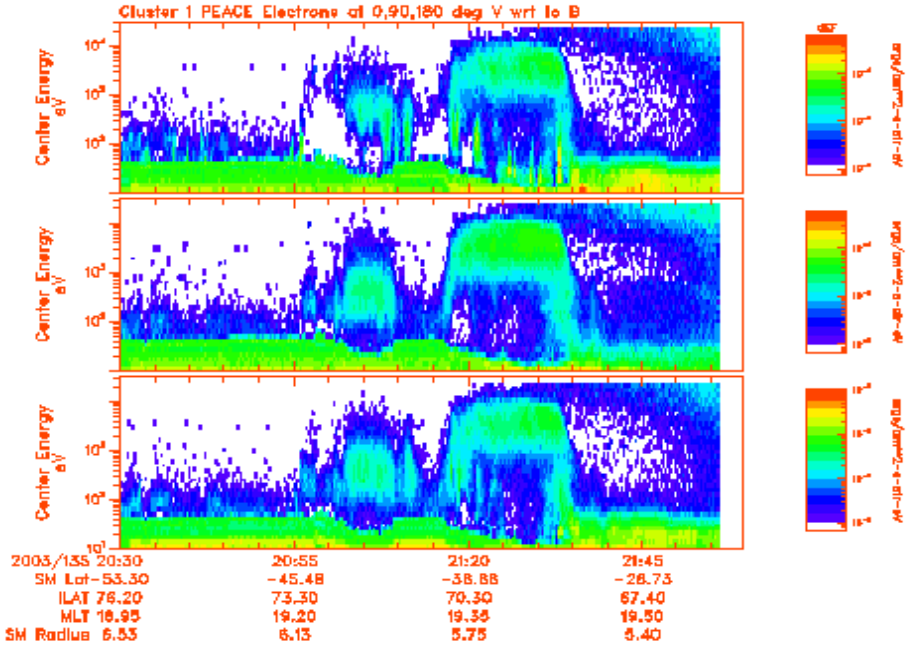

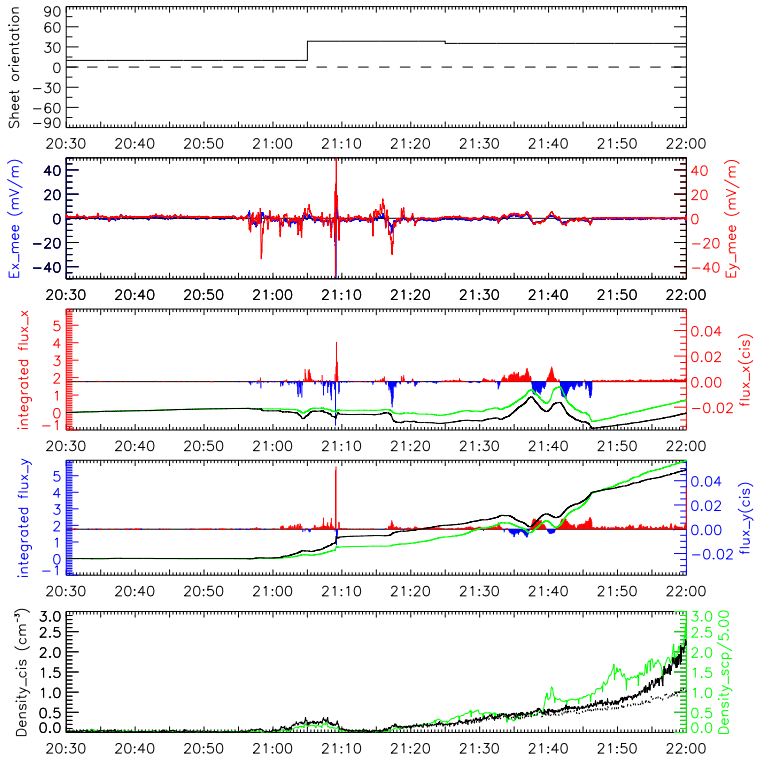

Figure C.27: 2003-05-15 Cluster 1

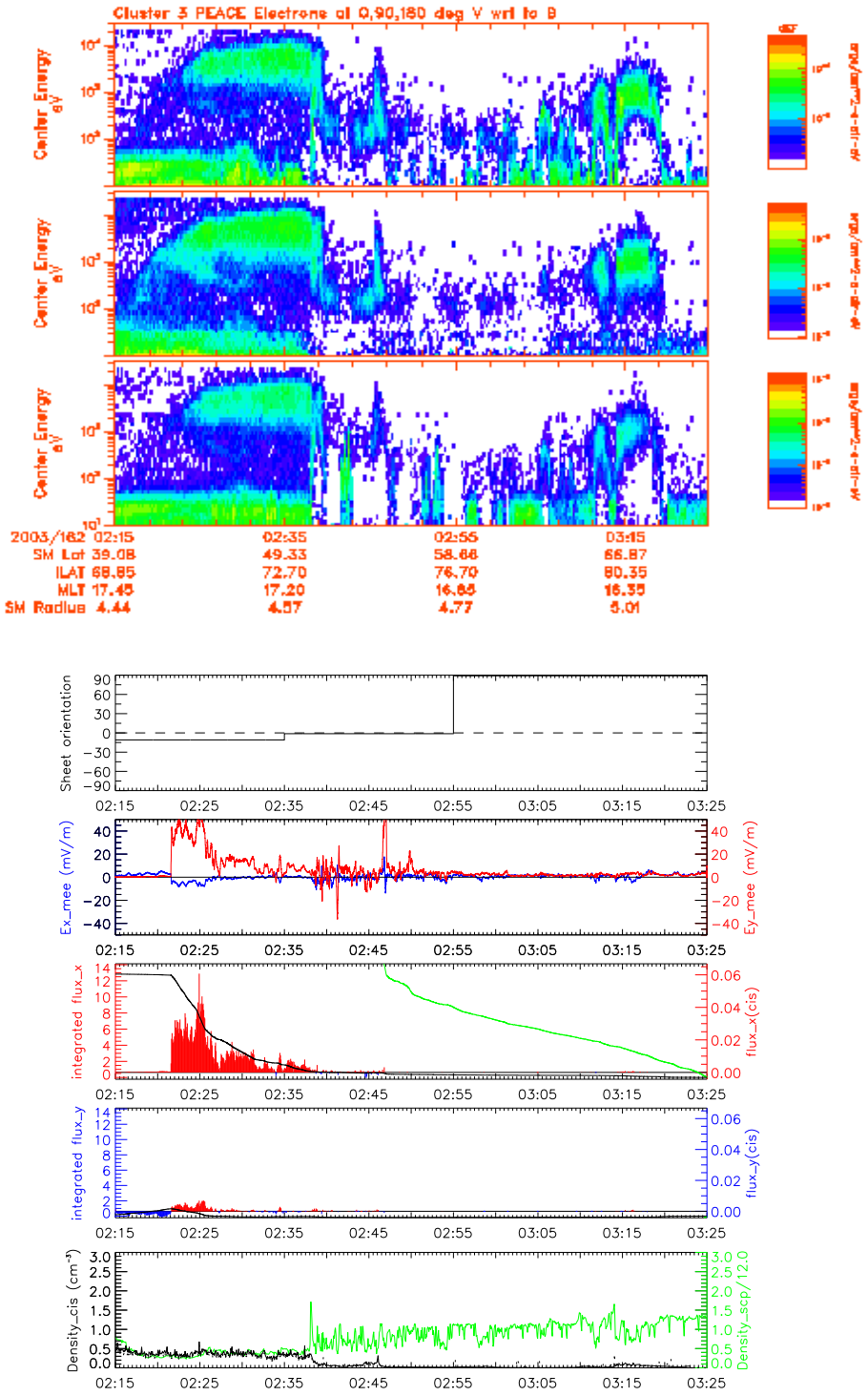

Figure C.28: 2003-06-11 Cluster 3

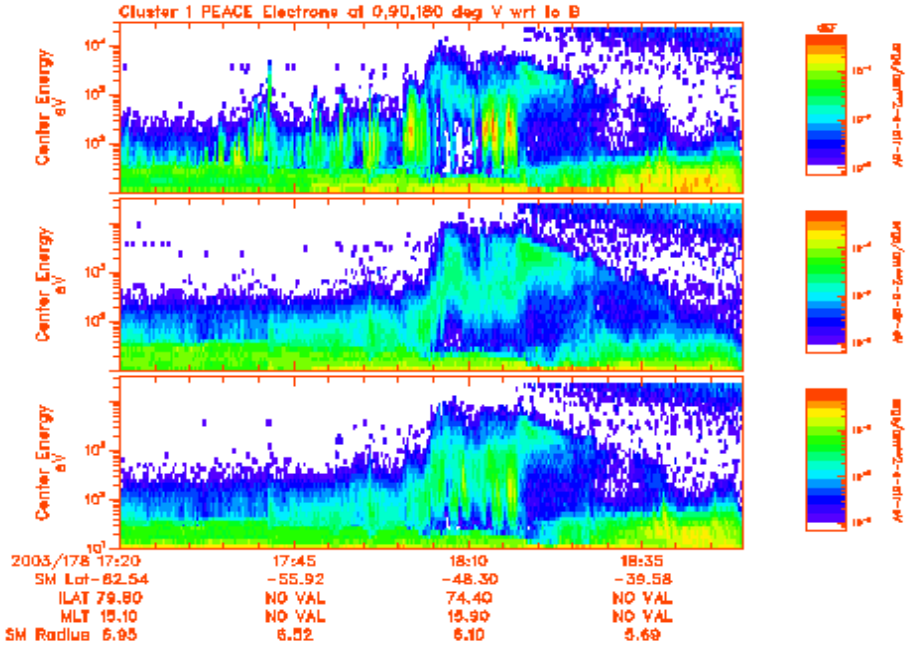

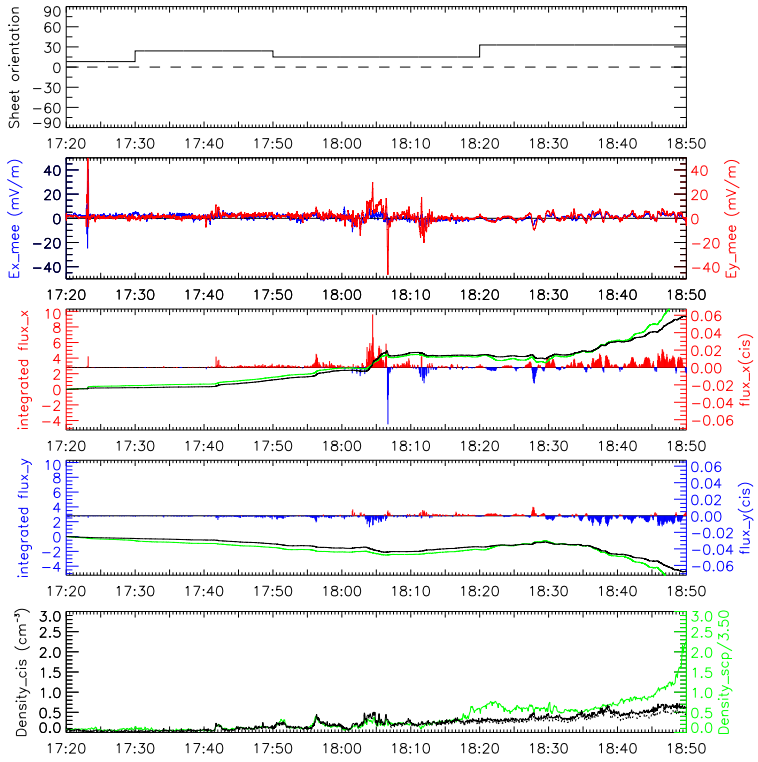

Figure C.29: 2003-06-27 Cluster 1

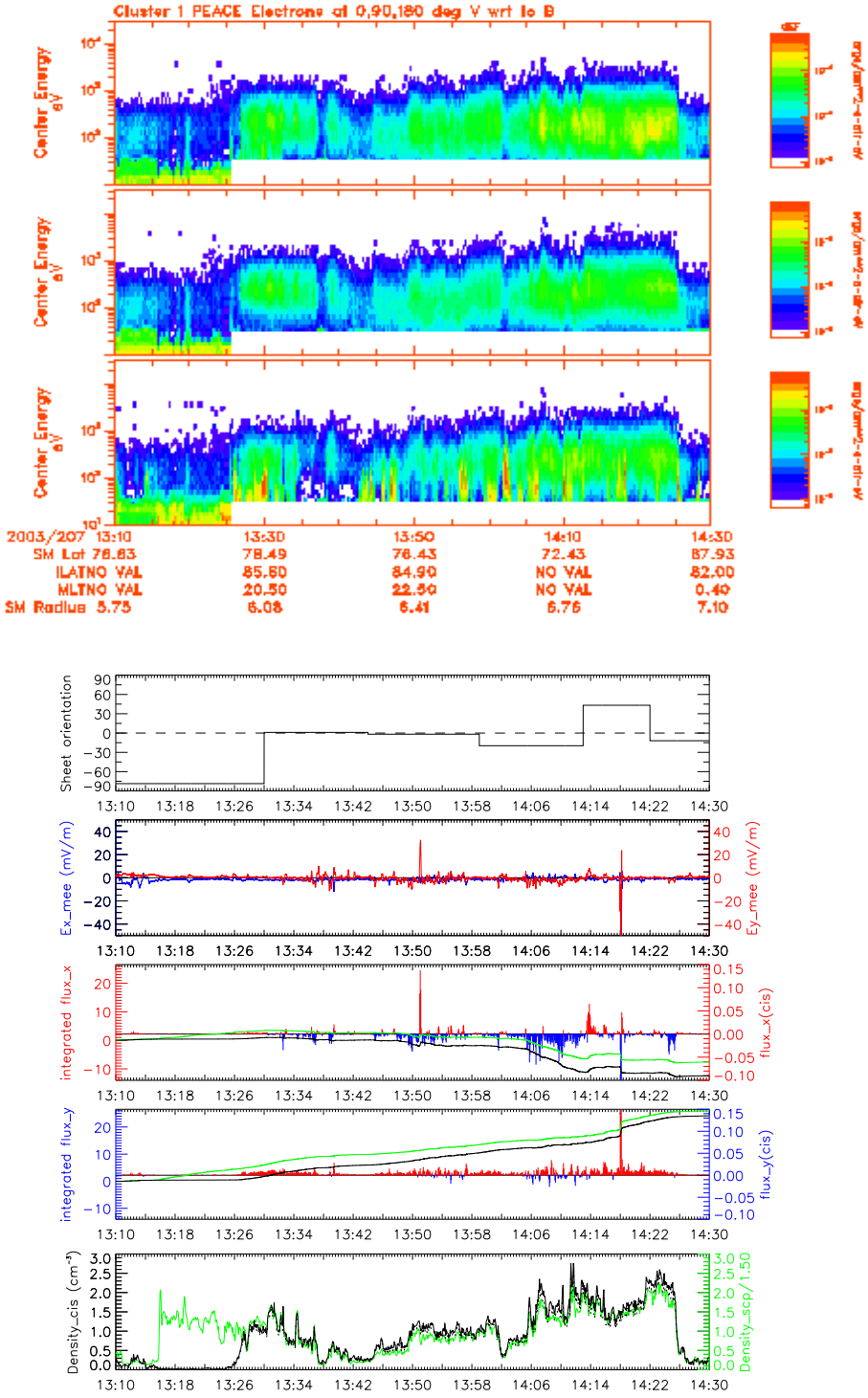

Figure C.30: 2003-07-26 Cluster 1

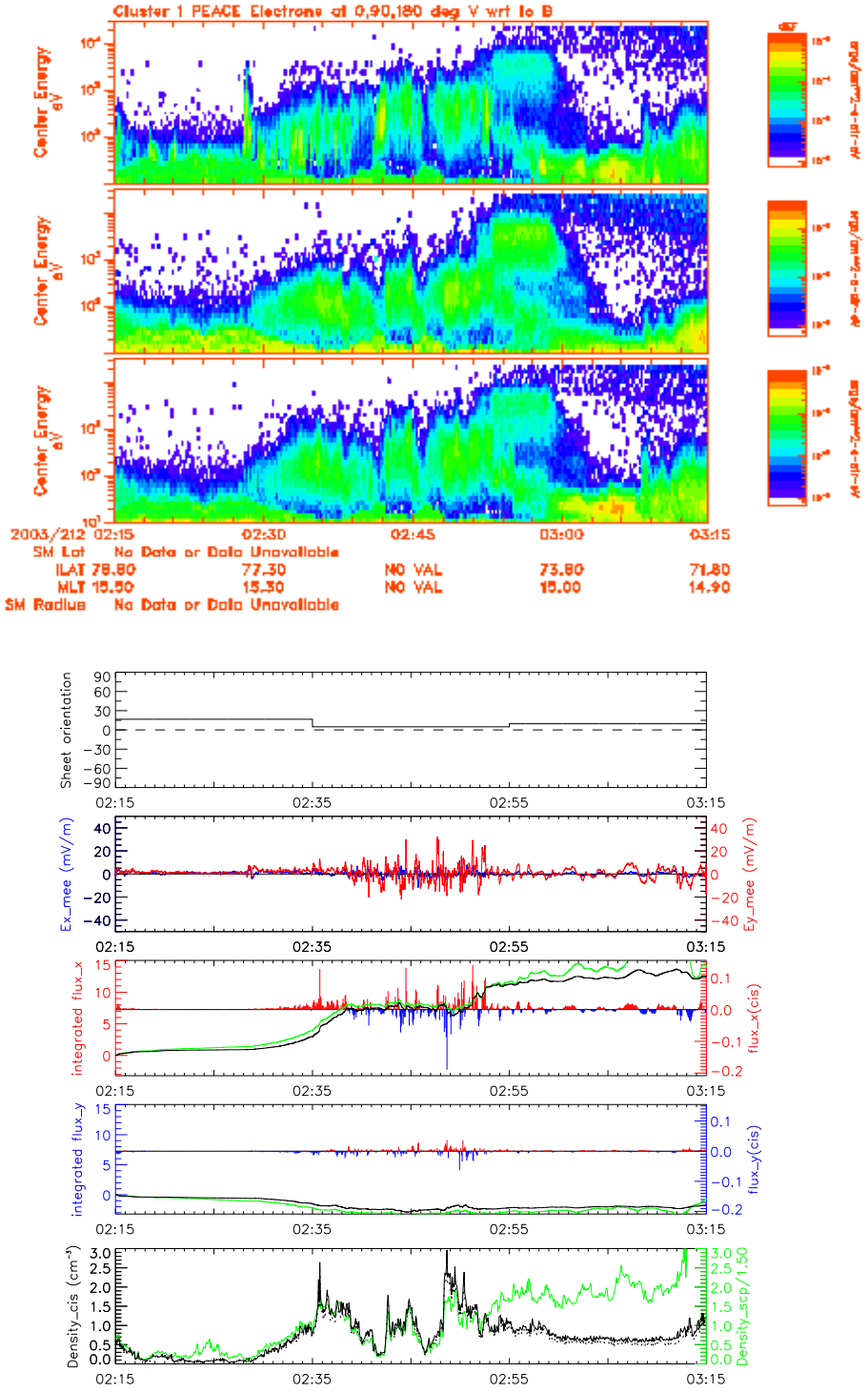

Figure C.31: 2003-07-31 Cluster 1

Appendix D

Field-aligned current plots

Plots that show PEACE data, potential, E-normal, B-normal, density, field-aligned currents and the particle flux in tangential direction. For plot description see chapter 5.2. Plot from one satellite per event is included. Plot from Cluster 1 2002-05-19 05.20-05.50 UT and plot from Cluster 1 2003-02-28 is missing because of wrong density data.

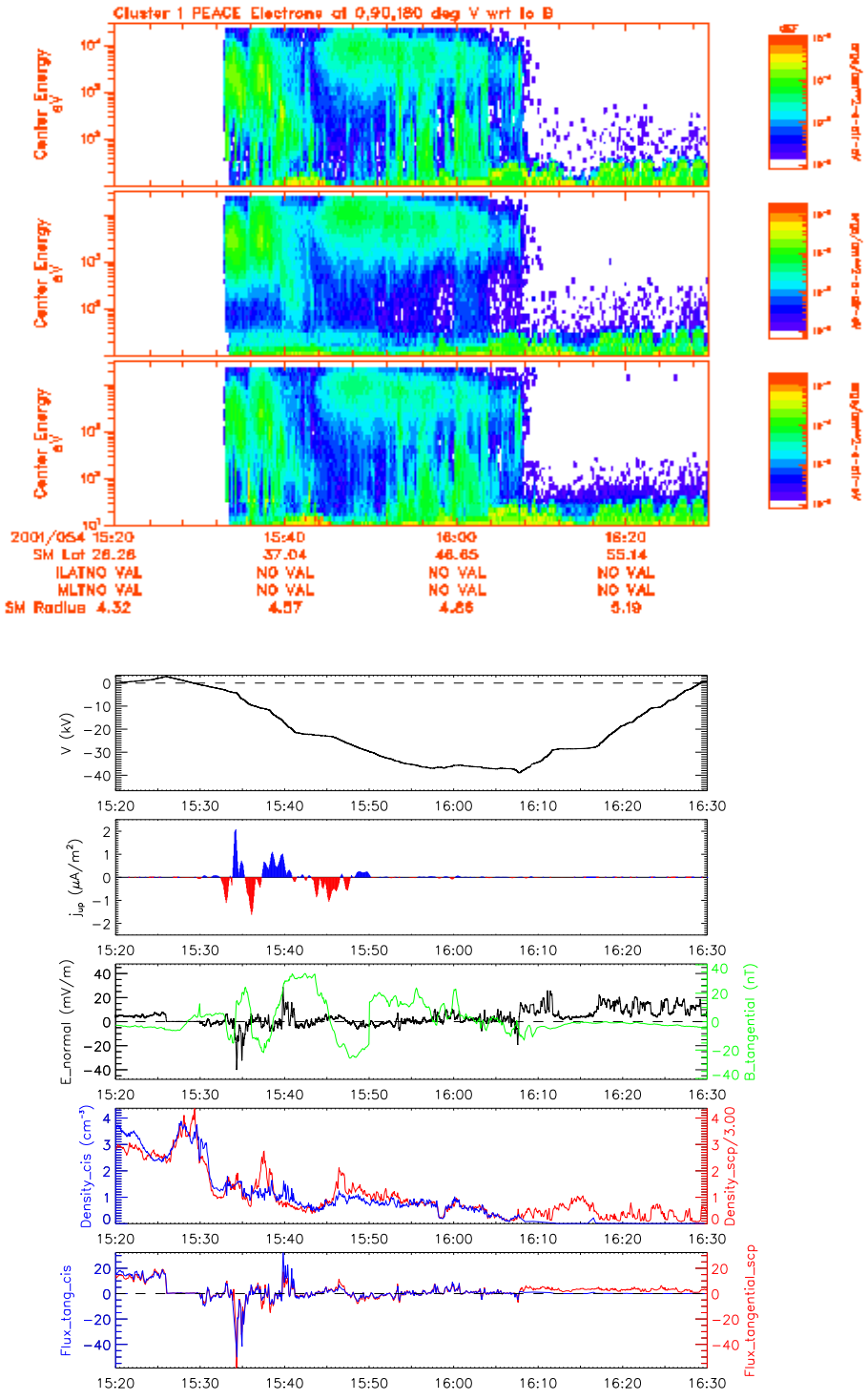

Figure D.1: 2001-02-23 Cluster 1

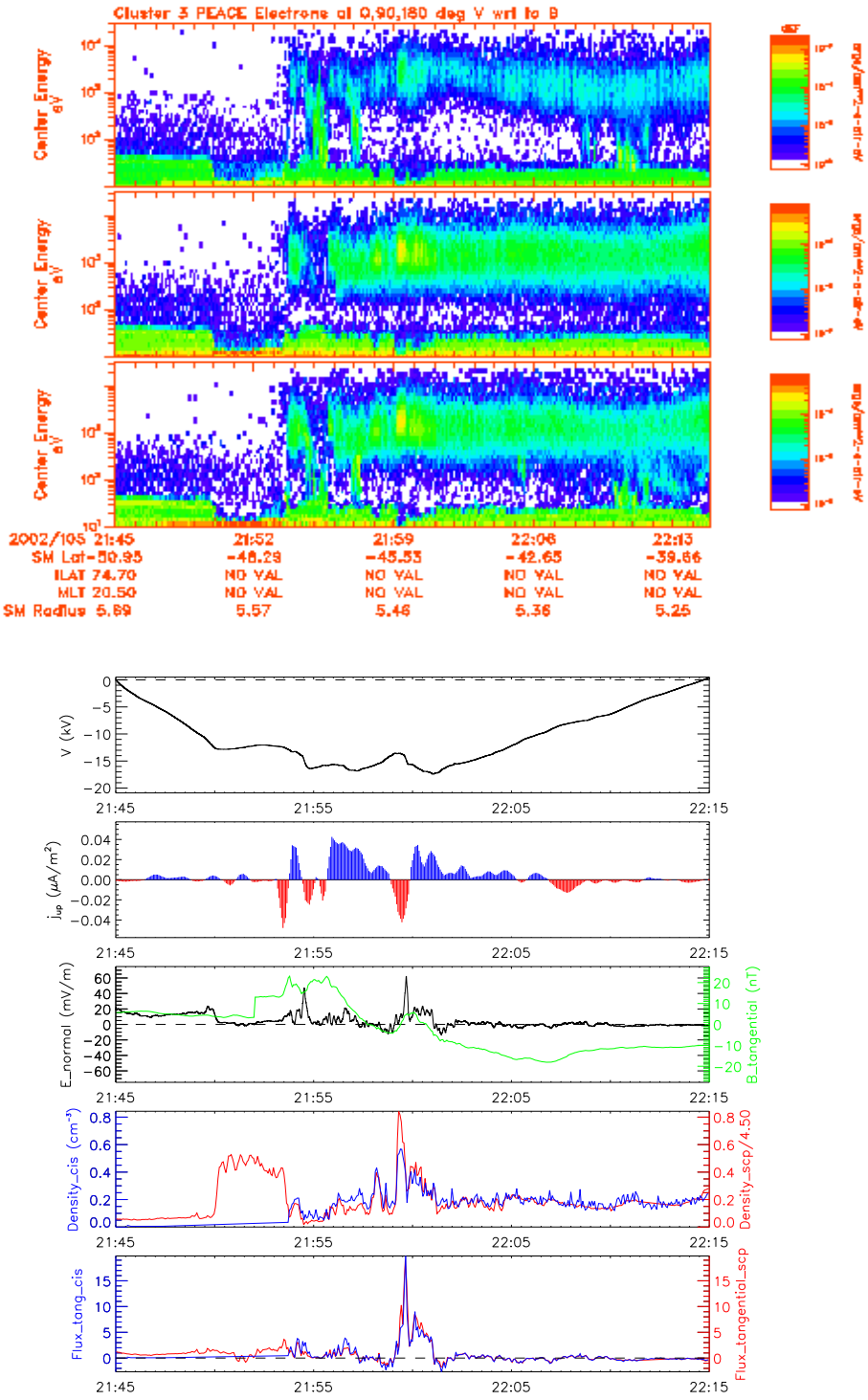

Figure D.2: 2002-04-15 Cluster 3

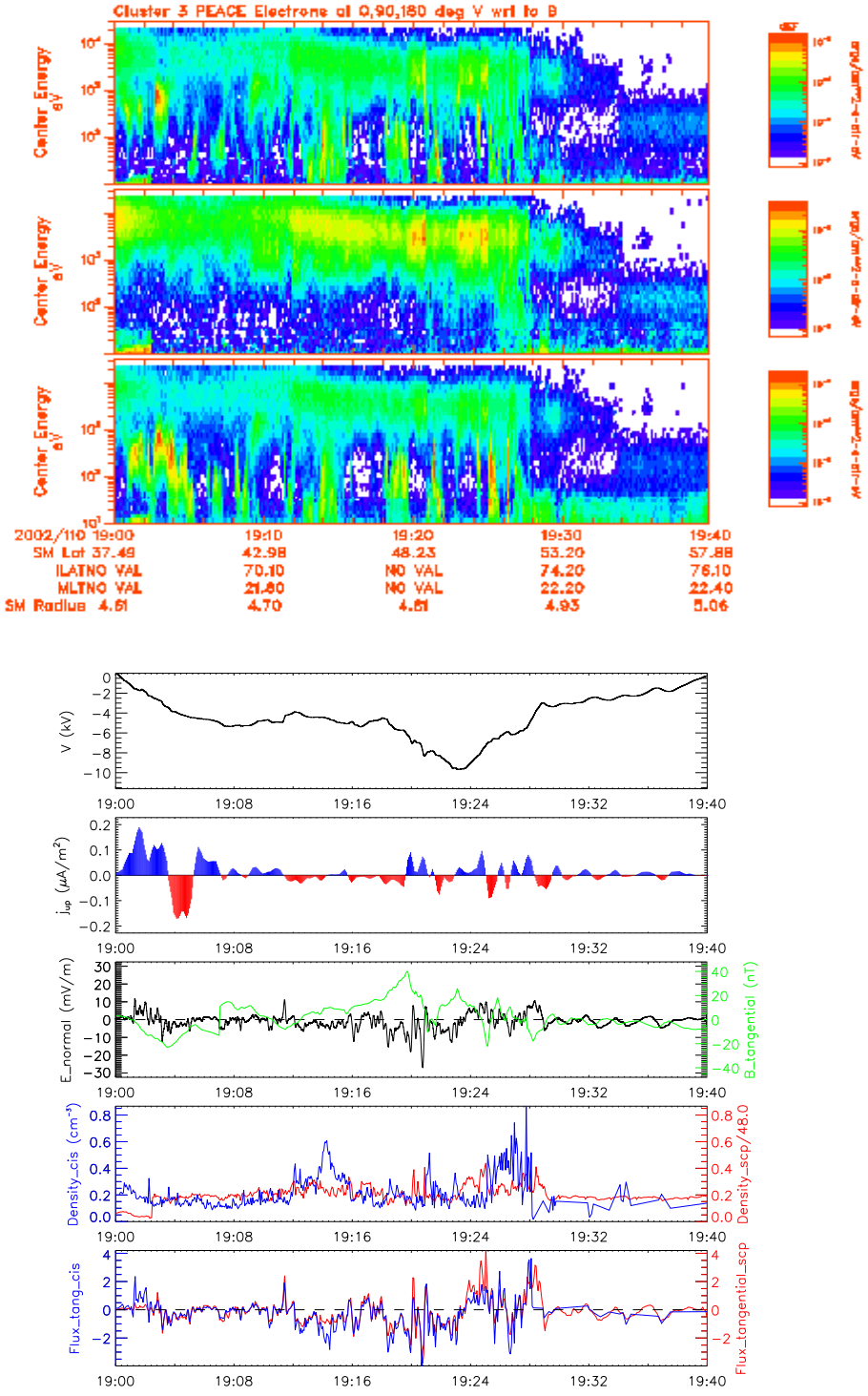

Figure D.3: 2002-04-20 Cluster 3

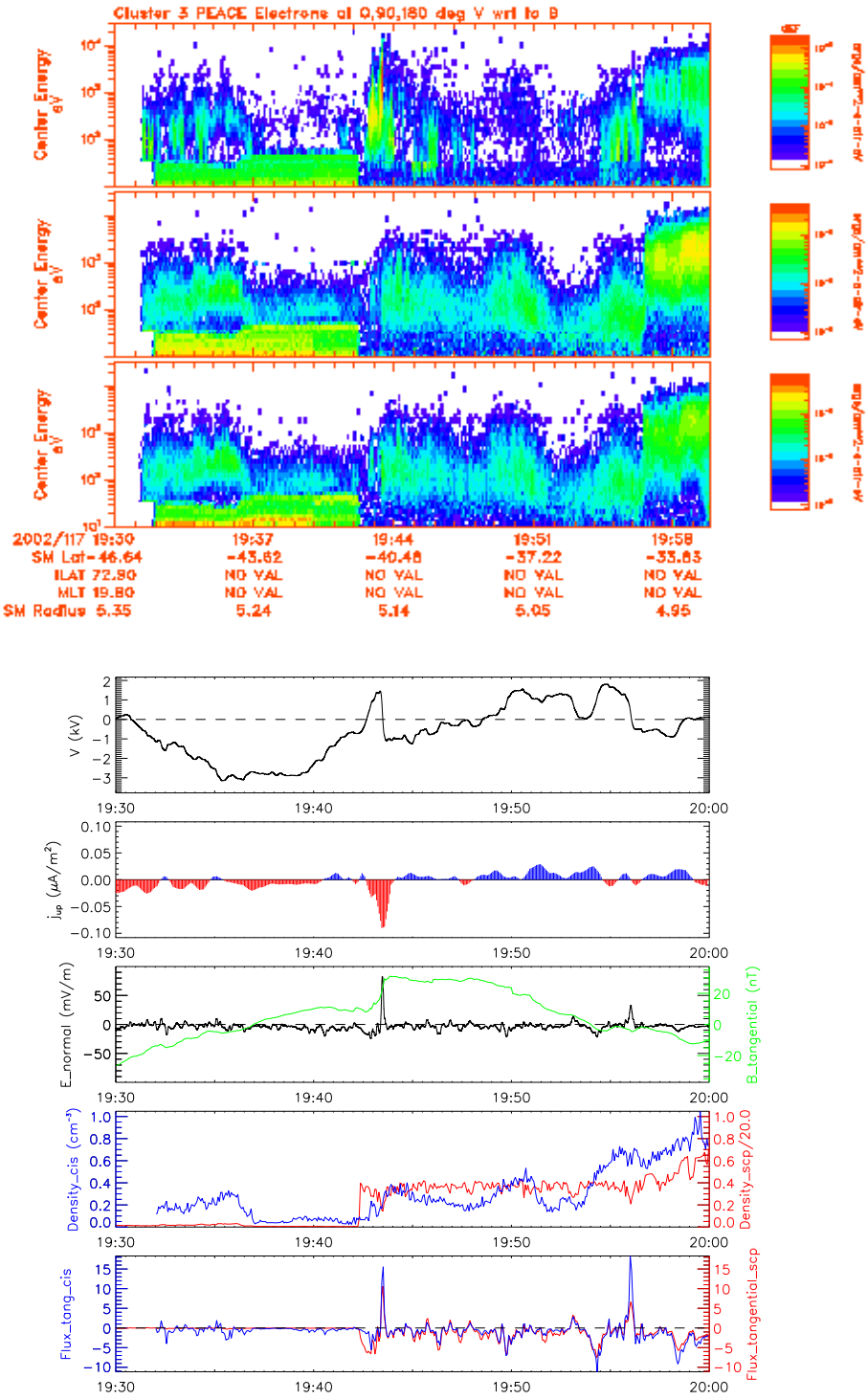

Figure D.4: 2002-04-27 Cluster 3

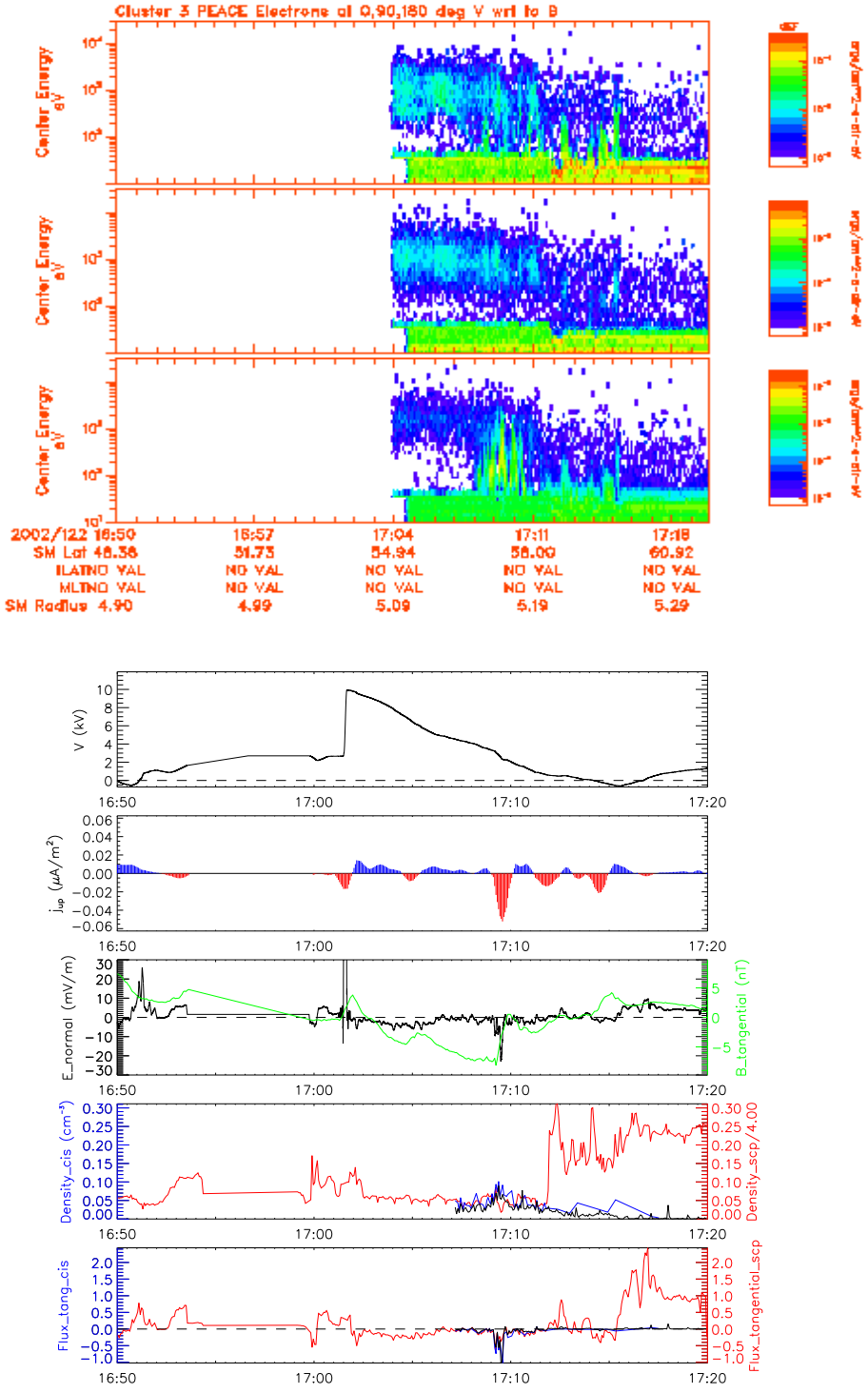

Figure D.5: 2002-05-02 Cluster 3

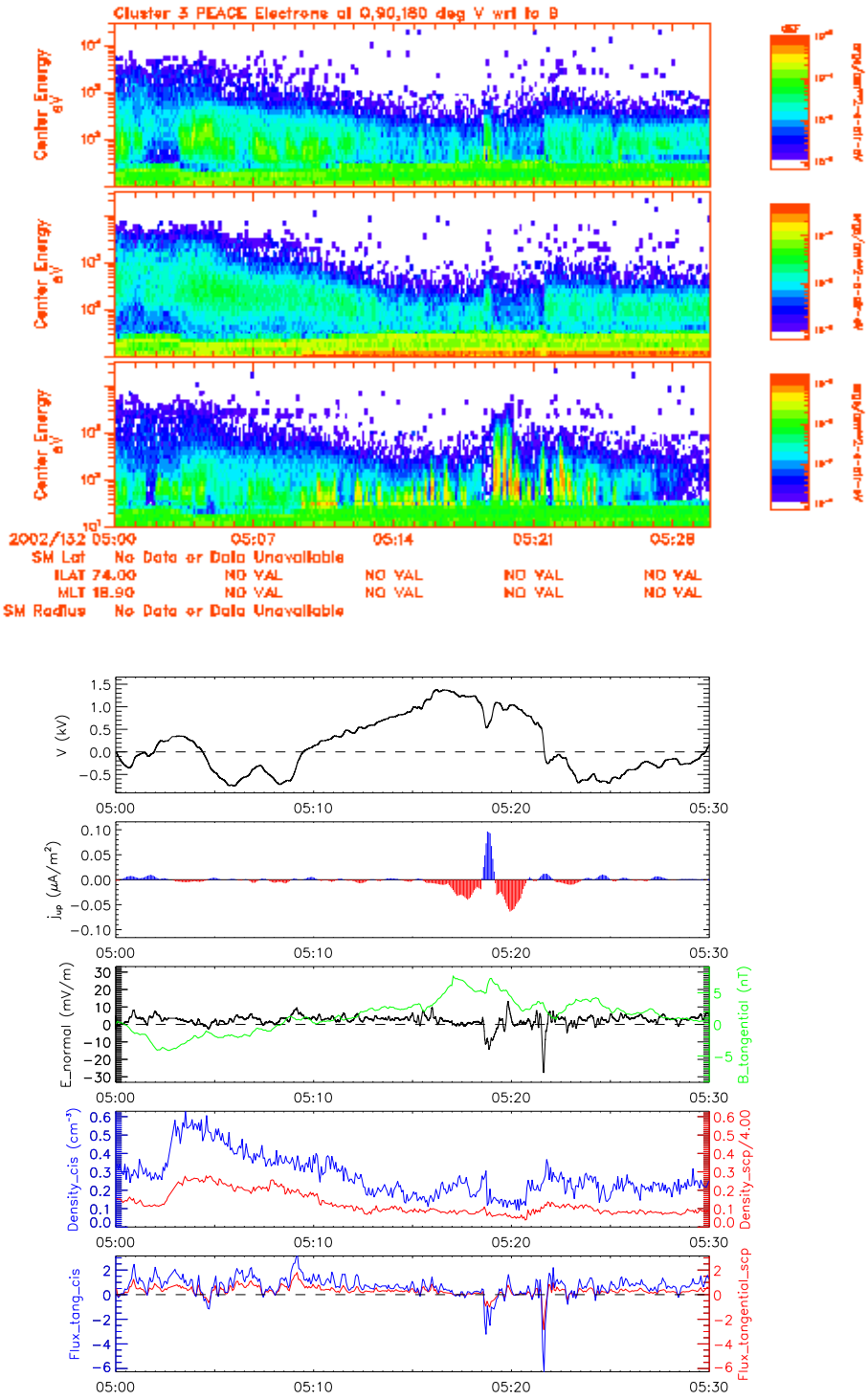

Figure D.6: 2002-05-12 Cluster 3

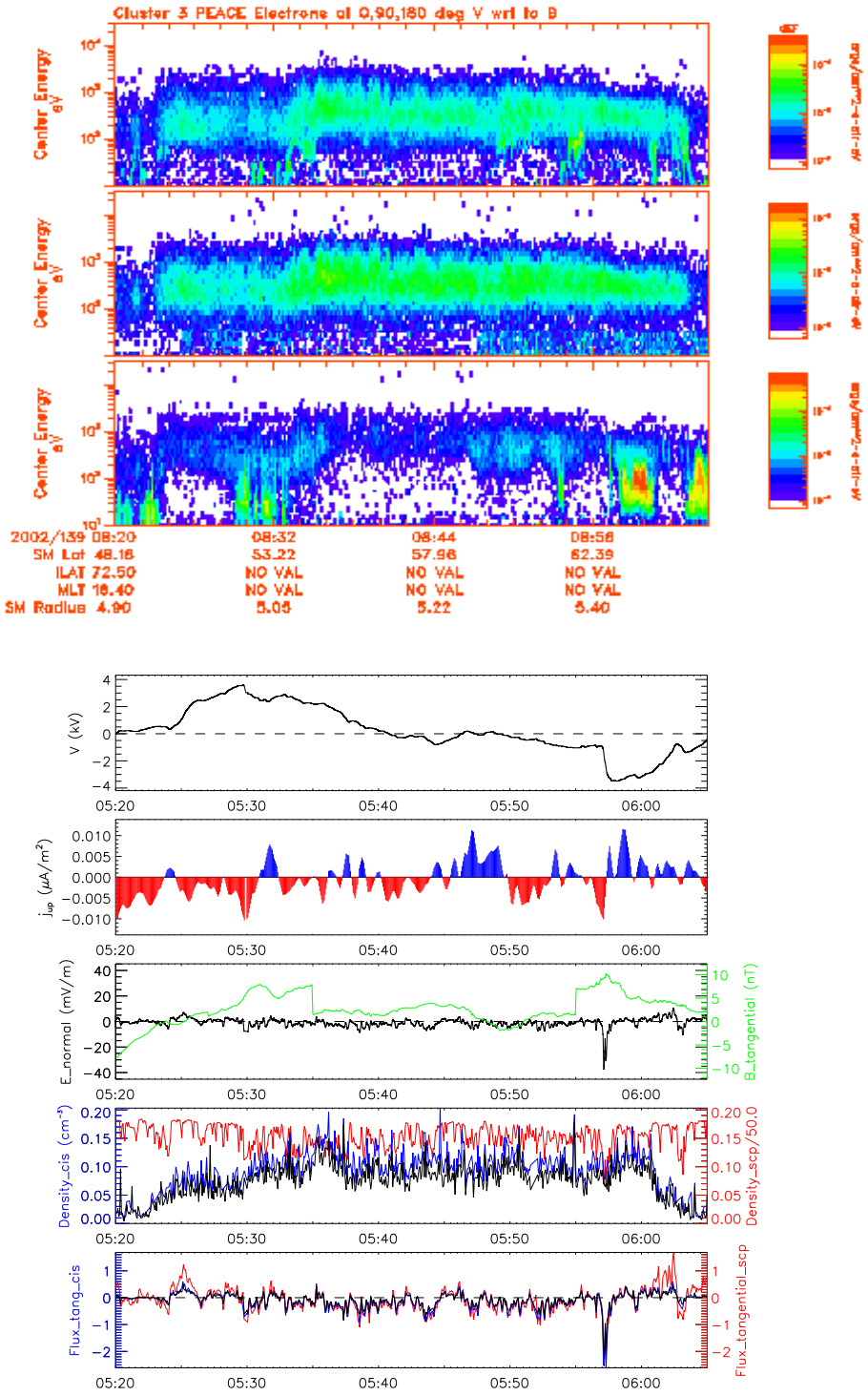

Figure D.7: 2002-05-19 Cluster 3

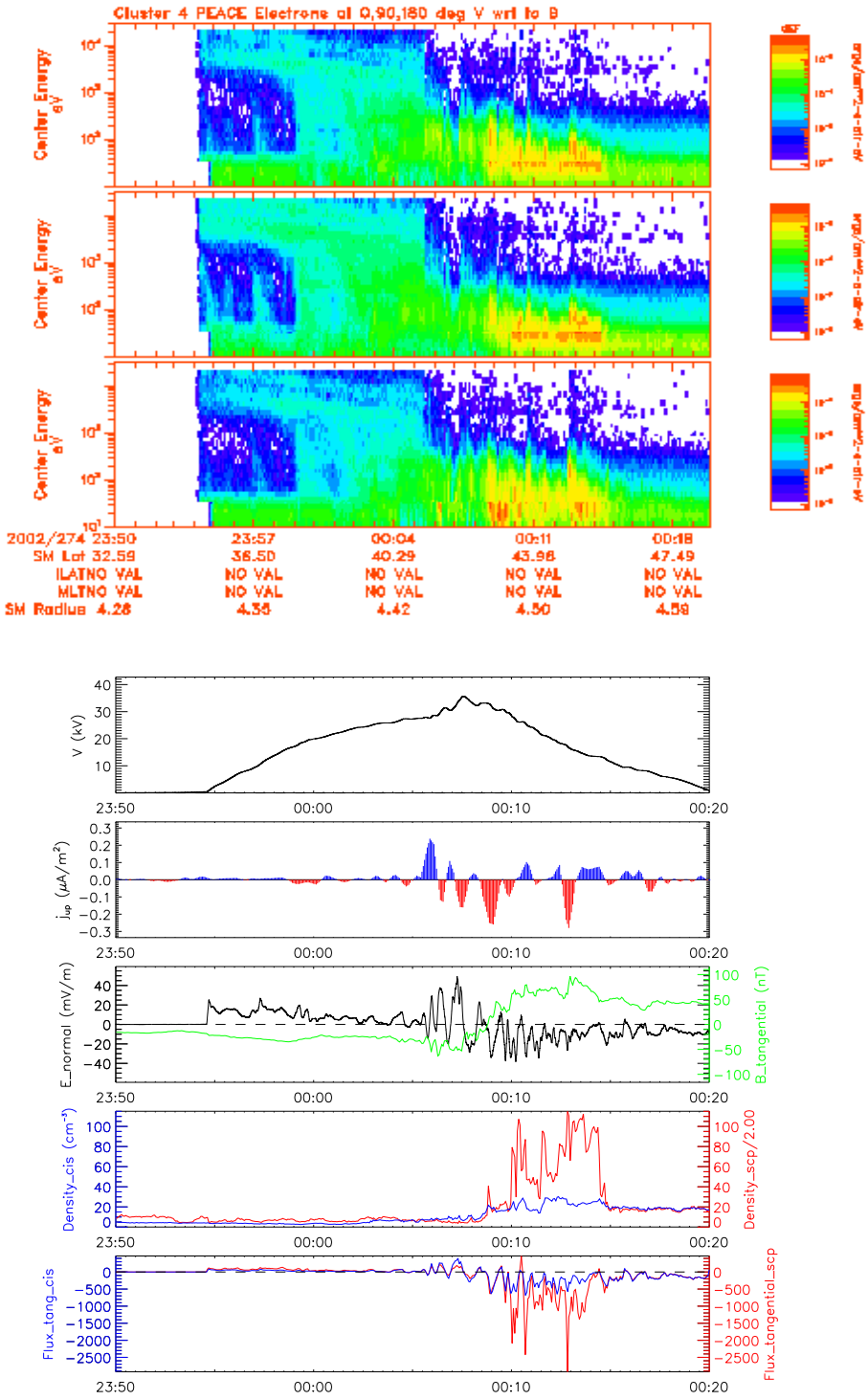

Figure D.8: 2002-10-01 Cluster 4

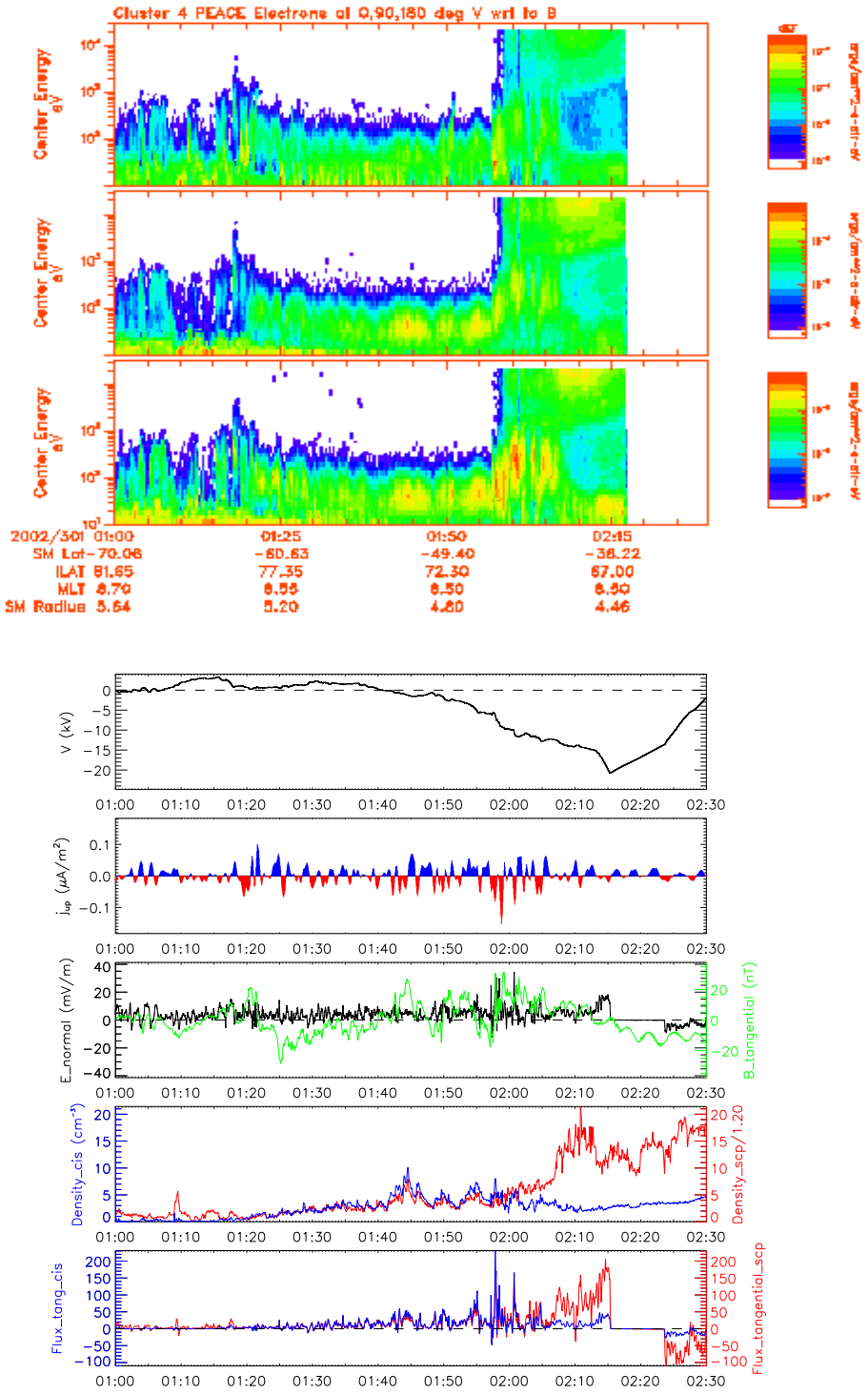

Figure D.9: 2002-10-28 Cluster 4

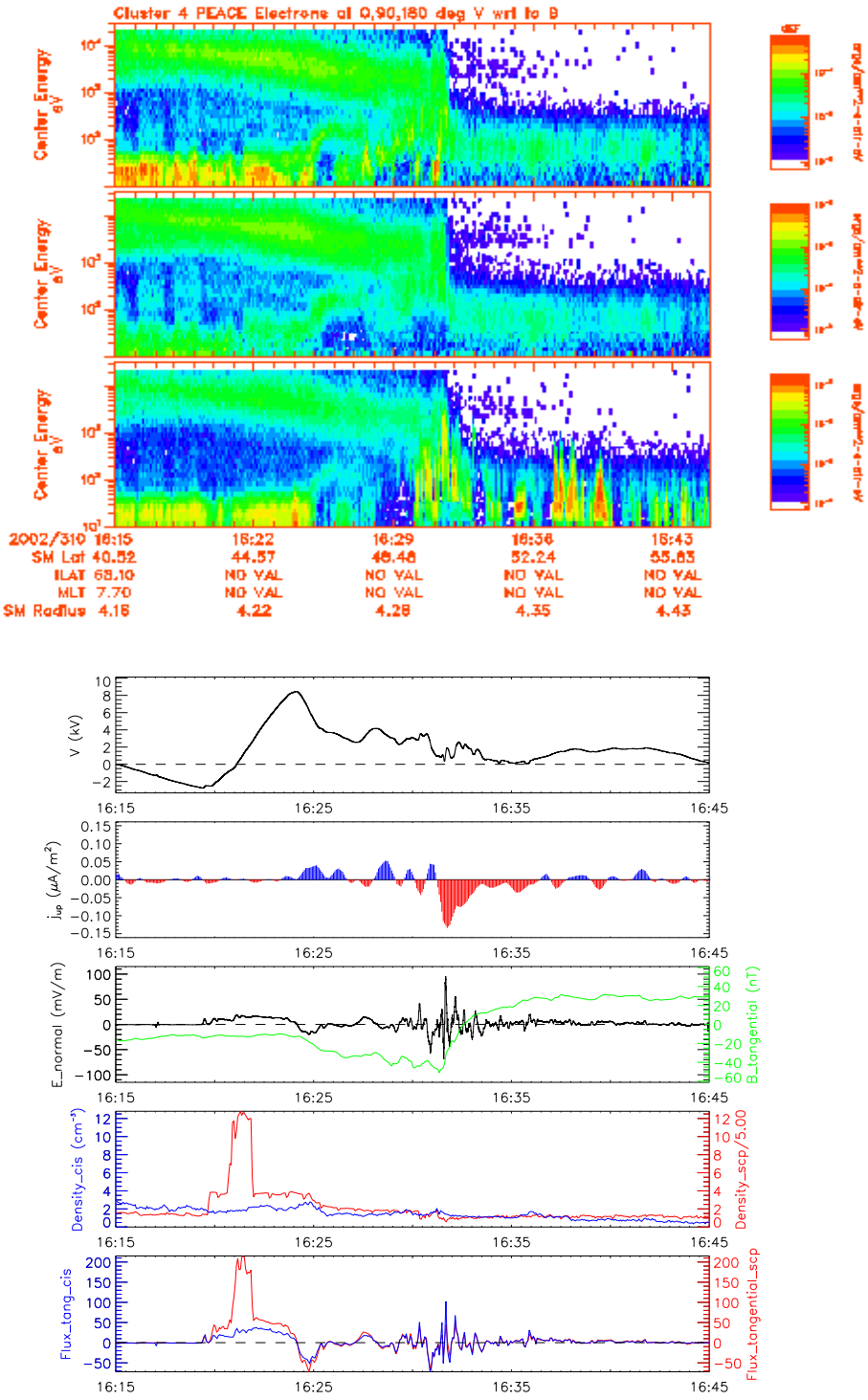

Figure D.10: 2002-11-06 Cluster 4

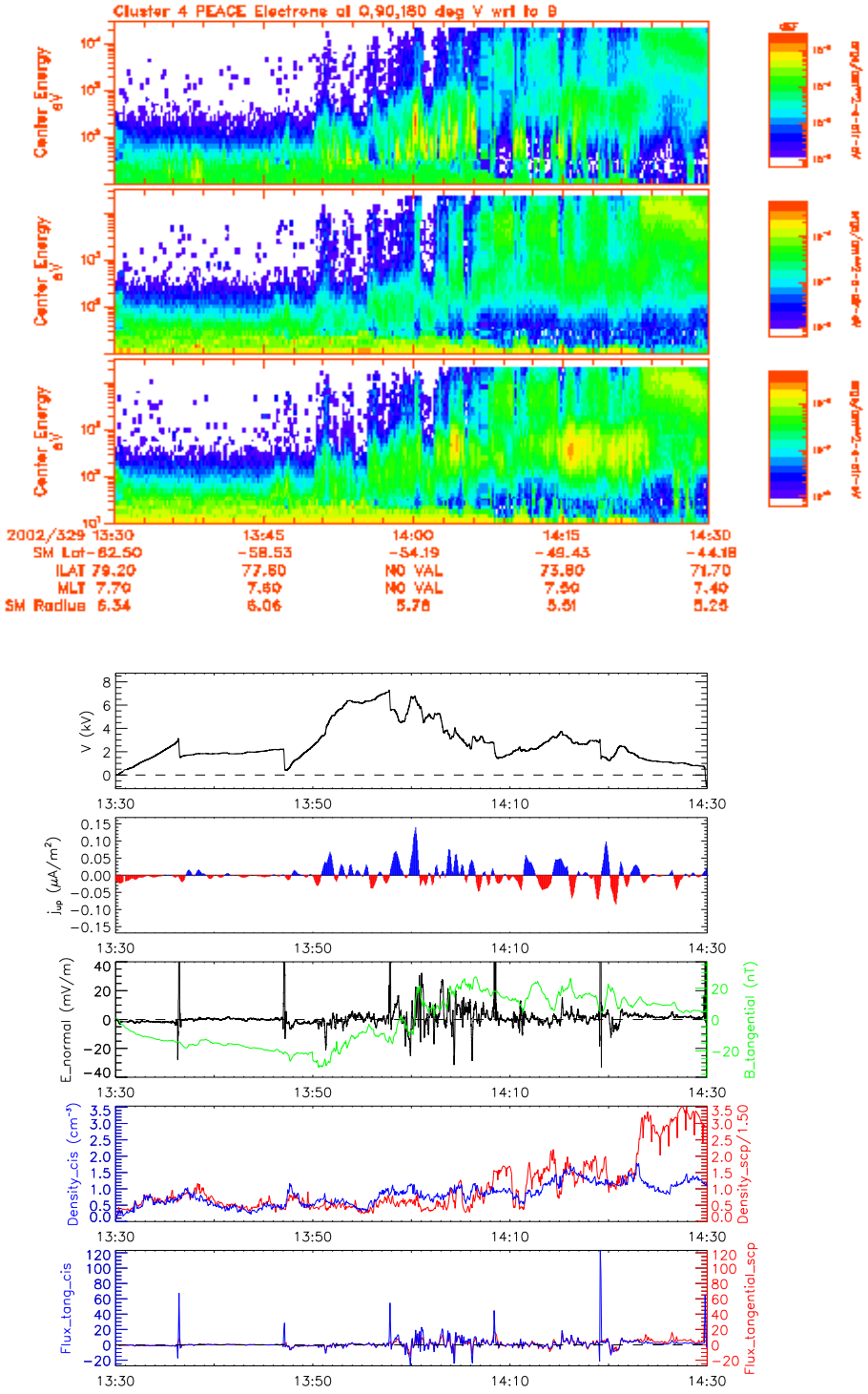

Figure D.11: 2002-11-25 Cluster 4

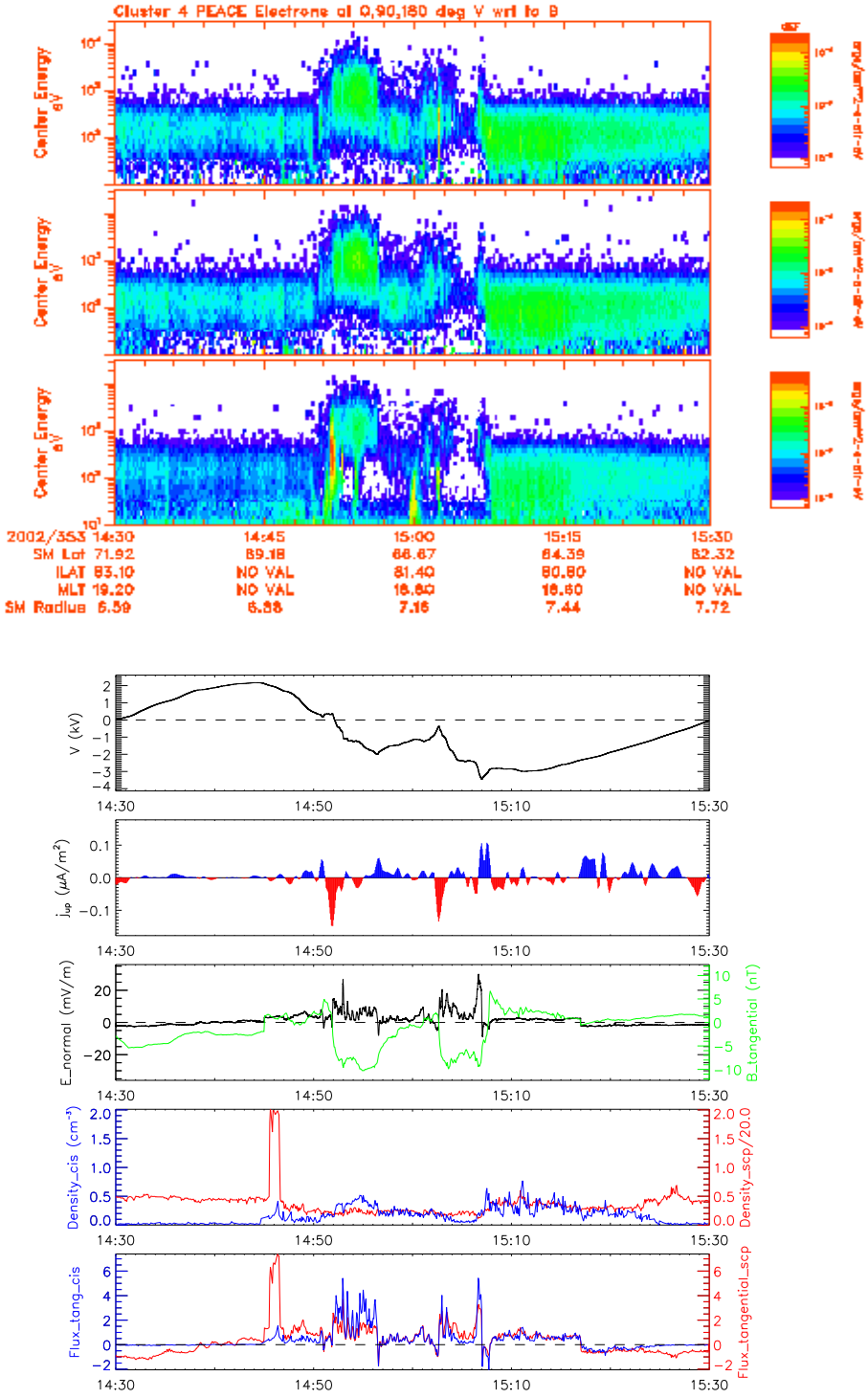

Figure D.12: 2002-12-19 Cluster 4

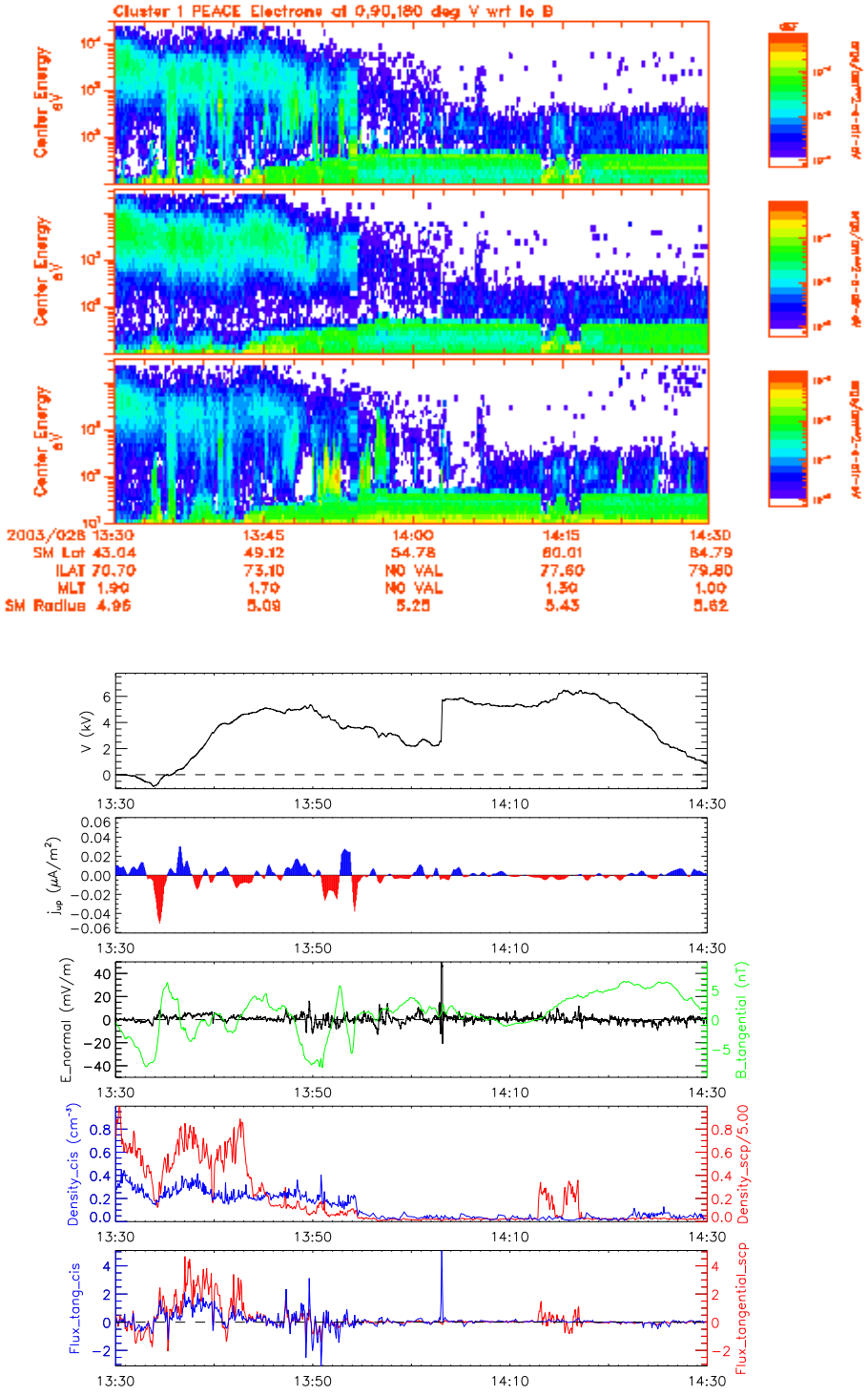

Figure D.13: 2003-01-26 Cluster 4

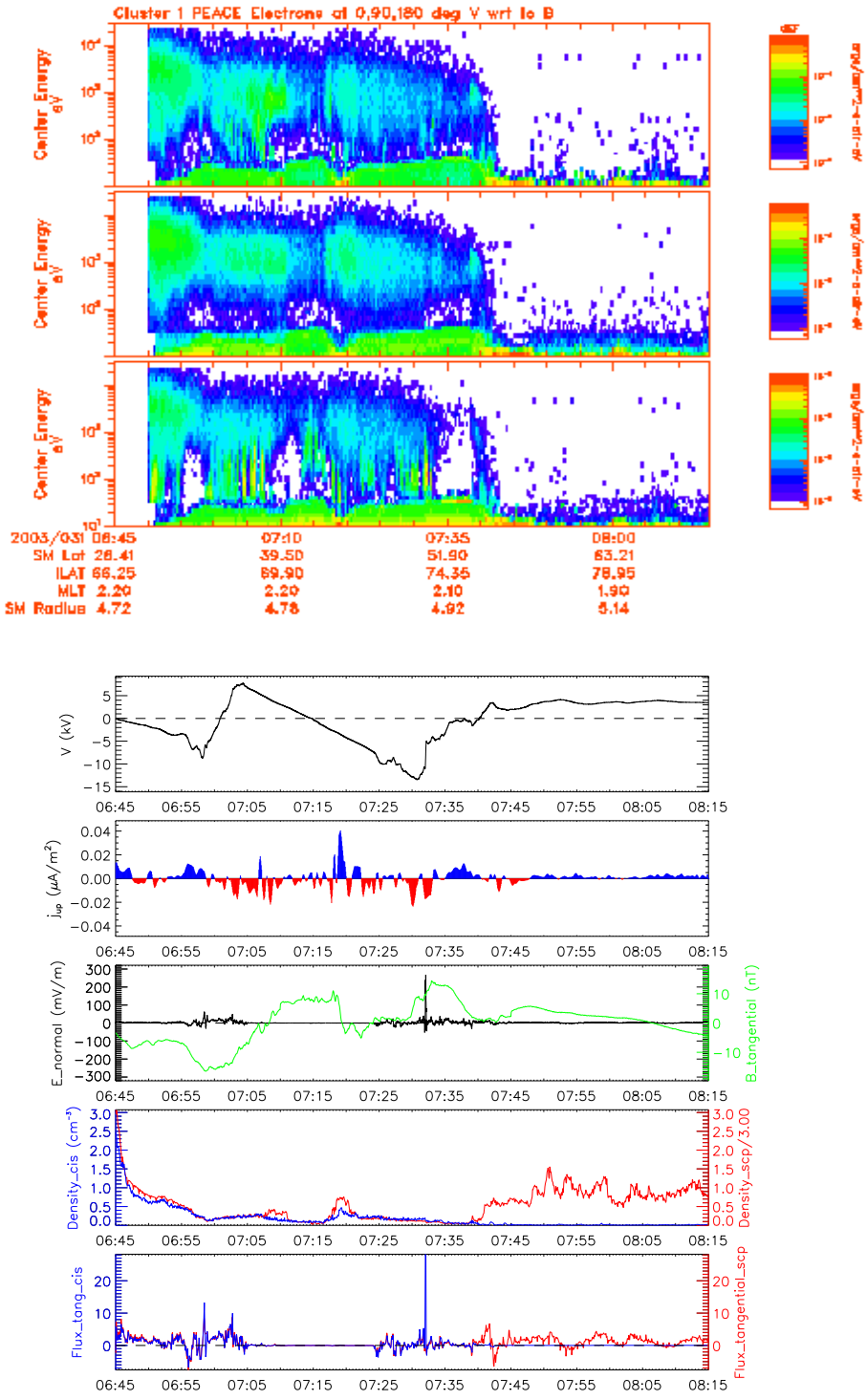

Figure D.14: 2003-01-31 Cluster 1

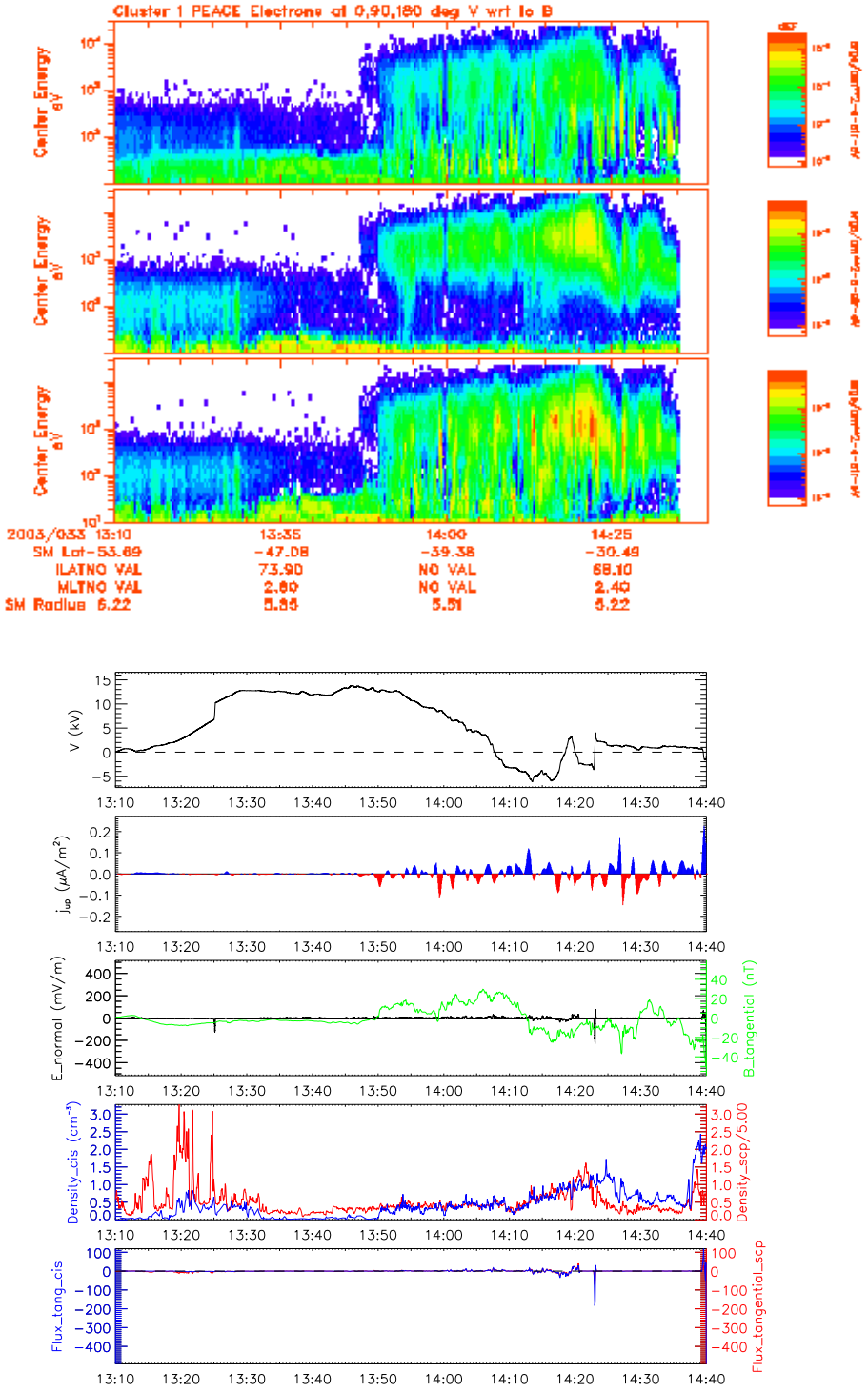

Figure D.15: 2003-02-02 Cluster 1

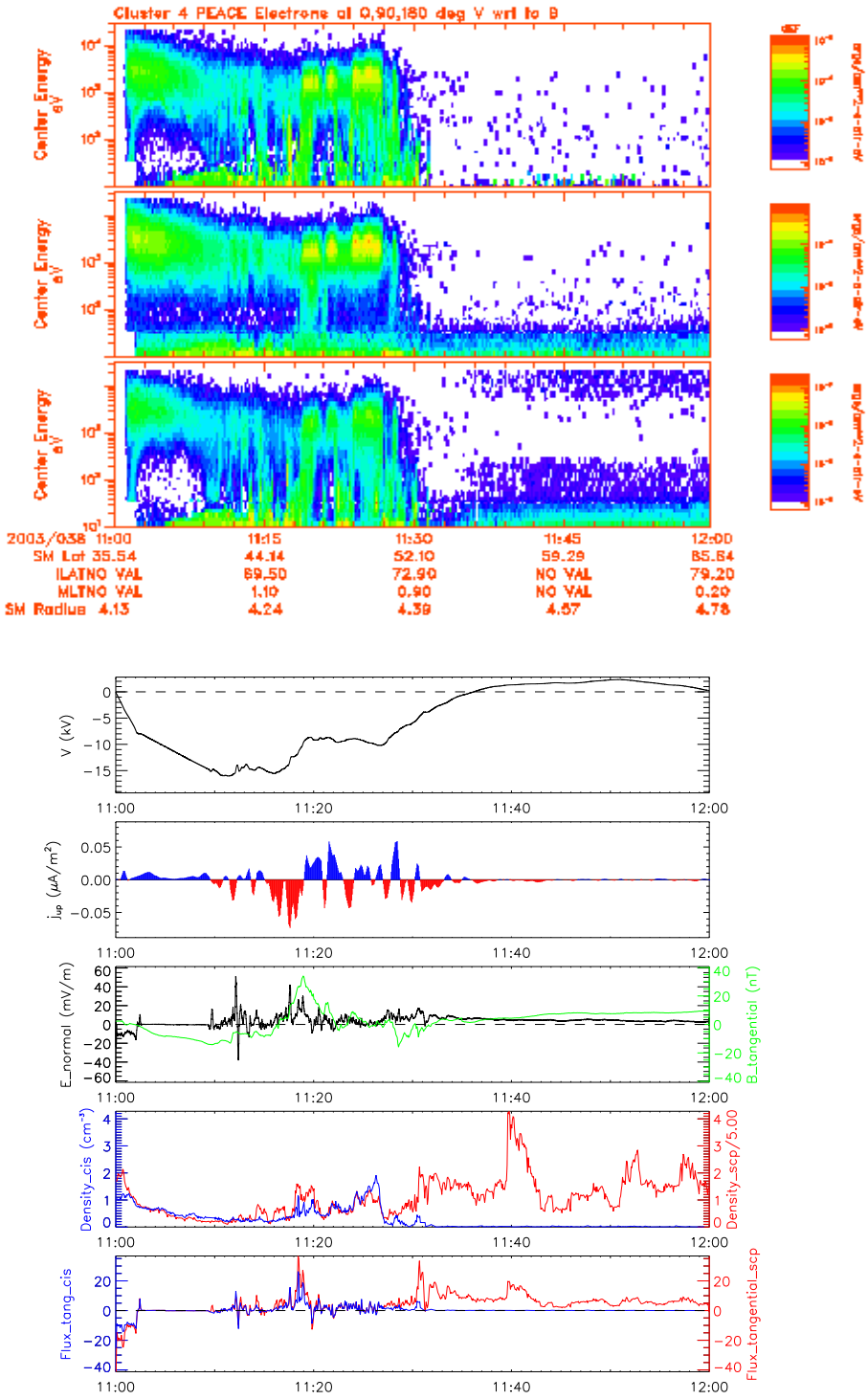

Figure D.16: 2003-02-07 Cluster 4

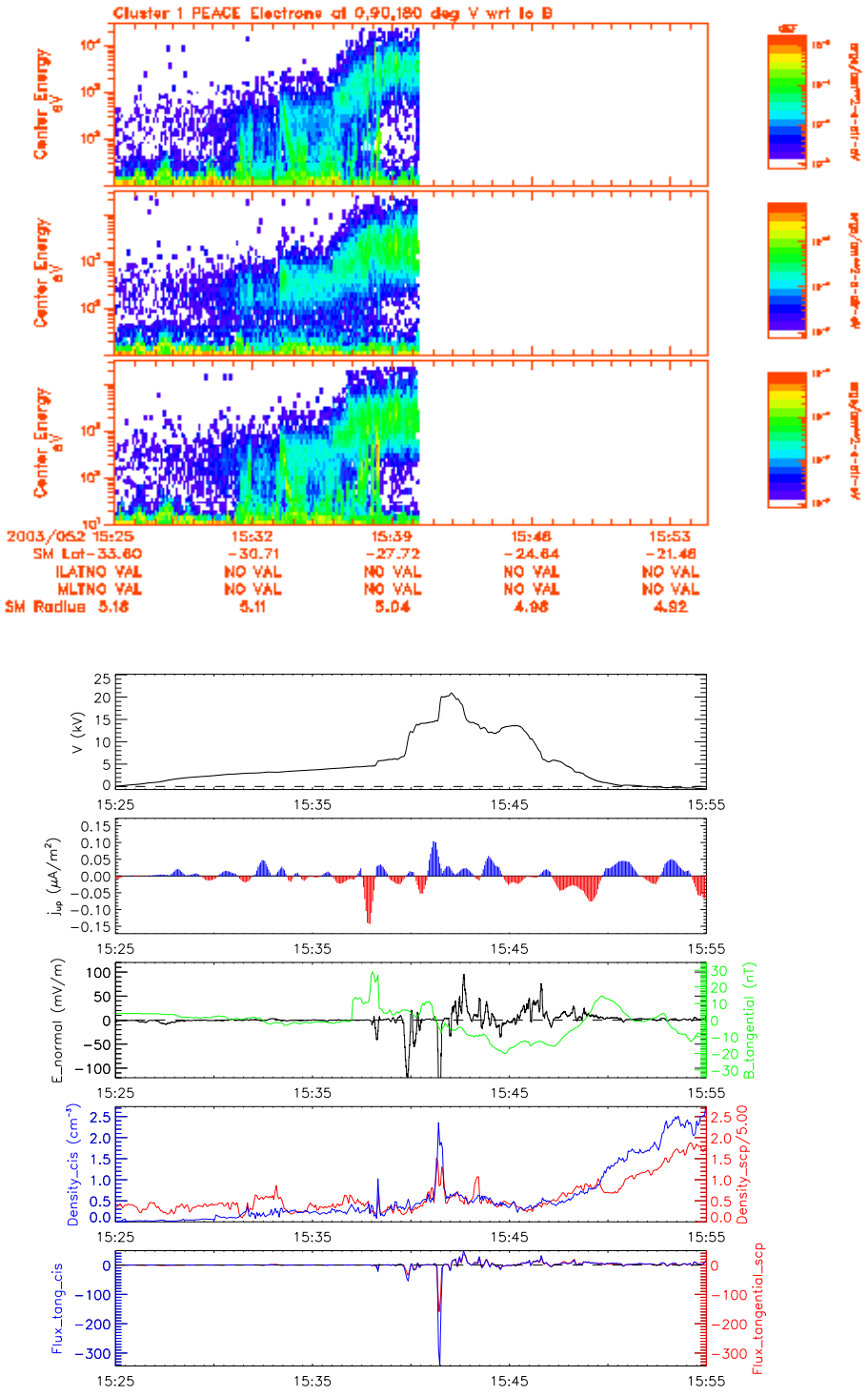

Figure D.17: 2003-02-21 Cluster 1

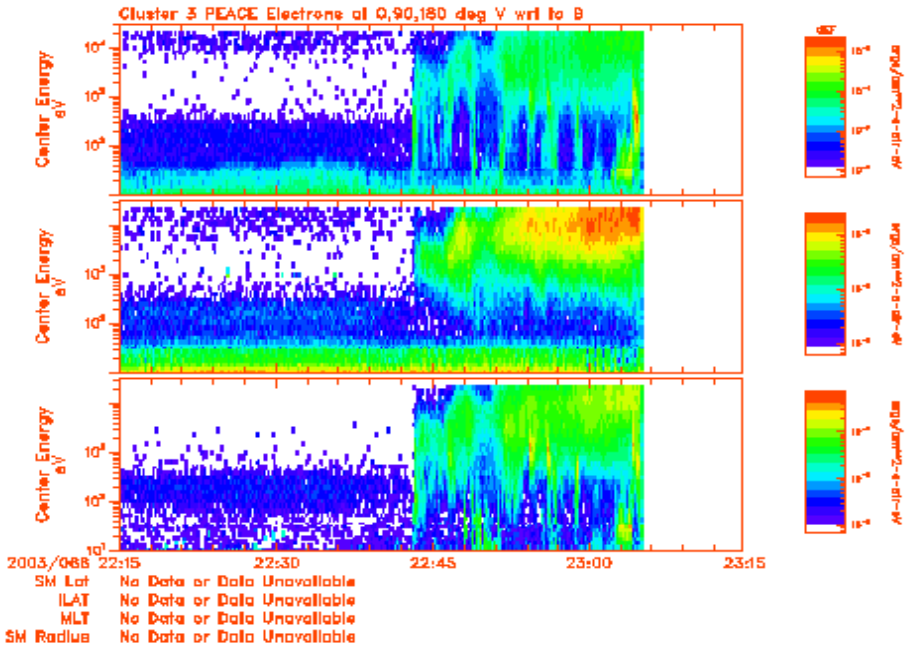

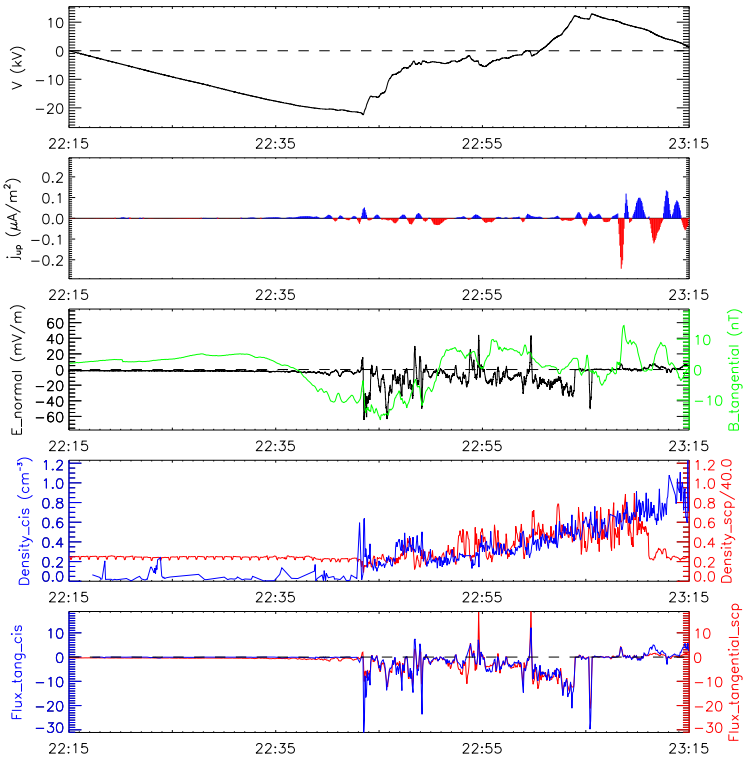

Figure D.18: 2003-03-07 Cluster 3

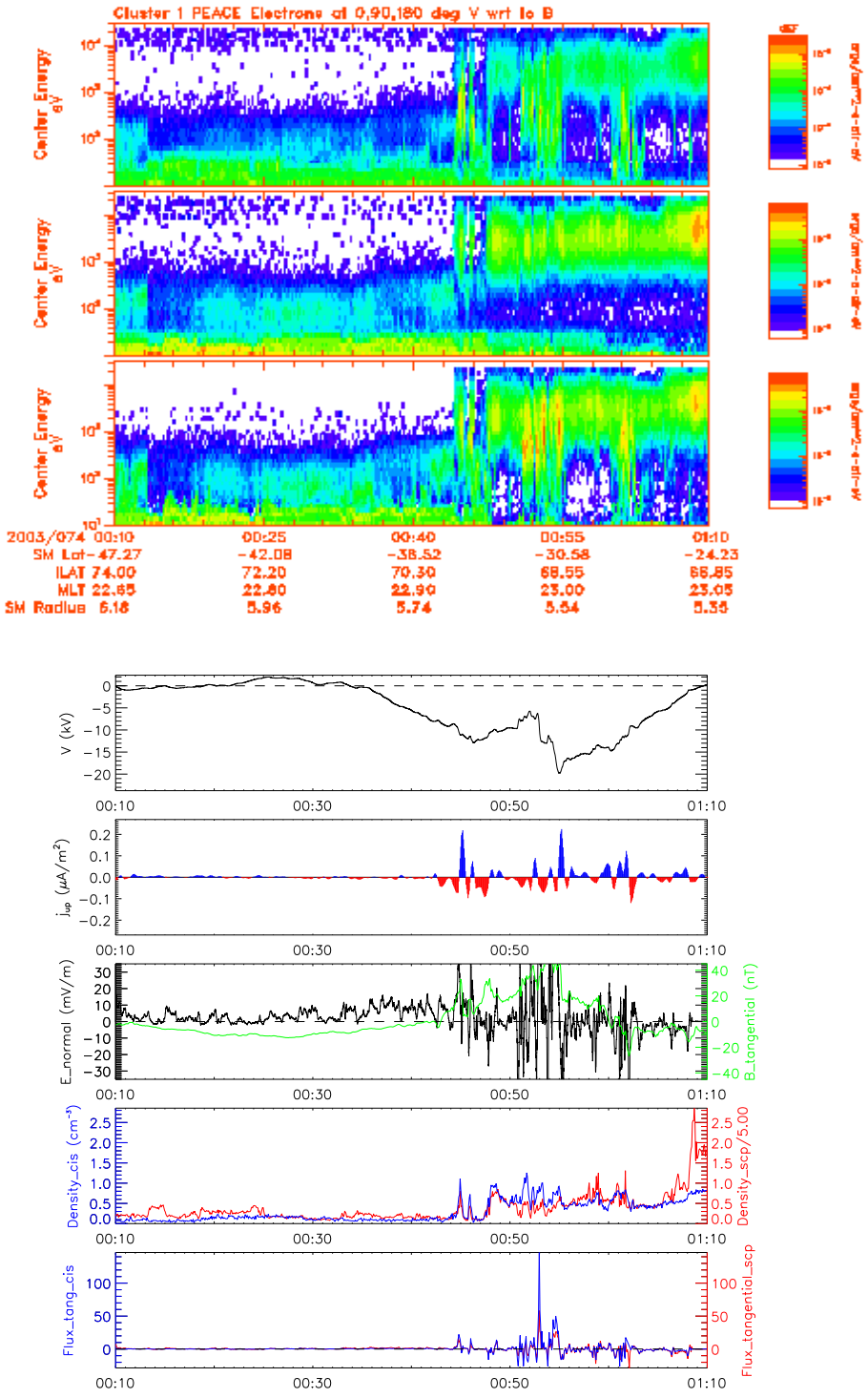

Figure D.19: 2003-03-15 Cluster 1

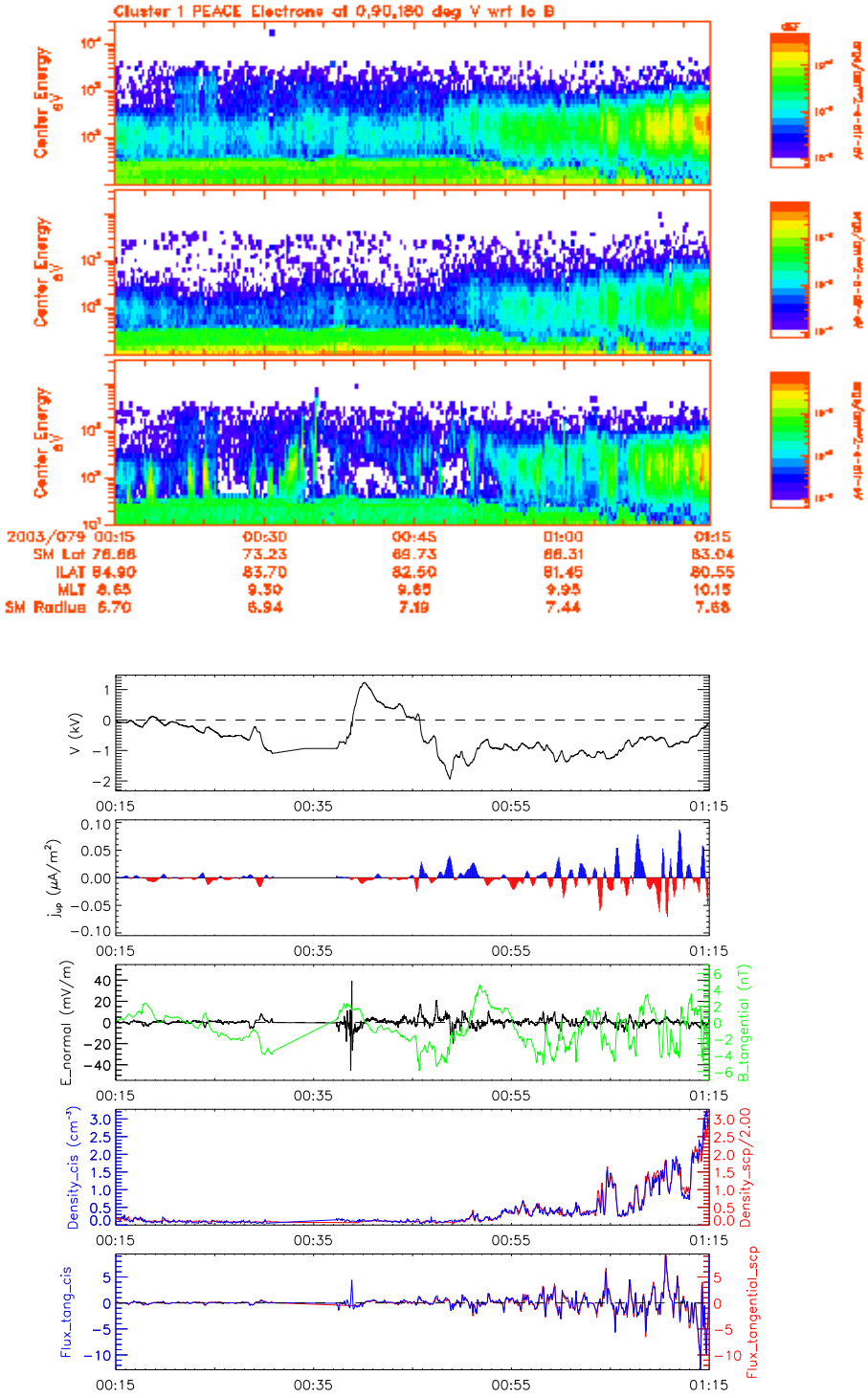

Figure D.20: 2003-03-20 Cluster 1

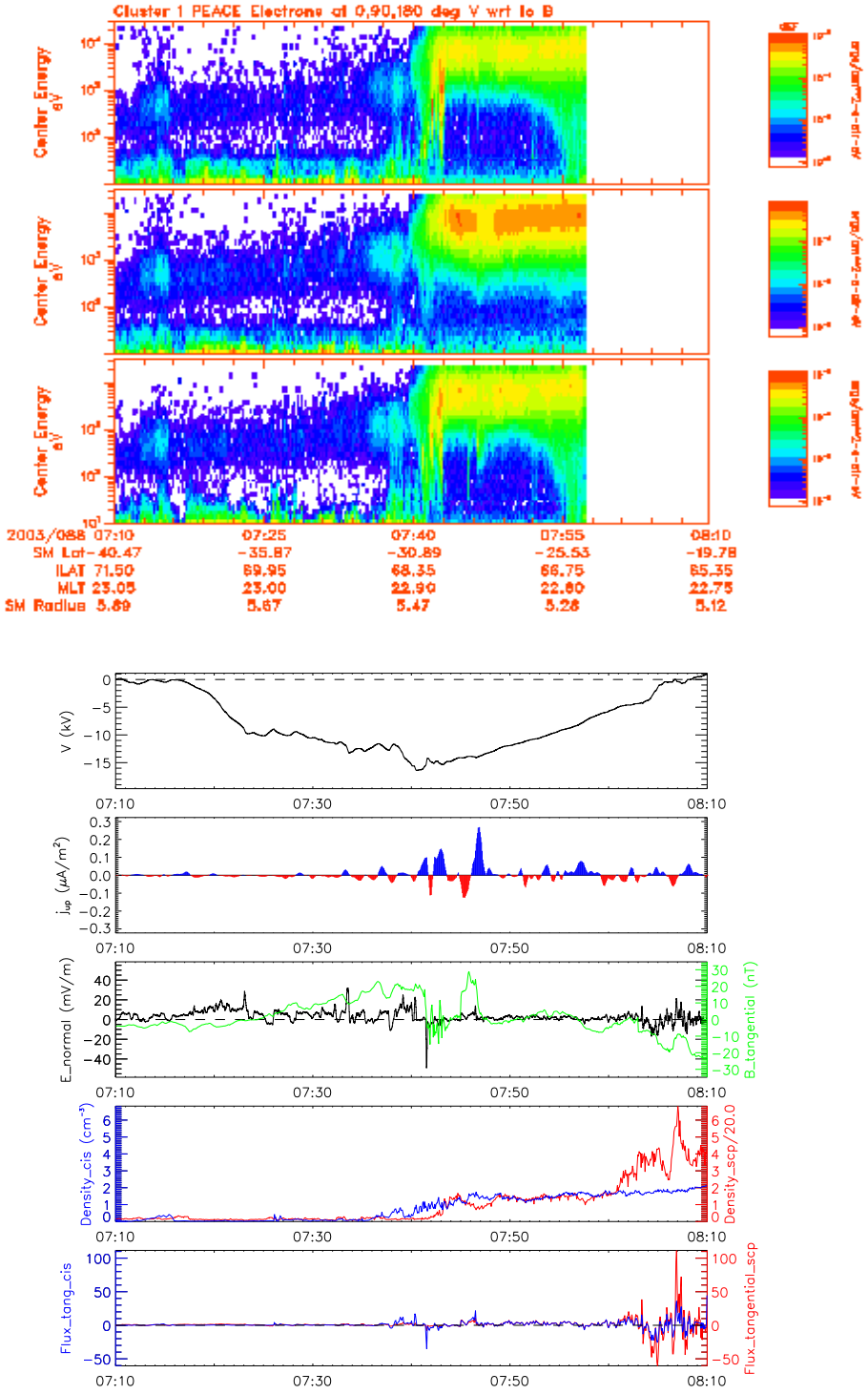

Figure D.21: 2003-03-29 Cluster 1

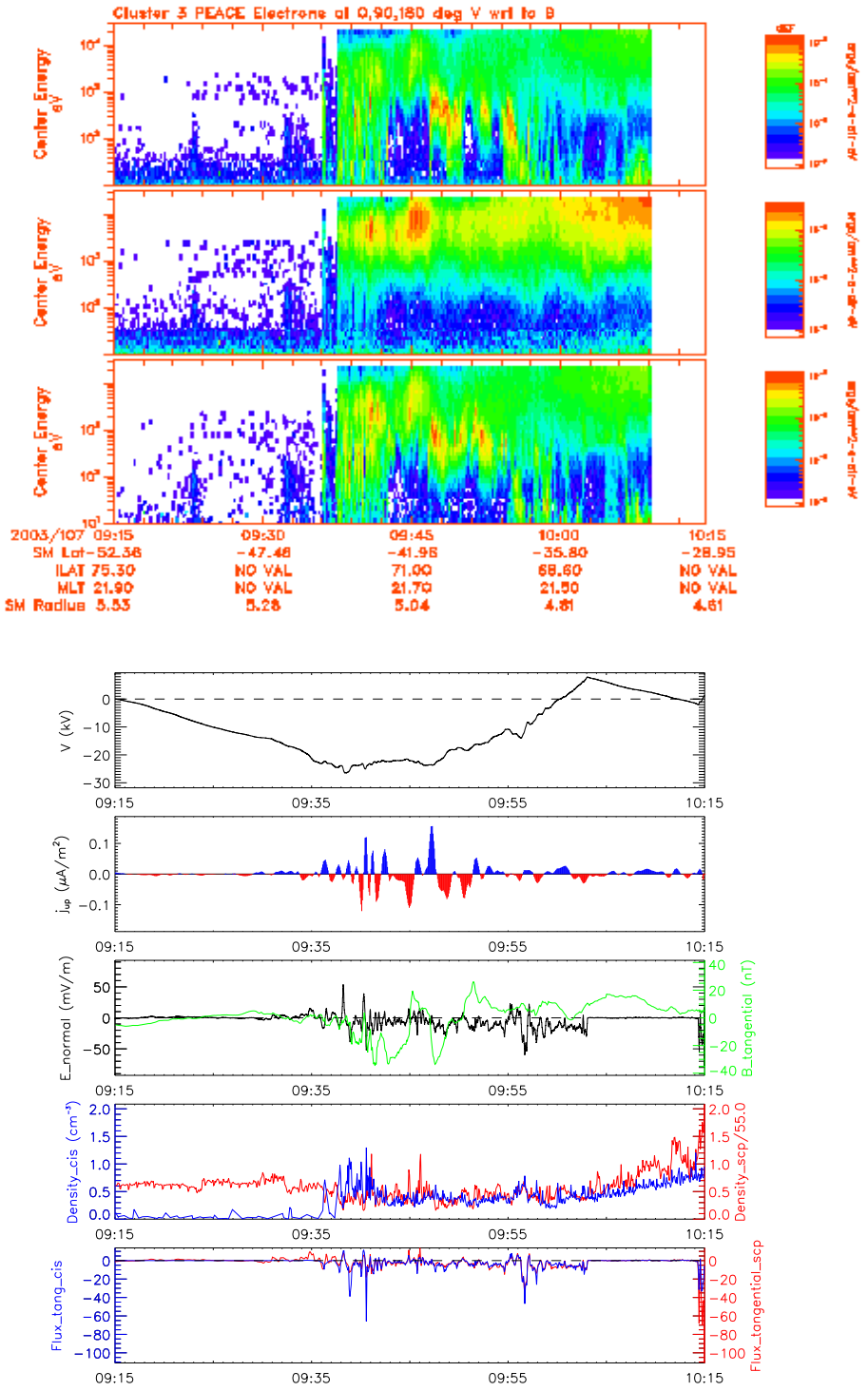

Figure D.22: 2003-04-17 Cluster 3

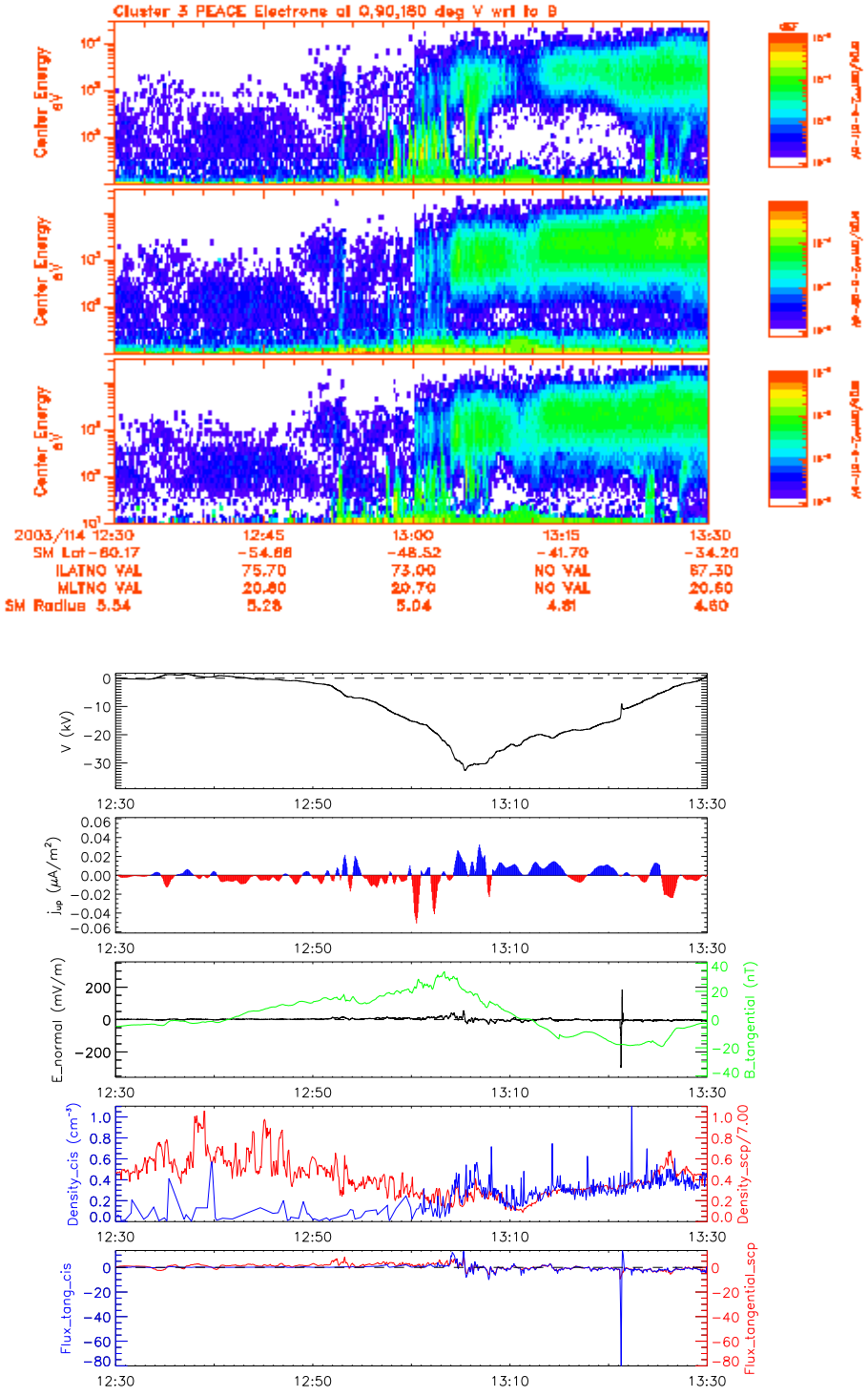

Figure D.23: 2003-04-24 Cluster 3

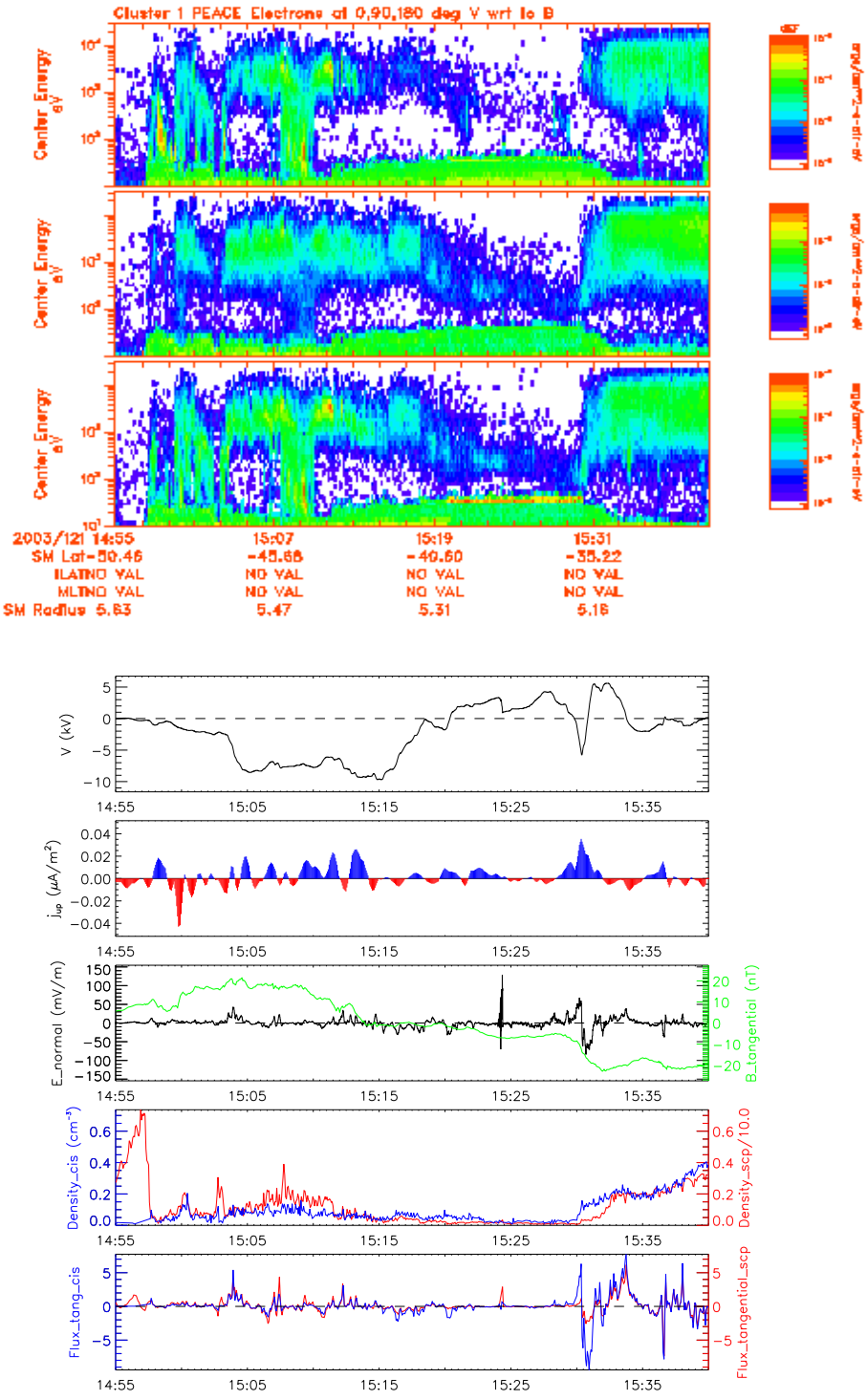

Figure D.24: 2003-05-01 Cluster 1

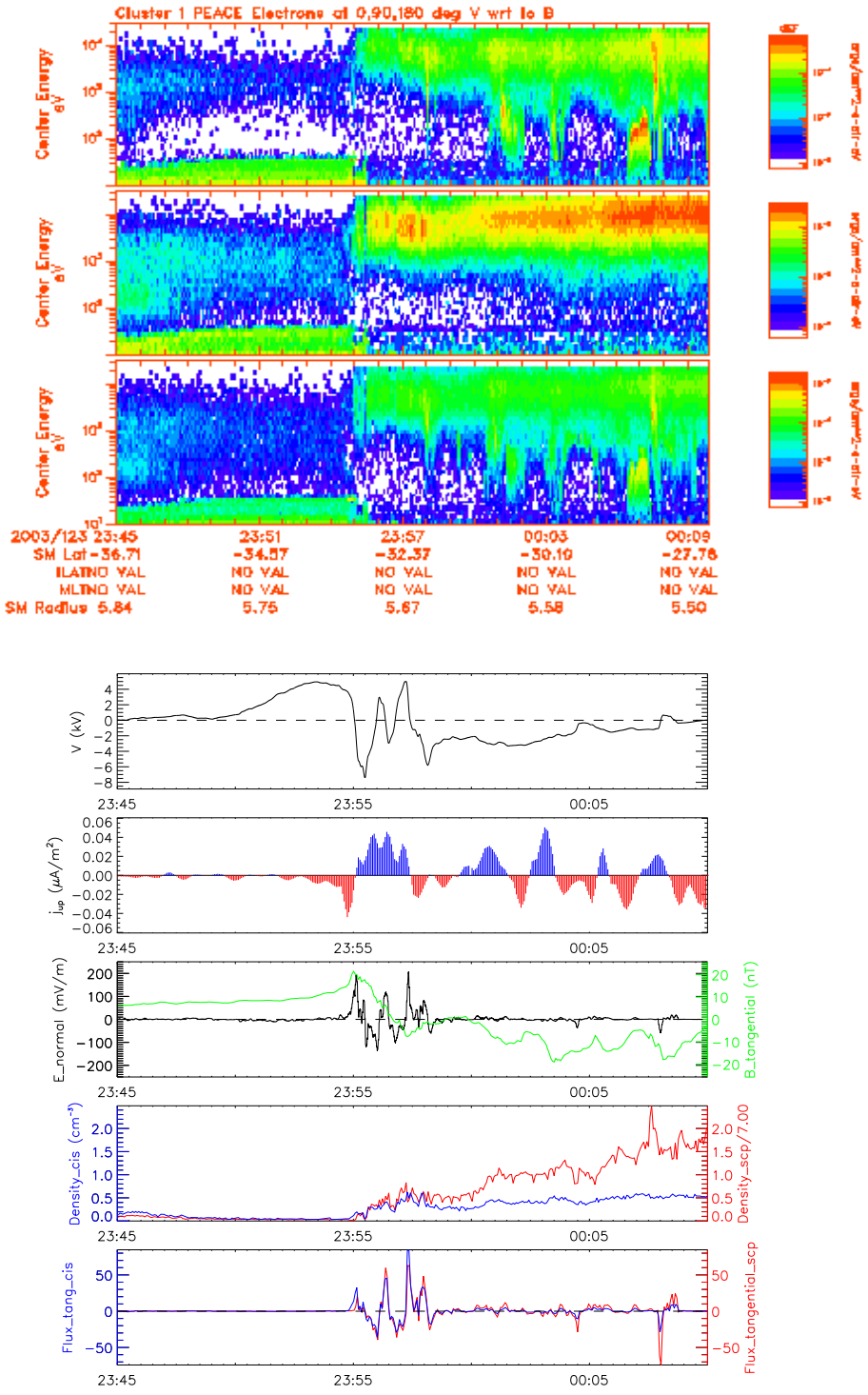

Figure D.25: 2003-05-03 Cluster 1

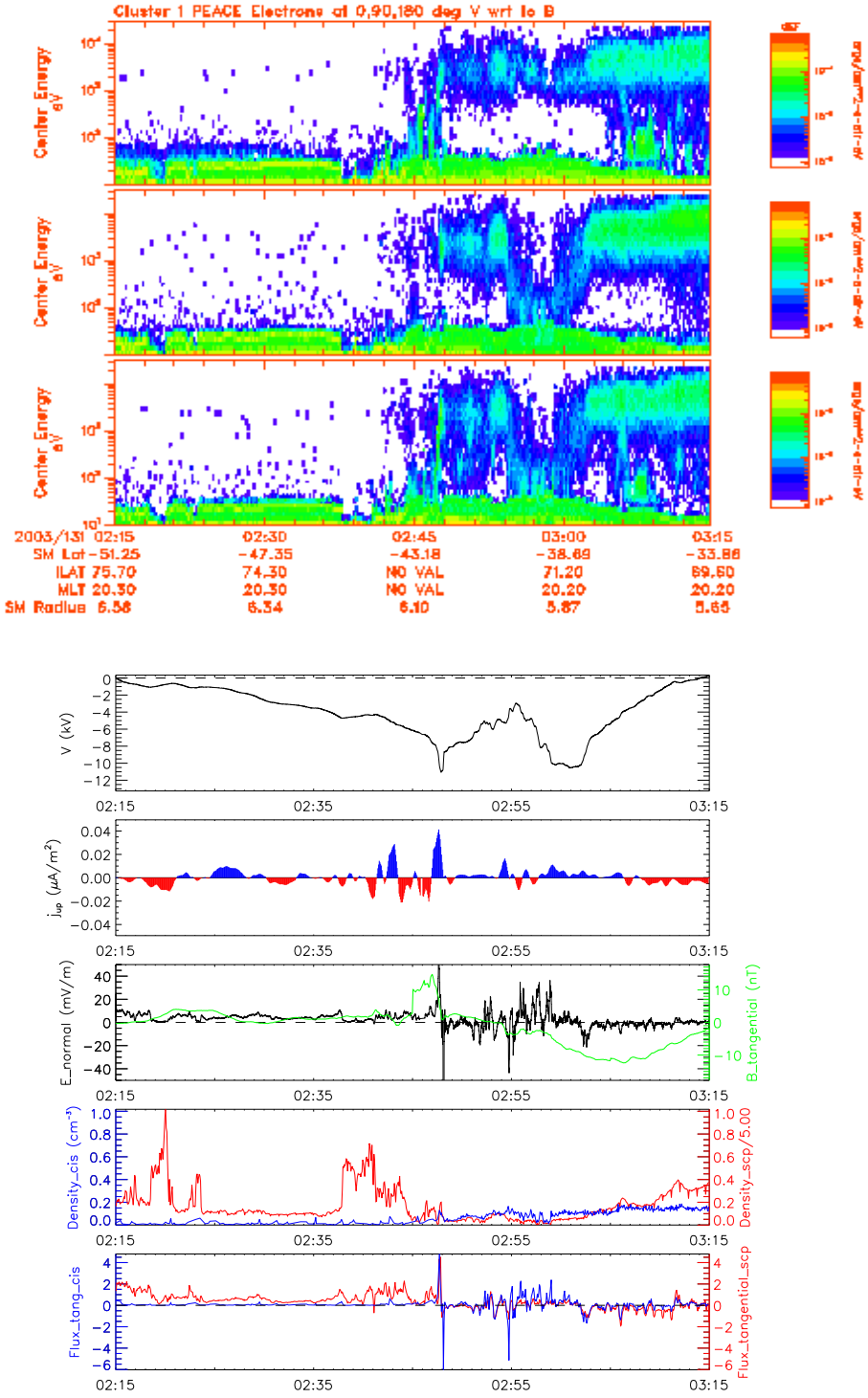

Figure D.26: 2003-05-11 Cluster 1

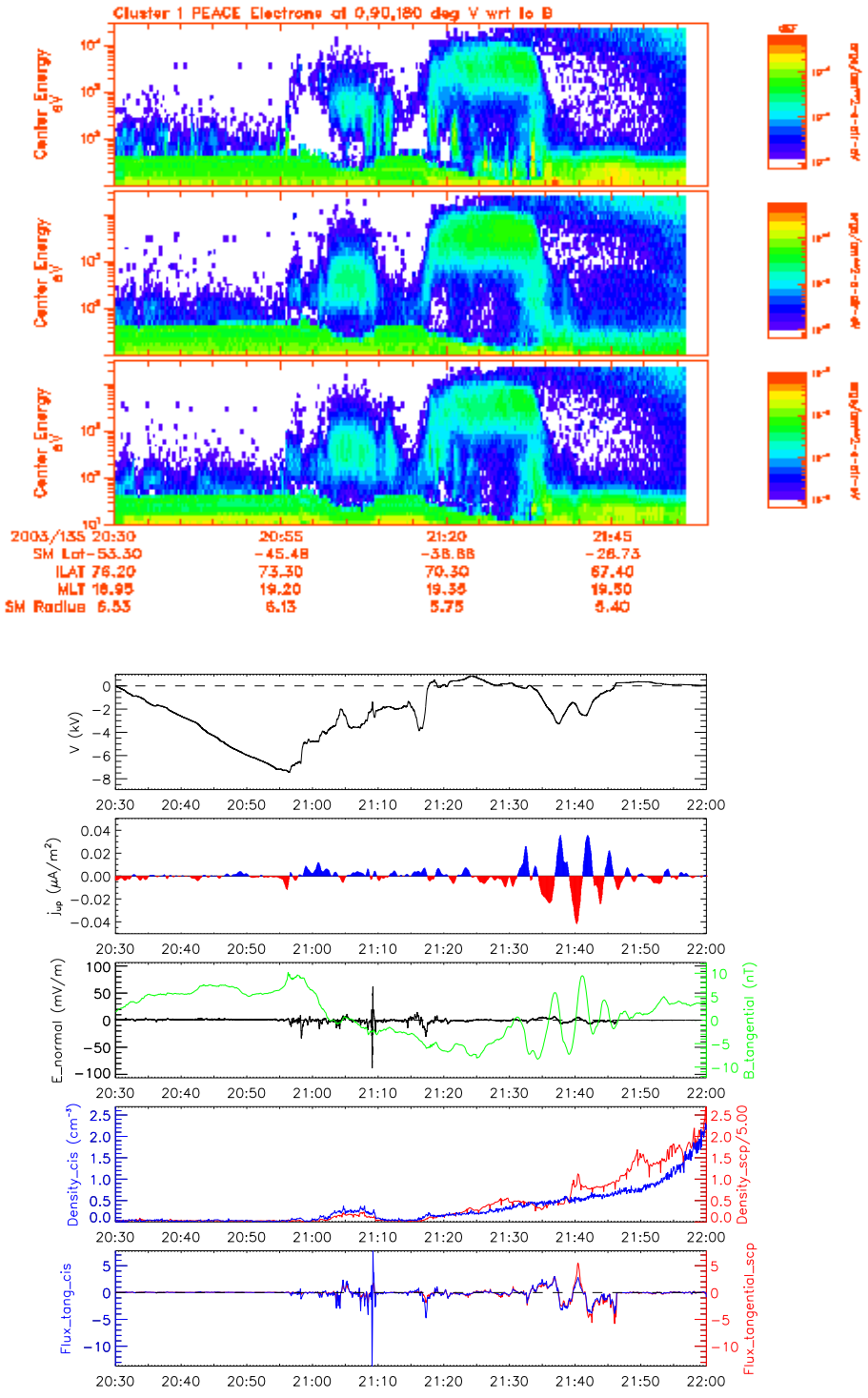

Figure D.27: 2003-05-15 Cluster 1

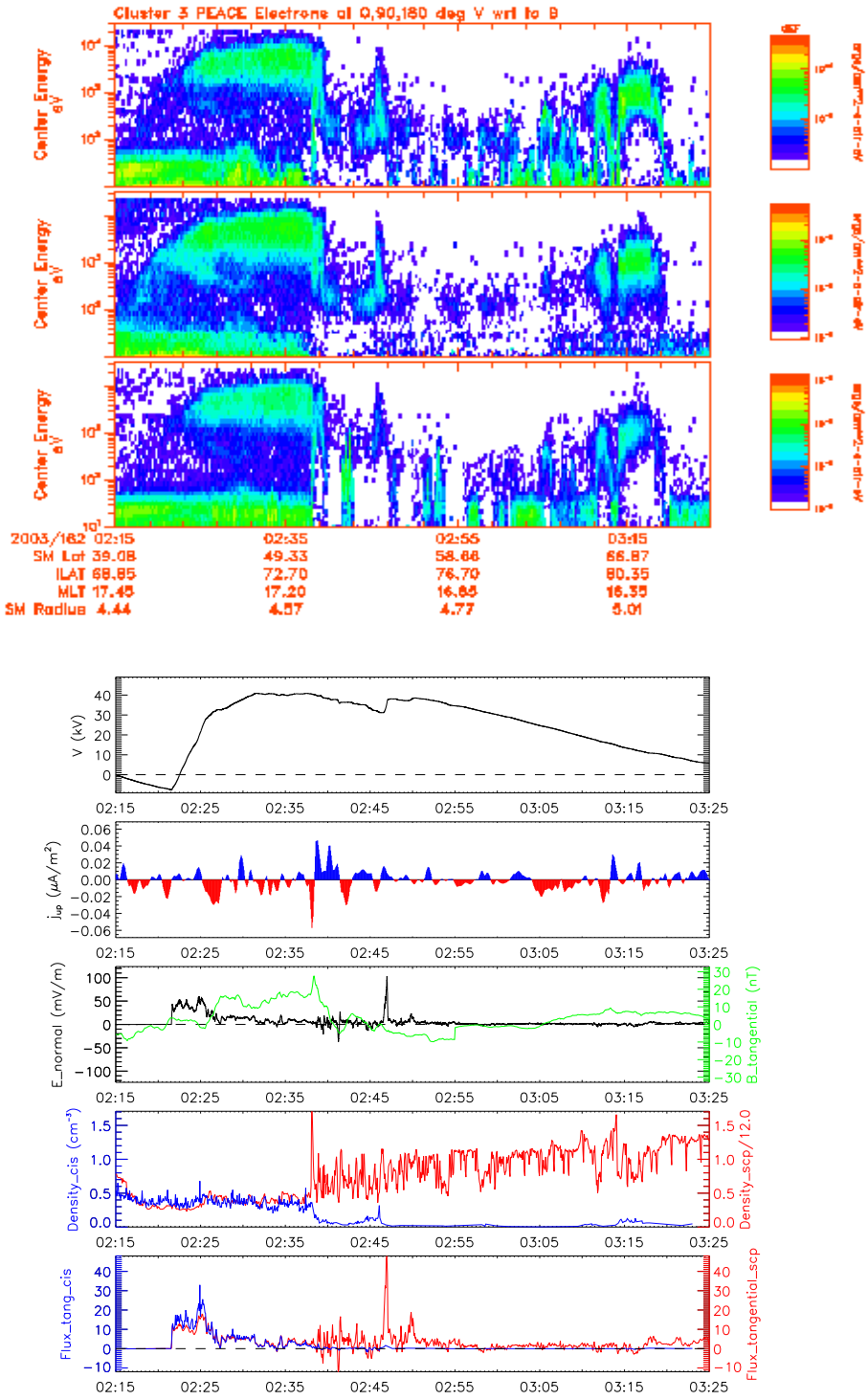

Figure D.28: 2003-06-11 Cluster 3

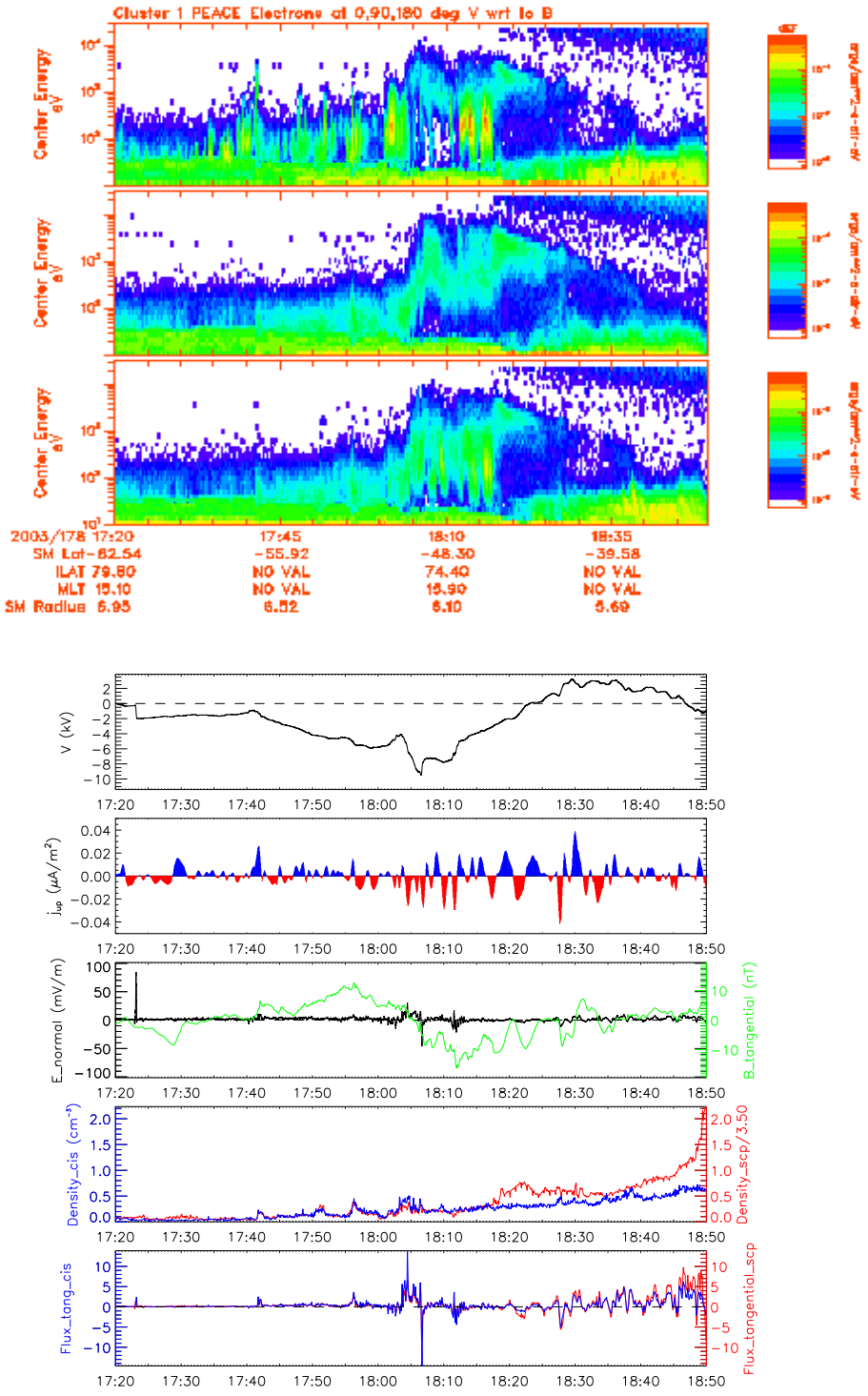

Figure D.29: 2003-06-27 Cluster 1

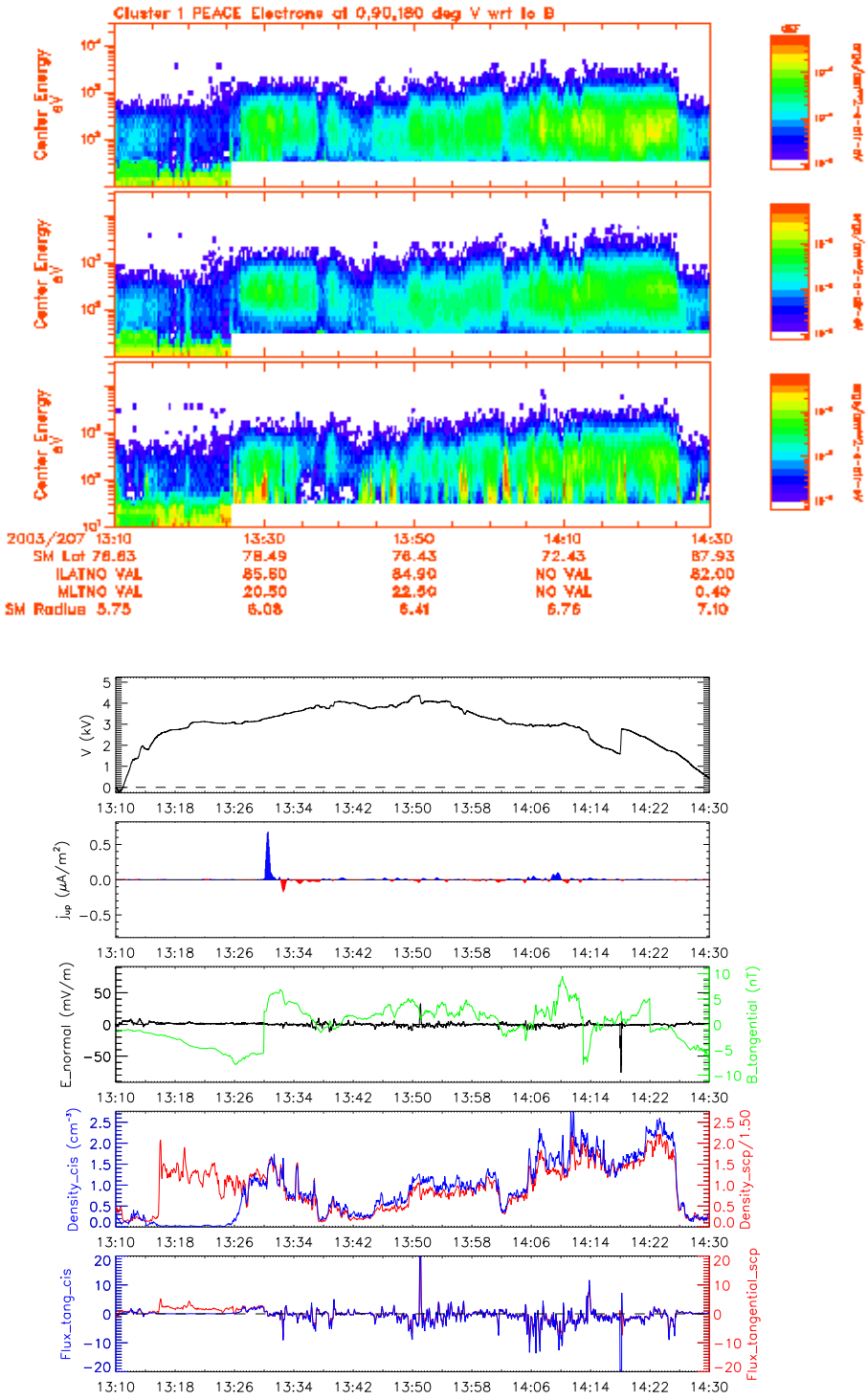

Figure D.30: 2003-07-26 Cluster 1

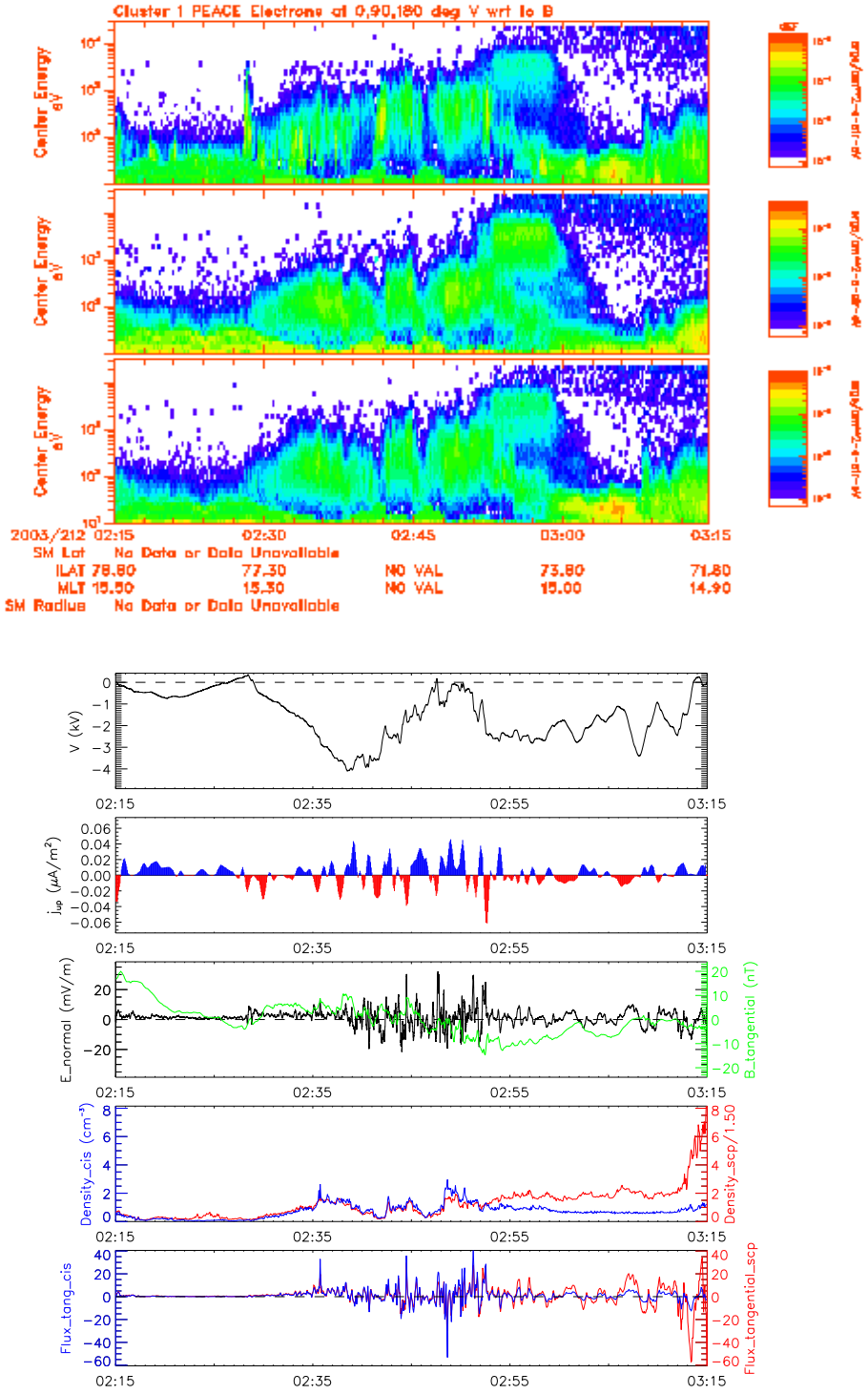

Figure D.31: 2003-07-31 Cluster 1